LBL-28489

Center for Advanced Materials

CAM

Fatigue Crack Propagation in Austenitic Stainless Steels at Cryogenic Temperatures

Zequn Mei
(Ph.D. Thesis)

January 1990

TWO-WEEK LOAN COPY
This is a Library Circulating Copy
which may be borrowed for two weeks.

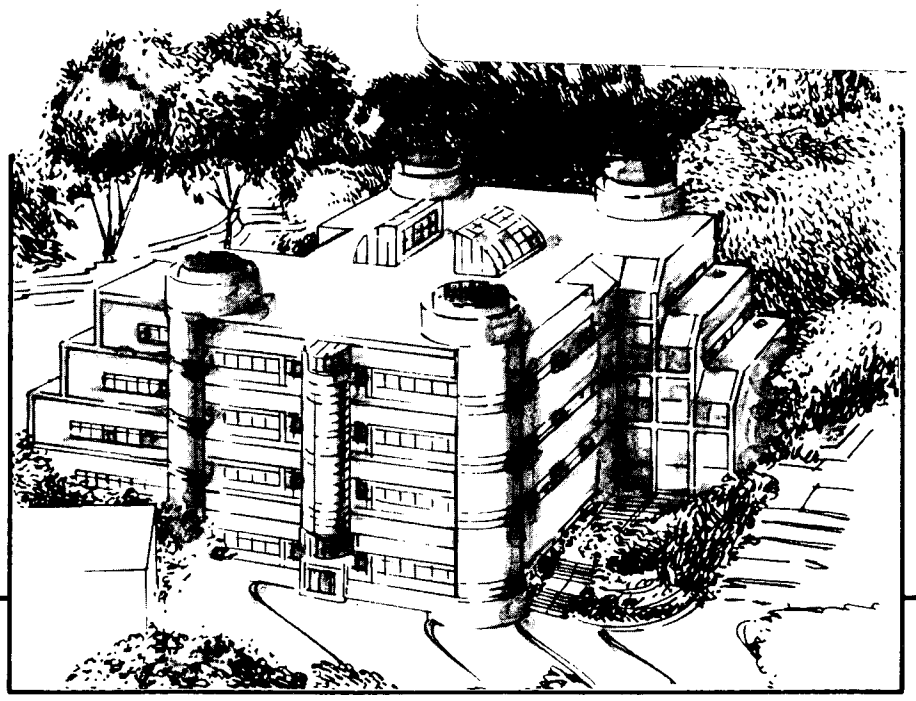

Materials and Chemical Sciences Division

Lawrence Berkeley Laboratory • University of California

ONE CYCLOTRON ROAD, BERKELEY, CA 94720 • (415) 486-4755

Prepared for the U.S. Department of Energy under Contract DE-AC03-76SF00098

LBL-28489 Copy 2
Bldg. 50 Library.

DISCLAIMER

This document was prepared as an account of work sponsored by the United States Government. While this document is believed to contain correct information, neither the United States Government nor any agency thereof, nor the Regents of the University of California, nor any of their employees, makes any warranty, express or implied, or assumes any legal responsibility for the accuracy, completeness, or usefulness of any information, apparatus, product, or process disclosed, or represents that its use would not infringe privately owned rights. Reference herein to any specific commercial product, process, or service by its trade name, trademark, manufacturer, or otherwise, does not necessarily constitute or imply its endorsement, recommendation, or favoring by the United States Government or any agency thereof, or the Regents of the University of California. The views and opinions of authors expressed herein do not necessarily state or reflect those of the United States Government or any agency thereof or the Regents of the University of California.

LBL-28489

Fatigue Crack Propagation in Austenitic Stainless Steels at Cryogenic Temperatures

Zequn Mei

Ph. D. Dissertation

Department of Materials Science and Mineral Engineering

University of California at Berkeley

and

Center for Advanced Materials

Materials and Chemical Sciences Division

Lawrence Berkeley Laboratory

1 Cyclotron Road

Berkeley, CA 94720

January 1990

This work was supported by the Director, Office of Energy Research, Office of Fusion Energy, Development and Technology Division of the U.S. Department of Energy, under Contract No. DE-AC03-76SF00098.

Fatigue Crack Propagation in Austenitic Stainless Steels at Cryogenic Temperatures

by

Zequn Mei

ABSTRACT

This dissertation contains a study, in two parts, that relates to fatigue crack propagation in austenitic stainless steels at cryogenic temperatures.

The first part of the research concentrates on the influence of the mechanically induced martensitic transformation on the fatigue crack growth rate in metastable austenitic stainless steels. The steels 304L and 304LN were used to test the influence of composition, the testing temperatures 298 K and 77K were used to study the influence of test temperature, and various load ratios were used to determine the influence of the mean stress. It was found that decreasing the mechanical stability of the austenite by changing composition or lowering temperature reduces the fatigue crack growth rate and increases the threshold stress intensity for crack growth. However, this beneficial effect diminishes as the load ratio increases, even though increasing the load ratio increases the extent of martensite transformation. Several mechanisms that may affect this phenomenon are discussed, including the perturbation of the crack-tip stress field, crack deflection, and the work hardening characteristics and relative brittleness of the transformed material. The perturbation of the stress field seems the most important; by modifying previous models we develop a quantitative analysis of the crack growth rate that provides a reasonable fit to the experimental results.

The second part of the research concerns the effect of low temperature on fatigue crack propagation in 310 austenitic stainless steel. Crack growth rates were measured at 298 K, 77 K, and 4 K. As temperature decreased the fatigue crack growth rate decreased while the threshold stress intensity increased. At all three temperatures the fatigue crack propagated in a quasi-cleavage mode along a zigzag path. The propagating crack branched to an extent that increased as the temperature decreased. Since no martensite was detected on the crack surfaces and the crack surfaces were smoother at lower temperatures, neither transformation toughening nor roughness-induced crack closure can account for the temperature dependence of the crack growth rate. Various factors that might contribute to the temperature dependence are discussed.

Thesis Committee Chair:

Prof. J. W. Morris, Jr.

ACKNOWLEDGEMENT

It has been 2 years and 8 month since I entered my Ph. D program, and 5 years and 5 months since I came to Berkeley to start my graduate study. As I am about to file my dissertation, my heart is full with joy. I would like to put my research supervisor, Professor J. W. Morris, Jr. on the top of my acknowledgement list. Without his guidance, encouragements, supports, and patience, this study would not have been possible. I am also deeply indebted to Professor R. O. Ritchie and his students Drs. W. Yu and J. Shang, for their valuable discussions throughout the whole research. It is my great honor to have Professors J. W. Morris, Jr., R. O. Ritchie, F. Hauser as my thesis committee members. I will always remember my qualifying examination committee members, Professors R. O. Ritchie, G. Thomas, T. Devine, and F. Hauser, not only their names but also tough questions they asked during the exam..

I would like to express my gratitude to all my fellow graduate students in Morris group, especially to G. Chang, Dana Tribular, Mark McCormack, Jin Chan, Judy Glazer, Steve Shaffer, Anne Sunwoo, Tammy Summers, and Choongun Kim, for their valuable discussions, assistance in doing experiments, and help with my English.

This work was supported by the Director, Office of Energy Research, Office of Fusion Energy, Development and Technology Division of the U. S. Department of Energy, under Contract No. DE-AC03-76SF00098.

I dedicate my dissertation to my mother Meiying Guan and wife Ping Xu.

TABLE OF CONTENTS

	Page
INTRODUCTION	1
PART A: Effects of Deformation-Induced Martensite on Fatigue Crack Propagation in Metastable Austenitic Stainless Steels	
I. REVIEW OF PREVIOUS STUDIES	5
II. EXPERIMENTAL METHODS	9
III. RESULTS	19
IV. DISCUSSION	47
V. CONCLUSIONS	74
PART B: Effects of Low Temperature on Fatigue Crack Propagation in Stable Austenitic Stainless Steel	
I. REVIEW OF PREVIOUS STUDIES	75
II. EXPERIMENTAL METHODS	76
III. RESULTS	77
IV. DISCUSSION	91
V. CONCLUSIONS	93
REFERENCE	94

LIST OF FIGURES

Fig. 1: Sketch showing a martensitic transformation zone induced by the stress / strain concentration at the crack tip. The constraint of the elastic medium on the transformation strain introduces a residual stress field.

Fig. 2: Optical micrographs of (a) annealed 304L stainless steel, and (b) annealed 304L after being rolled 13% at 77 K, showing the deformation-induced martensite. (XBB 884-3424)

Fig. 3: Relations between the volume fraction of induced martensite, determined by X-ray diffraction measurement,[9] and corresponding tensile strain for annealed 304L and as-received 304LN stainless steels. (XBL 829-6610)

Fig. 4: Specimen geometry and size for crack propagation test, and the locations of electric-current input leads and electric-potential measurement probes used for crack length measurement. (W = 2", and a_0 = 0.7").

Fig. 5: Scheme of the direct-current-electrical-potential crack monitoring system.

Fig. 6: Experimentally determined relation of a / W (crack length / specimen width) vs. V_a / V_0 (voltage at a / voltage at a_0, initial crack length) for the specimen with the geometry and size shown in Fig. 4, with V_0 = 1.3 mV, a_0 = 17.5 mm.

Fig. 7: Crack growth rates as a function of stress intensity range of (a) 304L and 304LN austenitic stainless steels tested at room temperature (RT) with load-ratio (R) 0.05; (b) 304L and 304LN steels tested at liquid nitrogen temperature (LNT) with load-ratio 0.05; (c) 304L and 304LN steels tested at LNT with load-ratio 0.5; (d) 304L steel tested at RT and LNT with load-ratio 0.05; (e) 304LN steel tested at RT and LNT with load-ratio 0.05; (f) 304L steel tested at LNT with load-ratio varying from 0.05 to 0.5, and (g) 304L steel tested twice at LNT with load-ratio of 0.3. (XBL 88114044 -- 4050, XBL 8993490).

Fig. 8: Optical micrographs of the fatigue crack profiles of (a) 304LN tested at room temperature (RT), with load-ratio (R) of 0.05, (b) 304L at RT with R = 0.05, (c) 304LN at liquid nitrogen temperature (LNT) with R = 0.05, (d) 304L at LNT with R = 0.05, (e) 304LN at LNT with R = 0.5, and (f) 304L at LNT with R = 0.5. In (c-f) the calculated maximum plastic zone size and ΔK are also indicated. (XBB 879-7964, 868-6196, 870-10652, 870-10653, 8712-10649, and 870-10651).

Fig. 9: Plots of the crack growth rates at load-ratio R normalized by that at R = 0.1 vs. the load-ratio for various austenitic stainless steels at different conditions, showing the abnormally high load-ratio effect on crack growth rate for metastable 304L at 77 K.

Fig. 10: All fatigue crack growth rate data measured in this research. (XBL 895-1865).

Fig. 11: Picture taken on an oscilloscope, showing the bending of the elastic compliance curve, measured from a back face strain gauge, indicating the crack closure. (XBB 880-9794).

Fig. 12: (a) Stress intensity factor at the crack closure, K_{cl}, normalize by the maximum stress intensity factor, K_{max}, and (b) K_{cl}, as a function of stress intensity factor range.

Fig. 13: Optical micrograph of the fatigue crack profile of 304L austenitic stainless steel tested at liquid nitrogen temperature with ΔK = 25 MPa $m^{1/2}$. The sample was covered with a thin layer of ferro-fluid in which 100 Å magnetic particles highlight the magnetic α' martensite. (XBB 884-3426).

Fig. 14: Martensite zone sizes, determined by metallography, around the fatigue cracks of 304L tested at liquid nitrogen temperature with three load-ratios (R) as functions of (a) cyclic intensity factor (ΔK) and (b) maximum stress intensity factor (K_{max})

Fig. 15: Scanning Electron Micrographs of the fatigue fracture surfaces of (a) 304LN at 298 K with R = 0.05 and ΔK = 33 MPa-$m^{1/2}$, (b) 304L at 298 K with R = 0.05

and ΔK = 20 MPa-m$^{1/2}$, (c) 304LN at 77 K with R = 0.05 and ΔK = 7 MPa-m$^{1/2}$, (d) 304L at 77 K with R = 0.5 and ΔK = 8 MPa-m$^{1/2}$, (e) 304L at 77 K with R = 0.5 and ΔK = 6.5 MPa-m$^{1/2}$, and (f) 304L at 77 K with R = 0.5 and ΔK = 18 MPa-m$^{1/2}$. (g) Low magnification optical micrograph of a 304L specimen that was tested half at 298 K and half at 77 K. (XBB 8811-1113, 8811-11108, 8811-11115, 8811-11107, 8811-11109, 8811-11117, and 896-5047)

Fig. 16: (a) Assumed transformation zone shapes before the crack propagates into it -- constant hydrostatic stress contour and equivalent stress contour. (b) Predicted R curves for plane strain and a Poisson's ratio of 1/3 for the two initial zone shapes.

Fig. 17: Deformation-induced martensitic transformation zones in (a) fatigue specimen of AISI 301 steel,[26] and (b) J_{IC} test specimen of 304 steel.[61] (XBB 880-9765)

Fig. 18: The reduction of stress intensity factor -K_{tran} , calculated from equation (19) and the transformation zone size plotted in Fig. 14 (a), vs. the cyclic stress intensity factor (ΔK) of fatigue tests of 304L at 77 K with load-ratios (R) of (a) 0.05, (b) 0.3, and (c) 0.5. The maximum and minimum stress intensity factors are also plotted for comparison.

Fig. 19: Crack growth rates vs. effective stress intensity factor range for 304L austenitic stainless steel tested at 77 K with three load-ratios.

Fig. 20: Crack growth rates vs stress intensity range of (a) cold-rolled 304L, annealed 304L, and as-received 304LN steels tested with load-ratio (R) 0.05 at (a) 298 K and (b) 77 K, (XBL 8812-4051, 4052). SEM fractographs of cold-rolled 304L fatigue-tested at 298 K with (a) $\Delta K \approx 4$ MPa-m$^{1/2}$, and (b) $\Delta K \approx 35$ MPa-m$^{1/2}$. (XBB 8811-11110, 11114)

Fig. 21: Optical micrograph of a crack propagated in an extensively transformed area, showing that the tendance for the crack extension between martensite laths produces a zigzag crack path. (XBB 8712-10651 B)

Fig. 22: Sketch showing the trend of variation of the da/dn vs. ΔK plots with temperature for (a) most of b.c.c alloys, and (b) most of f.c.c alloys.

Fig. 23: Crack growth rate vs. stress intensity range of 310 and 304 austenitic stainless steels at room, liquid nitrogen, and liquid helium temperatures. (XBL 897-2552).

Fig. 24: Optical micrographs of fatigue crack profile of the 310 stainless steel specimen tested at liquid helium temperature. (XBB 897-5501, 5840).

Fig. 25: Scanning electron micrographs of the fatigue fracture surfaces of the 310 stainless steel specimens under the conditions of (a) room temperature, $\Delta K \approx 32$ MPa-m$^{1/2}$, da/dN $\approx$ 1 μm/cycle; (b) liquid nitrogen temperature, $\Delta K \approx 10.5$ MPa-m$^{1/2}$, da/dN $\approx 1.1 \times 10^{-2}$ μm/cycle; (c) liquid helium temperature, $\Delta K \approx 20$ MPa-m$^{1/2}$, da/dN $\approx 7 \times 10^{-3}$ μm/cycle; (d) liquid helium temperature, $\Delta K \approx 20$ MPa-m$^{1/2}$, da/dN $\approx 7 \times 10^{-3}$μm/cycle. (XBB 896-5051A, 5059A, 5061A, 5060)

Fig. 26: Profilometer line scannings of the fatigue fracture surfaces of the specimens that were tested at room, liquid nitrogen, and liquid helium temperatures. (XBL 899-3488).

Fig. 27: X-ray diffraction data of (a) fracture surface of the fatigue specimen tested at liquid helium temperature and (b) the surface 3mm below the fracture surface.

Fig. 28. Pole figures of (a) fracture surface of the fatigue specimen tested at liquid helium temperature and (b) the surface 3mm below the fracture surface.

Fig. 29: Plots of ln(da/dN) vs. 1/T at $\Delta K = 20$ and 16 MPa-m$^{1/2}$.

INTRODUCTION

The structural materials used in a superconducting magnet in a fusion reactor sustain high cyclic stresses at cryogenic temperatures.[1] Designing the magnet requires an understanding of fatigue crack propagation in the structural materials at cryogenic temperatures. Austenitic stainless steels are the candidates for the magnet structure because they retain excellent mechanical properties at low temperatures,[2] are readily available, are relatively ease to fabricate, and have a good service history.

This dissertation contains a study, in two parts, of fatigue crack propagation in austenitic stainless steels at cryogenic temperatures. These two parts are (a) an investigation of the effects and mechanisms of deformation-induced martensitic transformation on fatigue crack propagation in the metastable austenitic stainless steels - AISI 304L and 304LN steels, and (b) a determination of the effects of low temperatures (77K, and 4 K) on fatigue crack propagation in a stable austenitic stainless steel - AISI 310 steel.

A. Effects of Deformation-Induced Martensite on Fatigue Crack Propagation

Many austenitic stainless steels are metastable at cryogenic temperatures. Their fcc austenitic structure (γ) changes into a bcc martensitic structure (α') under sufficient stress and strain. This is the so-called mechanically induced or deformation-induced martensitic transformation. An overview on the γ to α' transformation in the austenitic stainless steels has been provided by Reed.[3]

For a crack under cyclic loading, the stress and strain concentration at the crack tip induces a local martensitic transformation, as shown in Fig. 1. The martensitic transformation is a shear type transformation; it involves a shear strain and sometimes a volume change. The shear and volume change inside the local transformation zone are

constrained by the surrounding elastic medium. A stress field results from that constraint, and is superimposed on the stress field due to the external loading. The martensitic transformation at the crack tip also changes other factors, such as the fracture mode, crack extension path, cyclic softening/hardening behavior, etc.. All these factors affect the fatigue crack growth rate.

One of the research objectives of this dissertation is to understand the effects and mechanisms of the mechanically induced martensitic transformation on the fatigue crack propagation. For that purpose crack growth rates were determined in relatively unstable AISI 304L and relatively stable AISI 304LN austenitic stainless steels at both room and

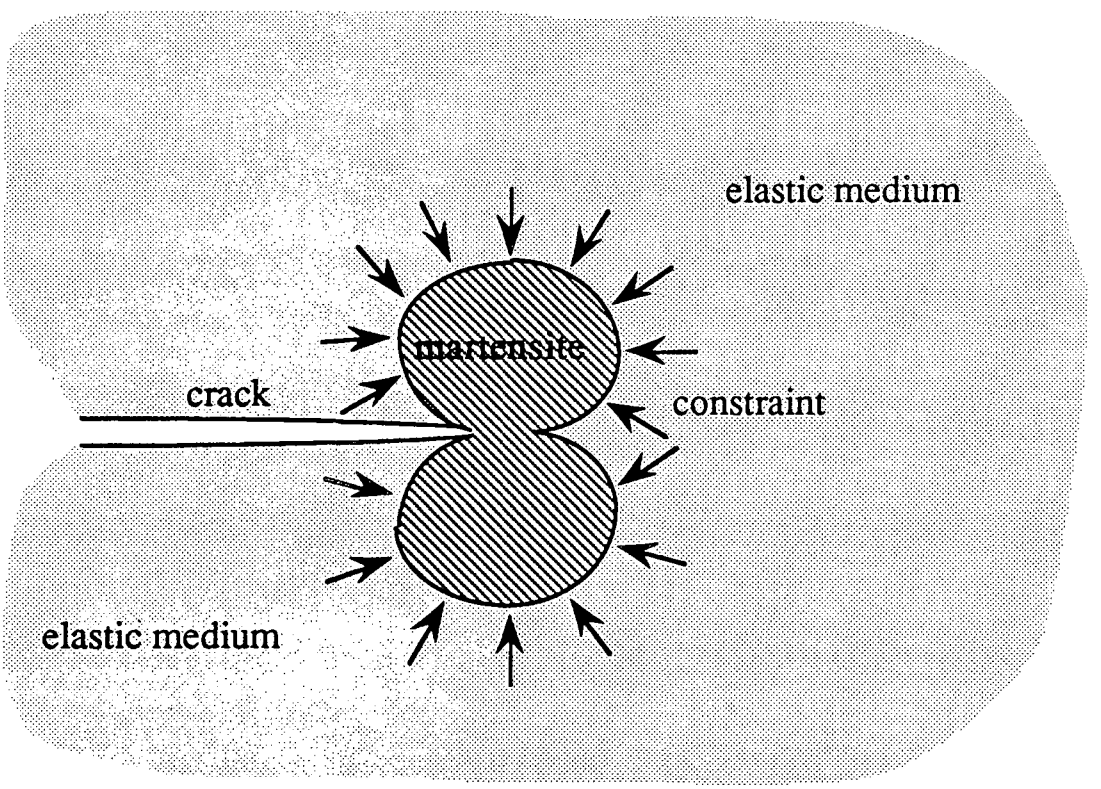

Fig. 1: Sketch showing the martensitic transformation zone induced by the stress / strain concentration at the crack tip. The constraint of the elastic medium on the transformation strain introduces a residual stress field.

liquid nitrogen temperatures (298 K and 77 K) with load-ratio varying between 0.05 to 0.5. In other words, the amount of the deformation-induced martensite produced by the cyclic load was controlled by varying the chemical composition, the testing temperature, and the average load.

Comparing the crack growth rate when the transformation occurred and that when it did not occur revealed a clear picture of the effects of the transformation on the crack growth rate. The morphology and distribution of the martensite particles around the cracks, the crack extension paths, and the fracture surfaces were studied after fatigue tests with optical and scanning electronic microscopies. Based on these observations various mechanisms for the influence of the transformation on the crack growth rate were investigated.

B. Effects of Low Temperature on Crack Propagation in the Stable Austenitic Stainless Steel

As mentioned above, the crack growth rates at 298 K and 77 K were compared to reveal the influence of the martensitic transformation on crack propagation. The comparison can not be conclusive since the crack growth rate depends on the testing temperature as well. The initial reason to study the low temperature effect on crack propagation in a stable austenitic stainless steel was to support the study on the metastable austenitic steels. Actually, the temperature effect on crack propagation is a separate and more general subject than the transformation effect. In the research field of fatigue at low temperature, the foremost question is probably -- would a fatigue crack grow faster or slower as the temperature decrease to cryogenic temperatures? And why?

It is well known that as the temperature decreases from room temperature to cryogenic temperatures, metallic materials become usually stronger, less ductile, and more brittle. But, as far as the crack propagation behavior is concerned, the general trend as the

temperature decreases is not clear. In the literature, examples of both increased and decreased the fatigue crack propagation rates with the testing temperature can be found. In this thesis, fatigue crack propagation in the stable 310 austenitic stainless steel in the temperature range from 4 to 298 K was studied.

PART A: EFFECTS OF DEFORMATION-INDUCED MARTENSITE ON FATIGUE CRACK PROPAGATION

I. REVIEW OF PREVIOUS STUDIES

A. Effects of Deformation-Induced Martensite on Mechanical Properties Other than Crack Propagation

The effects of the mechanically induced martensitic transformation on the uniaxial tensile properties of metastable austenitic steels have been well documented in the literature.[4-10] The effects depend on the austenitic stability and the testing temperature between M_s and M_d, the temperatures for spontaneous transformation and for transformation under deformation respectively. In all the cases, the transformation increases the general work hardening rate. (This is simply because the martensitic phase is harder than the austenitic phase.) If a metastable steel is tested at temperatures close to and above M_s where the austenitic structure is unstable with respect to small deformations, a low yield point results. The stress needed to initiate the martensitic transformation is lower than the stress to start slip, therefore the transformation strain before slip strain terminates the elastic range of the stress vs. strain plot. If a metastable steel is tested at a temperature close to and below M_d where transformation occurs only after large deformation, a relatively large elongation results. This is why TRIP (TRansformation Induced Plasticity) steel has extraordinary ductility in a certain temperature range.[11]

The plane strain fracture toughness, K_{IC}, of metastable austenitic steels have been shown to depend on the martensitic transformation during fracture.[12,13] For example, Antolovich[12] determined the K_{IC} of a high carbon TRIP alloy over a range of temperature, from -196°C to 200°C. The toughness decreased as the testing temperature

decreased but jumped to a high level when passing the M_d temperature. The enhancement of the fracture toughness was thought to result from the absorption of energy by the γ to α' transformation at the fracture surface. Various models were proposed to calculate the amount of the energy.[12-14]

Low cycle fatigue studies have been reported for metastable TRIP alloys,[15,16] Fe-18Cr-6.5Ni-0.19C stainless steel,[17] the AISI 300 series of austenitic stainless steels,[18,19] and the AISI 200 series of austenitic stainless steels.[20] Generally speaking, for constant strain fatigue test, at a given plastic strain amplitude, the formation of α' martensite leads to a substantial cyclic hardening of the material and to a decrease in fatigue life. The exceptions are the 300 series austenitic stainless steels, where the slight transformation at small strain amplitude improves the fatigue life, while massive transformation at large strain amplitude decreases the fatigue life.

B. Effects of Deformation-Induced Martensite on Crack Propagation

While there have been many research studies on the influence of the mechanically induced martensitic transformation on tensile properties, there is relatively little prior work on fatigue crack propagation in metastable austenitic steels. However, the TRIP alloys,[21-23] and AISI 300 series austenitic stainless steels have been studied.[9,22-29] Most of the studies concentrated on crack propagation in the Paris region of the da/dN (crack growth rate) vs. ΔK (cyclic stress intensity factor) plot, only some[27-29] investigated near-threshold crack propagation. The experimental data shown in all these studies lead to the conclusions that the transformation decreases the fatigue crack growth rate and enhances the threshold stress intensity factor for crack growth.

These conclusions were reached by comparative experiments, i.e. (1) fatigue test at the temperature above M_d vs. that between M_s and M_d,[9,22-24,18,29] (2) fatigue test of the stable austenitic steels vs. that of the metastable austenitic steels;[9,22-26] (3) fatigue tests of the steels with certain thermo-mechanical treatments which alter its austenitic stability vs.

that of same steels without the treatments;[21] and (4) fatigue test of metastable steels in the air vs. in a vacuum, testing in a vacuum was shown to promote the martensitic transformation.[27]

Several mechanisms were proposed for the reduction of the fatigue crack growth rate by the transformation. The compressive residual stress mechanism was raised[30,25] based on the fact that there is a volume expansion associated with the γ to α' transformation in the 300 series austenitic stainless steels.[31-33] The elastic constraint of the materials around a dilated transformed zone puts that zone into compression. Thus the stress due to the applied external tensile loading is reduced at the crack tip by the compressive residual stress.

Schuster and Altstetter[25] did an interesting experiment to prove the existence of compressive residual transformation stress. They prepared several 1.5 mm thick specimens with different notch lengths for zero load ratio fatigue test; therefore for loading to the same ΔK level, each specimen has a different net section tensile stress. For long notch length specimens (low net section stress), the crack growth rate in the unstable AISI 301 austenitic stainless steel was slower than that in the relative stable AISI 302 austenitic stainless steel. For short notch length specimens (high net section stress), the difference in crack growth rate between 301 and 302 steels disappeared. However the crack growth rate data they collected with the short notch length specimens are not valid, as pointed by themselves, because the specimens had already generally yielded.

Work hardening mechanism was proposed[23] based on the arguments that the strong work hardening rate due to the transformation reduces the crack tip opening displacement. However the work hardening effect was believed not large enough to explain the experimental results.[23] The phenomenon of crack closure was observed during fatigue crack propagation tests in metastable AISI 300 series austenitic stainless steels, however the crack closure measurement data could not satisfactorily explain the change of crack growth rate due to the transformation.[27-29]

It is seen after reviewing the previous research that the study of fatigue crack propagation in metastable austenitic steels has been confined to the Paris, or power-law region of the da/dN vs. ΔK plot and the mechanisms for the influence of the transformation on the crack propagation have not been understood.

II. EXPERIMENTAL METHODS

A. Materials

The materials used in this study were commercial grade AISI 304L and 304LN stainless steels. Their chemical compositions are listed in Table I. They differ primarily in nitrogen content, which is higher in 304LN. Increasing nitrogen raises the yield strength at low temperature (Table II) and stabilizes the austenite phase. 304L plates were processed in two different ways. The basic material was annealed at 1050 °C for 1 hour followed by a water quench to create a homogeneous austenite phase. Some of these plates were then rolled 13% at liquid nitrogen temperature to form a two-phase mixture of austenite and martensite. 304LN was used in the as-received (annealed and quenched) condition. The average grain sizes of 304L and 304LN were 100 μm and 70 μm, respectively. Optical micrographs of the annealed 304L and cold-rolled 304L are shown in Fig. 2. X-ray diffraction tests confirmed that the annealed 304L and as-received 304LN were essentially pure austenite (γ), while the cold-rolled 304L was about 50% austenite, 50% martensite (α') with a small admixture of the hexagonal, ε-martensite phase. The tensile properties of the annealed and as-received 304LN were measured and are listed in Table II.[9]

Table I - Chemical compositions (wt %) of 304L and 304LN stainless steels

	Fe	Cr	Ni	Mn	P	S	Si	C	N
304L	Bal.	18.7	8.64	1.63	0.021	0.010	0.51	0.024	0.074
304LN	Bal.	18.54	9.55	1.77	0.014	0.009	0.78	0.021	0.139

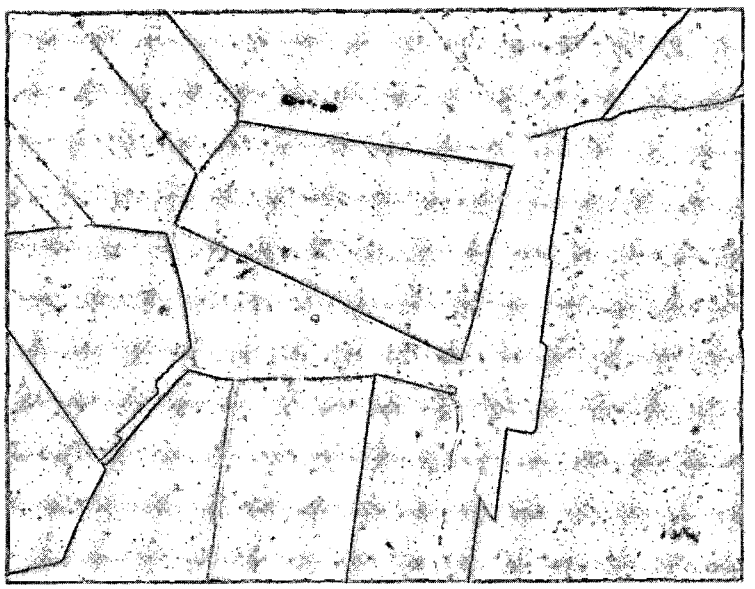

304L, Austenized 1hr at 1050°C + Quench 25 um

(a)

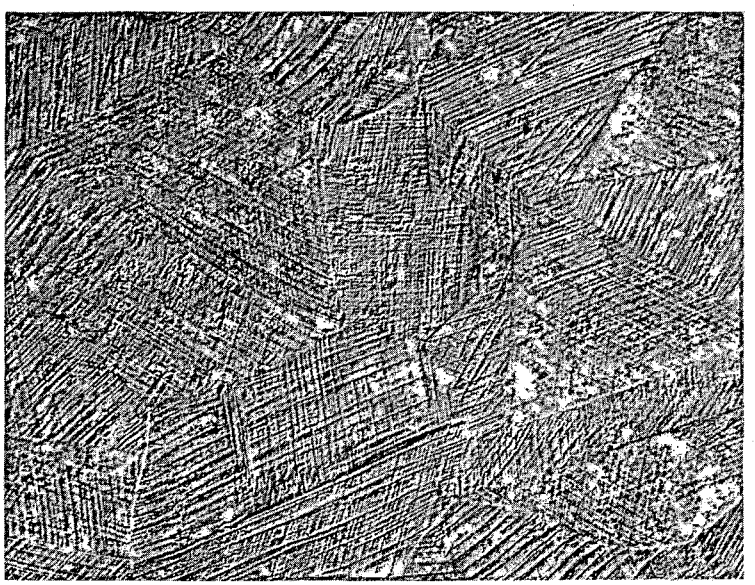

304L, Rolled 13% at LNT 25 um

(b)

Fig. 2: Optical micrographs of (a) annealed 304L stainless steel, and (b) annealed 304L after being rolled 13% at 77 K, showing the deformation-induced martensite. XBB 884-3424

The martensite start temperatures on cooling (M_s) and deformation (M_d) were estimated from the empirical formulae given in references [34,35], and are: for 304LN, $M_s < 0$ K, $M_d < 255$ K, for 304L, $M_s < 38$ K, $M_d < 299$ K. The thermal stability of the annealed 304L steel was confirmed by soaking in liquid helium for more than 2 hours; no α' or ε-hcp martensite was detected by X-ray diffraction. The volume fractions of martensite as a function of tensile strain at room and liquid nitrogen temperatures were measured by x-ray diffraction.[9] The results are plotted in Fig. 3. Despite the similarity of the computed M_d temperatures, the austenite phase in 304L is very much less stable on mechanical deformation than that in 304LN.

Table II - Tensile properties of 304L and 304LN stainless steels

Materials	Testing Temperature (K)	Yield σ_y (MPa)	Ultimate tensile σ_u (MPa)	σ_u/σ_y	Elongation (%)
304L	298	294	658	2.2	85.5
	77	433	1524	3.5	48.1
304LN	298	341	643	1.89	71.7
	77	724	1476	2.0	51.3

B. Fatigue Crack Propagation

The fatigue crack propagation tests were conducted according to the procedures recommended in references [36,37]. Fatigue crack growth rates were measured on 12.7 mm and 25.4 mm thick compact tension specimens of the geometry and size suggested by ASTM standards, [36] as sketched in Fig. 4. The fatigue crack plane lay in the L-T

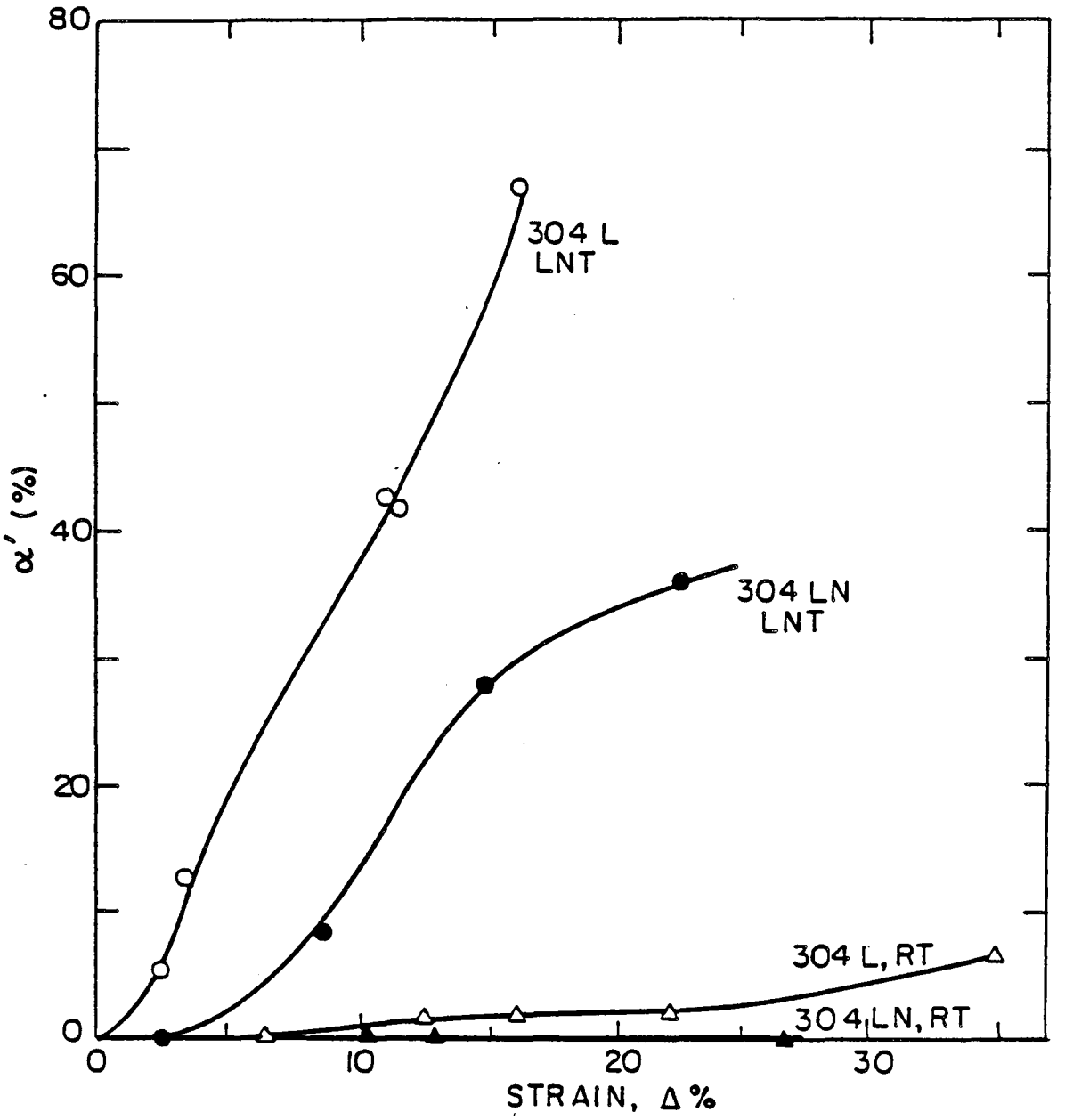

Fig. 3: Relations between the volume fraction of induced martensite, determined by X-ray diffraction measurement,[9] and corresponding tensile strain for annealed 304L and as-received 304LN stainless steels. (XBL 829-6610)

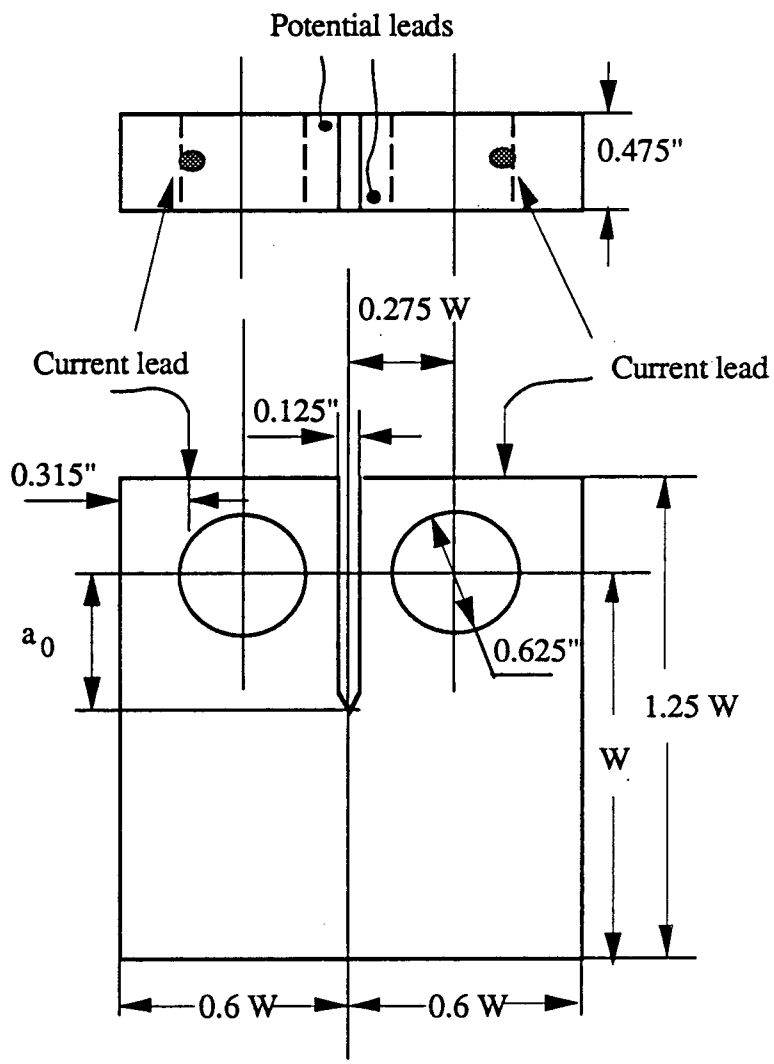

Fig. 4: Specimen geometry and size for crack propagation test, and the locations of electric-current input leads and electric-potential measurement probes used for crack length measurement. (W = 2", and a_0 = 0.7").

orientation. The specimens were tested under load control in a hydraulic testing machine with a compression-tube frame, using a sine-wave load form and a frequency of 10-30 Hz.

The cyclic stress intensity (ΔK) was calculated from the crack length (a), the specimen thickness (B), the specimen width (W), and cyclic load (ΔP), as suggested in reference [38],

$$K = \frac{\Delta P\, f(\frac{a}{W})}{B\, W^{1/2}} \tag{1}$$

where

$$f(\tfrac{a}{W}) = \sqrt{\pi}\,[\,16.7\,(\tfrac{a}{W})^{1/2} - 104.7\,(\tfrac{a}{W})^{3/2} + 369.9\,(\tfrac{a}{W})^{3/2} - 573\,(\tfrac{a}{W})^{5/2} + 360.5\,(\tfrac{a}{W})^{7/2}\,]. \tag{2}$$

After completing fatigue crack propagation tests, the author of this thesis realized that the parameter $f(\frac{a}{W})$ adopted by ASTM standard is,[36]

$$f(\tfrac{a}{W}) = \frac{2+\frac{a}{W}}{(1-\frac{a}{W})^{3/2}}\,[\,0.886 + 4.64\,\tfrac{a}{W} - 13.32\,(\tfrac{a}{W})^2 + 14.72\,(\tfrac{a}{W})^3 - 5.6\,(\tfrac{a}{W})^4\,] \tag{3}$$

However, the difference between (2) and (3) is less than 1 % in the range of crack length monitored in this study.

The crack length was monitored continuously using the direct current electrical potential method,[37,39] as sketched in Fig. 5. Constant direct-current is driven through the cracked specimen, and the electric potential across the crack is measured. The relation of $\frac{a}{W}$ (crack length / specimen width) vs. $\frac{V_a}{V_0}$ (voltage at a / voltage at a_0, initial crack length)

was determined at both room and liquid nitrogen temperatures. The relations at both temperatures are almost the same, as expected, and are plotted in Fig. 6. The $\frac{a}{W}$ vs. $\frac{V_a}{V_0}$ plot from reference [72] is also plotted in Fig. 6; the specimen they used to determined the plot has pin hole size of 0.5" as opposed to 0.625" in this study. The crack length was recorded as a function of cycle number on a strip-chart recorder. The fatigue crack growth rate, da/dN, was determined from the slope of the curve.

Fatigue crack growth was monitored over a range of growth rates from 10^{-11} to 10^{-6} m/cycle to sample both the near-threshold and Paris regions. The near-threshold region crack growth rates were measured under decreasing ΔK conditions (so-called the load shedding method [37,40]), using a step-wise decrement in ΔK of less than 7 % at each step. At each load level, the crack was allowed to propagate at least 3 times the computed maximum plastic zone size formed at the previous load level. After establishing the

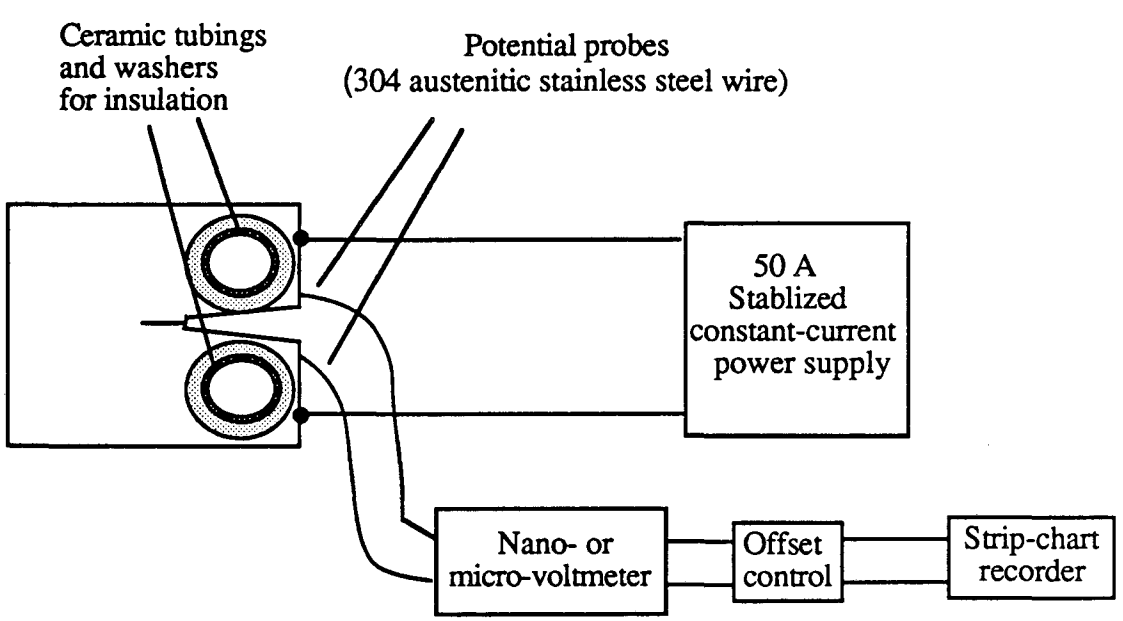

Fig. 5: Scheme of the direct-current electrical-potential crack monitoring system.

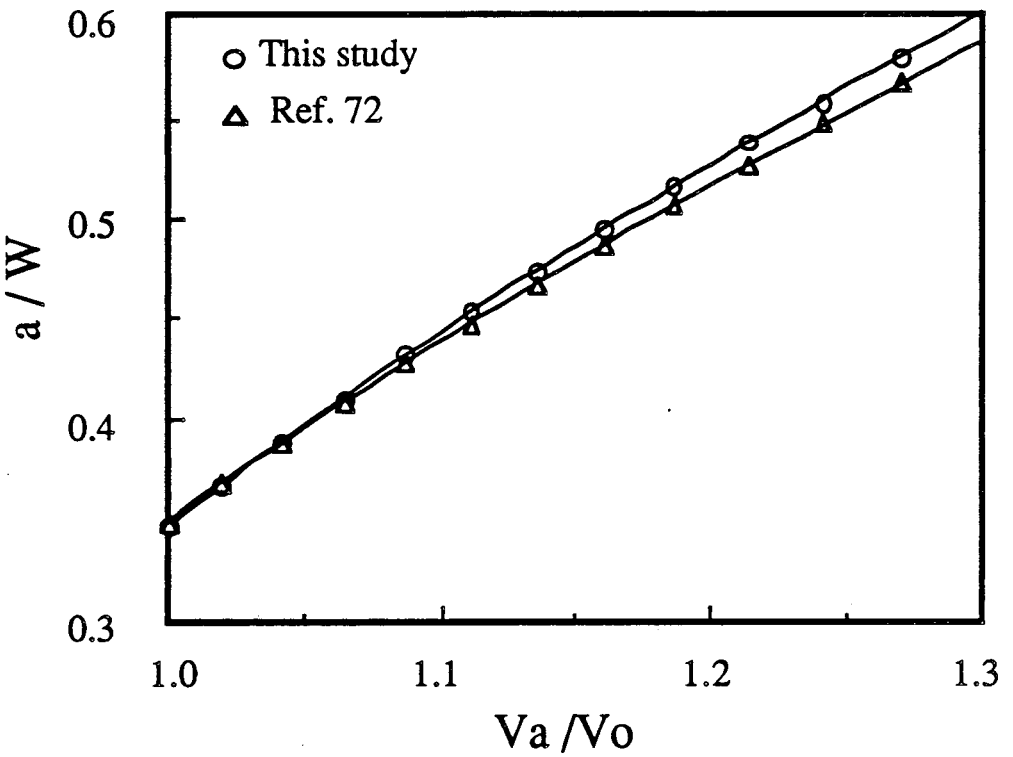

Fig. 6: Experimentally determined relation of $\frac{a}{W}$ (crack length / specimen width) vs. $\frac{V_a}{V_0}$ (voltage at a / voltage at a_0, initial crack length) for the specimen with the geometry and size shown in Fig. 4, with V_0 = 1.3 mV, a_0 = 17.5 mm. The relation from reference [72] is also plotted as comparison. The numerically fitted expression of the curve is

$$\frac{a}{W} = -2.7510 + 6.2023\frac{V_a}{V_0} - 4.1620\left(\frac{V_a}{V_0}\right)^2 + 1.0576\left(\frac{V_a}{V_0}\right)^3 ,$$

while the expression from reference [72] is

$$\frac{a}{W} = -1.9296 + 4.2365\frac{V_a}{V_0} - 2.5825\left(\frac{V_a}{V_0}\right)^2 + 0.62541\left(\frac{V_a}{V_0}\right)^3 .$$

threshold, the load was increased step-wise and da/dN values were recorded until the specimen sustained general yield. The fatigue tests at room temperature were conducted in air at about 298 K; the tests at 77 K were done by immersing the specimens and the compression tube into a 25 liter dewar filled with liquid nitrogen.

The extent of crack closure during fatigue crack growth was monitored continuously using the back-face strain gauge technique.[41,42] In this technique a strain gauge is mounted on the back face of the specimen and the closure stress intensity, which represents the macroscopic contact of the fracture surfaces during unloading, is determined from the load at which the elastic compliance curve first deviates from linearity.

C. Optical Microscopy

The deformation-induced martensite around the fatigue crack was observed after the fatigue test by optical microscopy on samples that were sectioned perpendicular to the crack plane at center thickness. Tests showed that no martensite was induced during grinding or polishing. Two methods were used to reveal the martensite: (1) chemical etching in a solution of 15 ml HNO_3, 45 ml HCl, 20 ml methanol for about 1 minute, which reveals the grain boundaries and interfaces between martensite and austenite, and (2) painting the surface with ferrofluid,[43,44] which highlights the magnetic α' martensite particles in the paramagnetic austenite matrix. While all of the optical metallography was done at room temperature, there was no evidence of martensite reversion during heating from 77 K and none is believed to occur.[45]

D. X-ray Diffraction and Scanning Electron Microscopy

The fatigue fracture surfaces of the specimens were studied under a scanning electron microscope. The γ, α' and ε phase fractions in the material near the fracture surface were measured by x-ray diffraction. The relative volume fractions of the three phases were

determined by comparing the integrated intensities of the $(200)_{\gamma}$, $(200)_{\alpha'}$, and $(10.1)_{\varepsilon}$ peaks.

III. RESULTS

A. Fatigue Crack Propagation

To explore the influence of the martensite transformation on the fatigue crack growth rate the extent of transformation during fatigue was varied in three different ways: (1) by changing the chemical composition from that of 304L to that of 304LN, (2) by lowering the temperature from room temperature to liquid nitrogen temperature, and (3) by varying the load ratio. The consequences of these three changes are the following.

Chemical Composition

The measured crack growth rates of 304L and 304LN at 298 K and 77 K for the load ratio R = 0.05 are plotted in Figs. 7(a) and 7(b) respectively. The fatigue crack growth rates of the two alloys are very nearly the same at 298 K. However, at 77 K the crack growth rate of 304L is 10 times slower than that of 304LN at $\Delta K = 10$ MPa$\sqrt{m}$, and is 4 times slower at $\Delta K = 50$ MPa$\sqrt{m}$. These results correlate directly with the extent of martensitic transformation in the two alloys. Metallographic studies of the fatigue crack profiles show that at 298 K both 304L and 304LN remain essentially austenitic at the crack tip as ΔK is varied from 3 to 40 MPa$\sqrt{m}$. Figs. 8 (a,b) show the crack profiles of 304LN and 304L specimens tested at 298 K, respectively. Both cracks are shown widely opened, because the specimens had been generally yielded. No martensite particles could be observed in the 304LN specimen, while little could be seen in the 304L specimen. Hence the fatigue crack growth rate at room temperature is not significantly affected by martensitic transformation in either alloy. The fatigue crack growth rates are similar despite differences in the static mechanical properties of the two alloys (Table II). At 77 K, on the other hand, 304L is substantially transformed while 304LN is only transformed slightly at the higher values of ΔK. As shown in Fig. 8 (c), very little martensite appears near a fatigue crack in

304LN that grows at ΔK values as high as 15 MPa$\sqrt{m}$. However, as shown in Fig. 8(d), martensite coats a growing crack in 304L even when ΔK approaches the threshold cyclic stress intensity factor, ΔK_{th}, and a broad region of extensive transformation is present when ΔK is greater than about 20 MPa$\sqrt{m}$. The fatigue crack growth rate decreases significantly when the chemical composition is changed to promote deformation-induced martensite.

The fatigue crack growth rates of 304L and 304LN at 77 K at a higher load ratio (R = 0.5) are compared in Fig. 7(c). The crack growth rate is, again, significantly slower in 304L. The decrease is less at R = 0.5 than at R = 0.05 (compare Figs. 7(c) and 7(b)). However, the difference in the degree of martensitic transformation is greater. Increasing the load ratio from R = 0.05 to R = 0.5 for given ΔK results in a larger transformation zone with denser martensite in 304L, while about the same degree of transformation occurs in 304LN. Fig. 8 (e,f) show the crack profiles of specimens tested at 77 K for 304LN with R = 0.5 and 304L with R = 0.3, respectively.

Temperature

Fig. 7(d) illustrates the effect of decreasing the test temperature on the fatigue crack growth rate in the two metastable steels. The fatigue crack growth rate of 304L at room temperature, where the austenite phase is stable, is significantly greater than that at liquid nitrogen temperature, where the alloy undergoes extensive transformation. On the other hand, Fig. 7(e) shows that the fatigue crack growth rate in 304LN is relatively insensitive to temperature at lower ΔK values where the transformation is insignificant at both test temperatures. Again, the martensitic transformation reduces the fatigue crack growth rate.

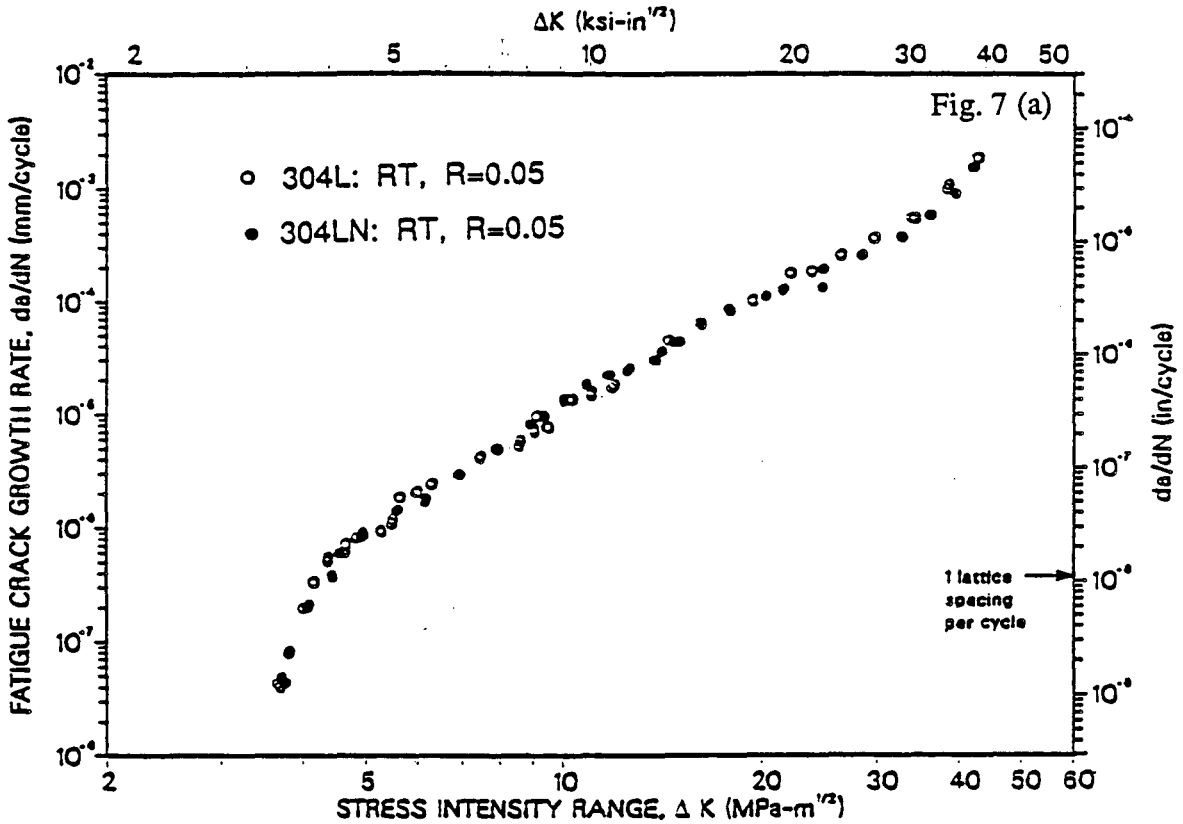

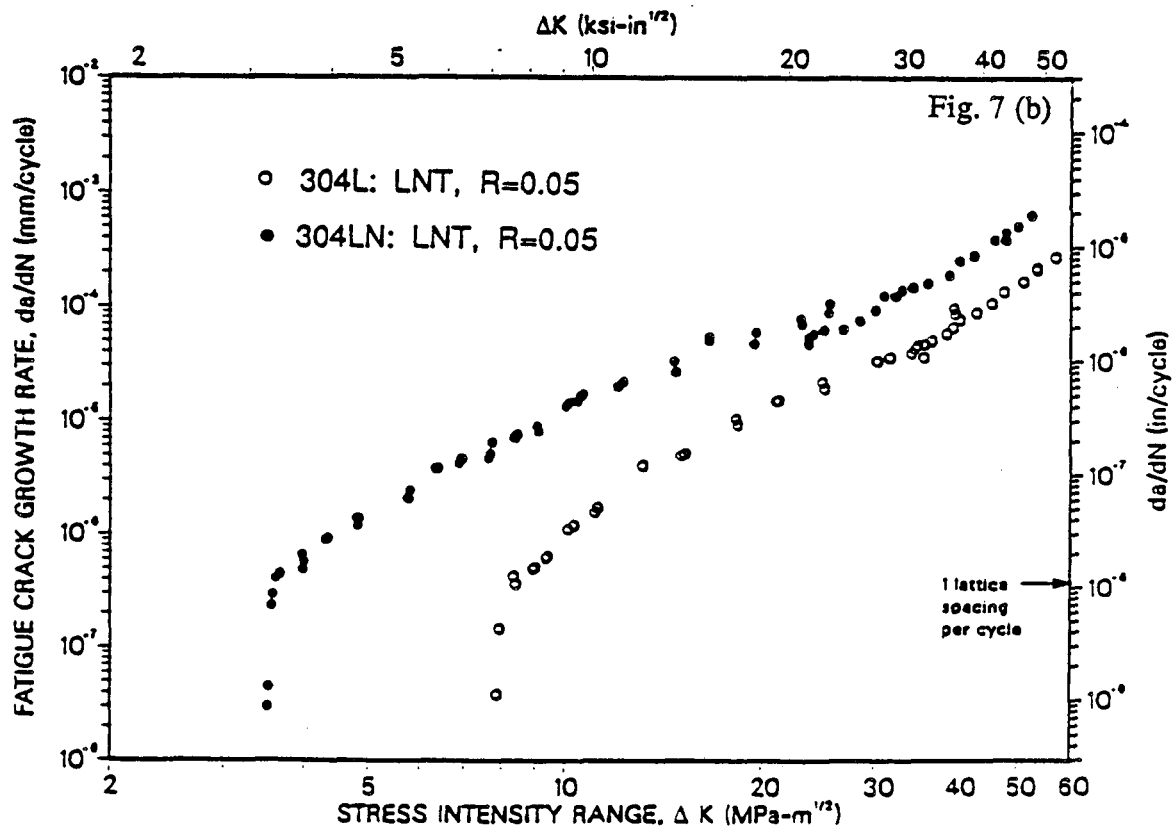

XBL 8811-4044 & XBL 8811-4045

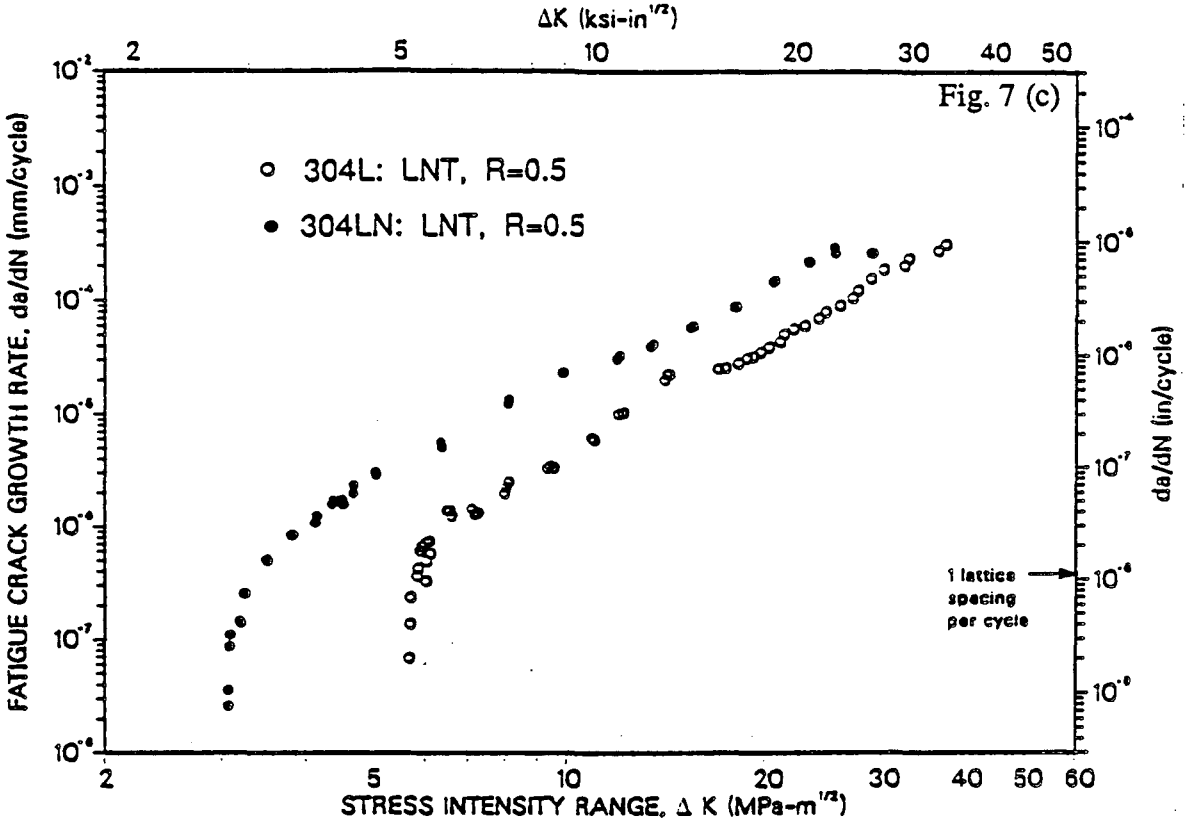

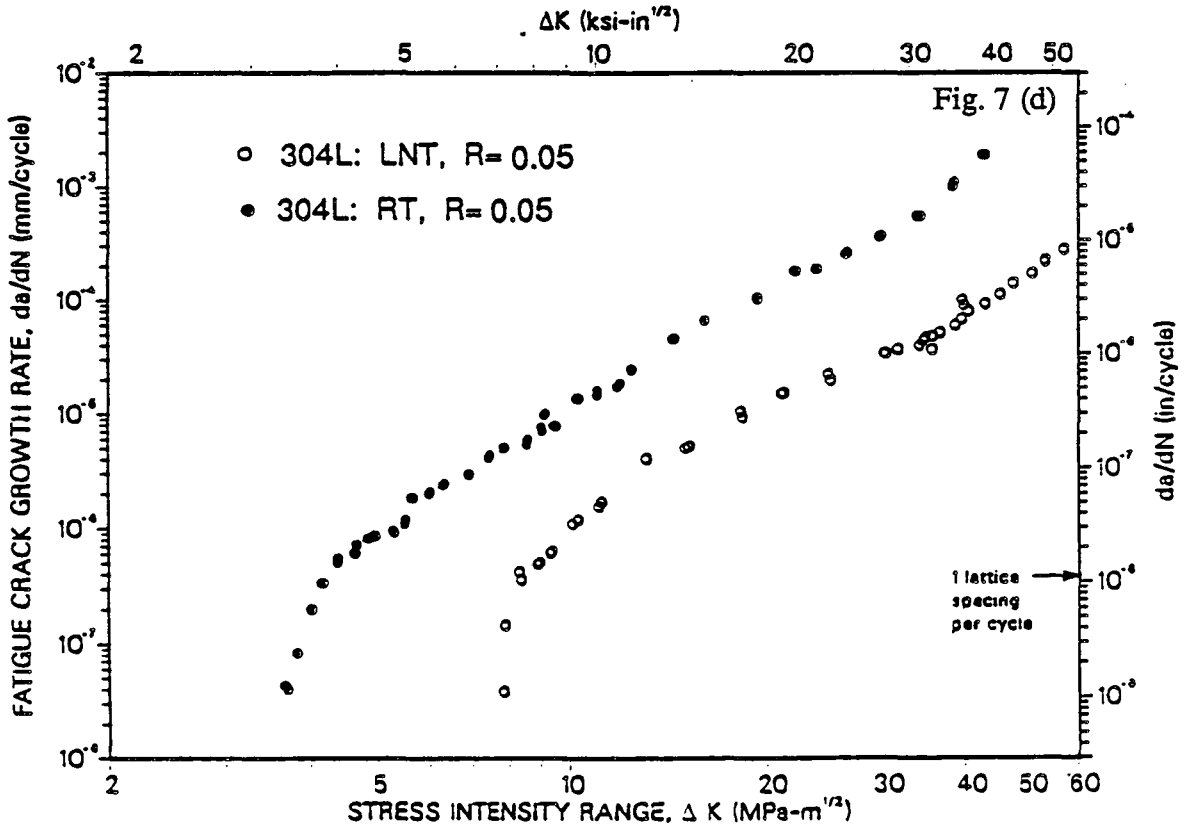

XBL 8811-4046 & XBL 8811-4047

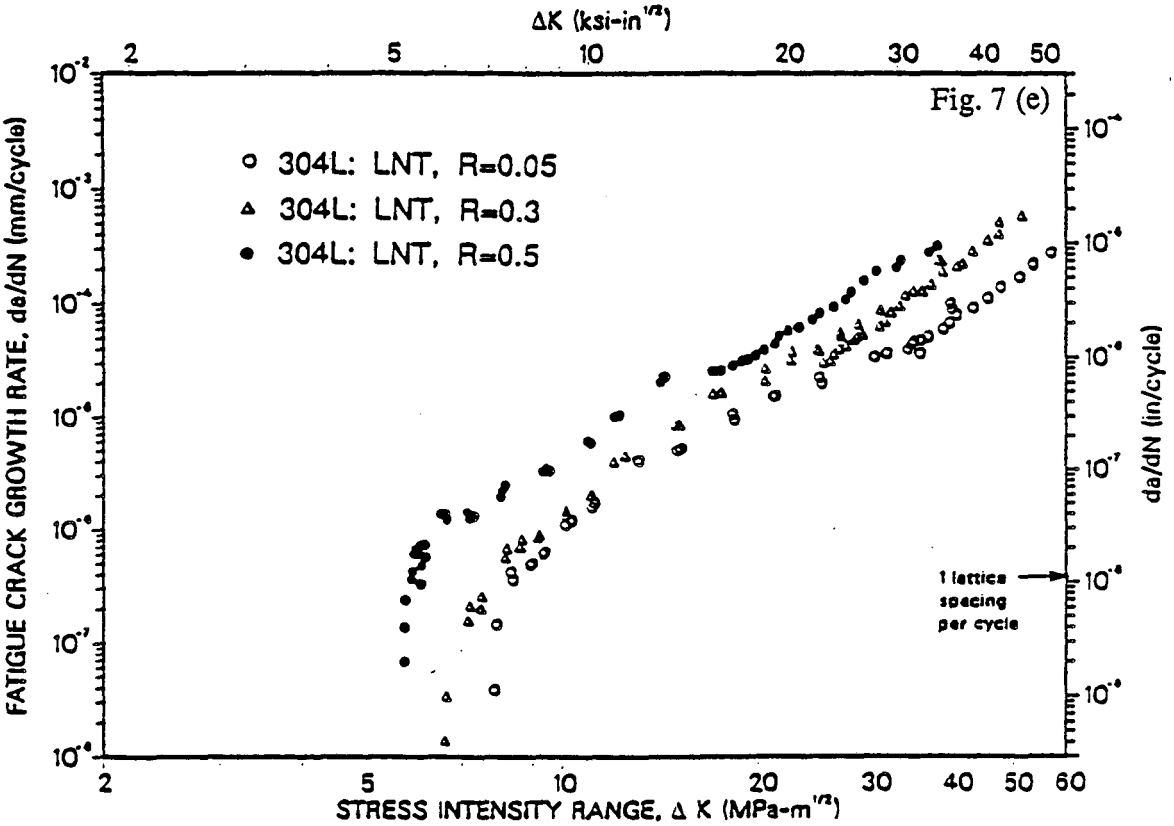

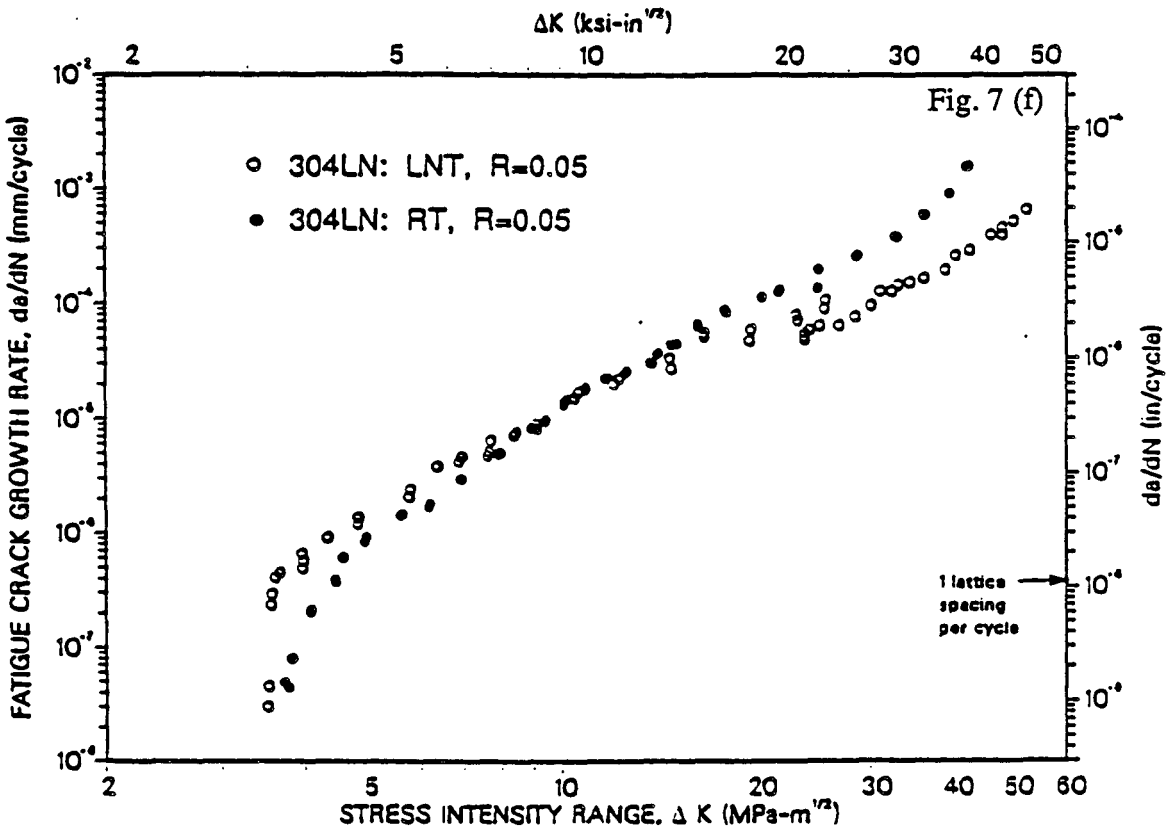

XBL 8811-4048 & XBL 8811-4049

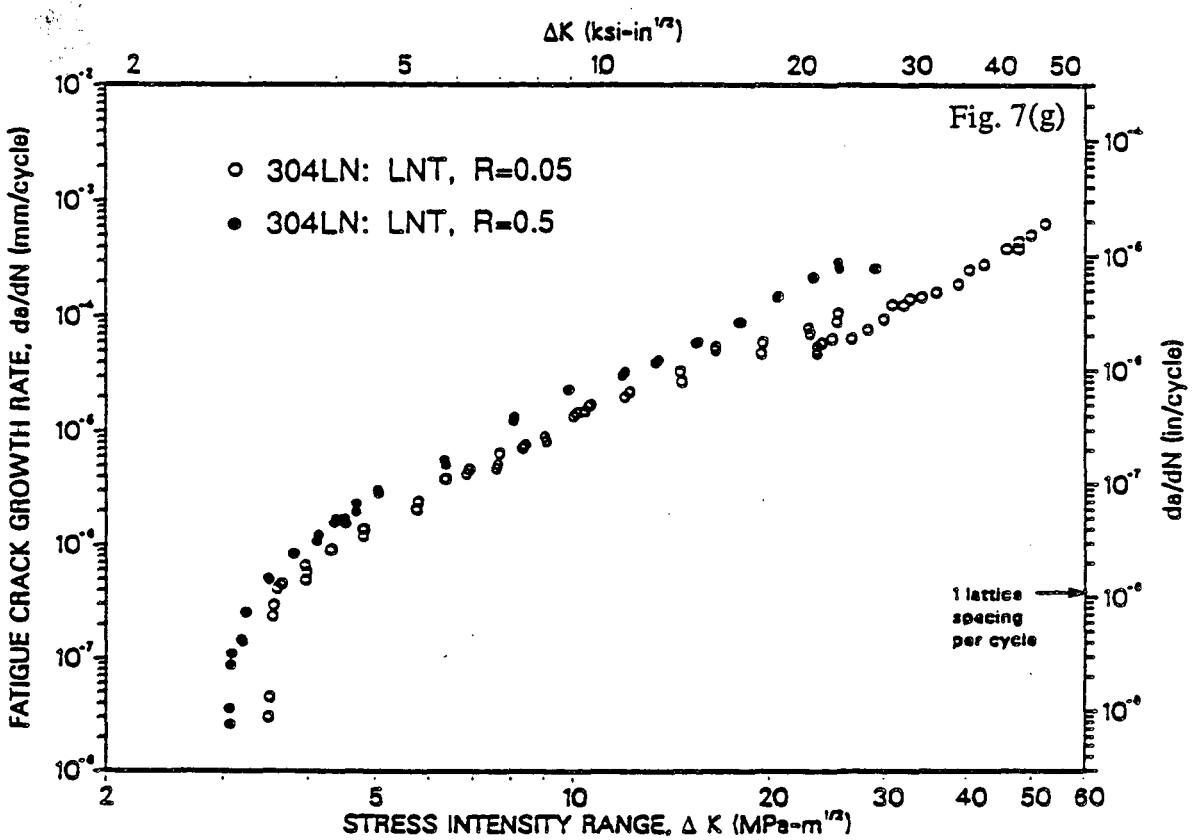

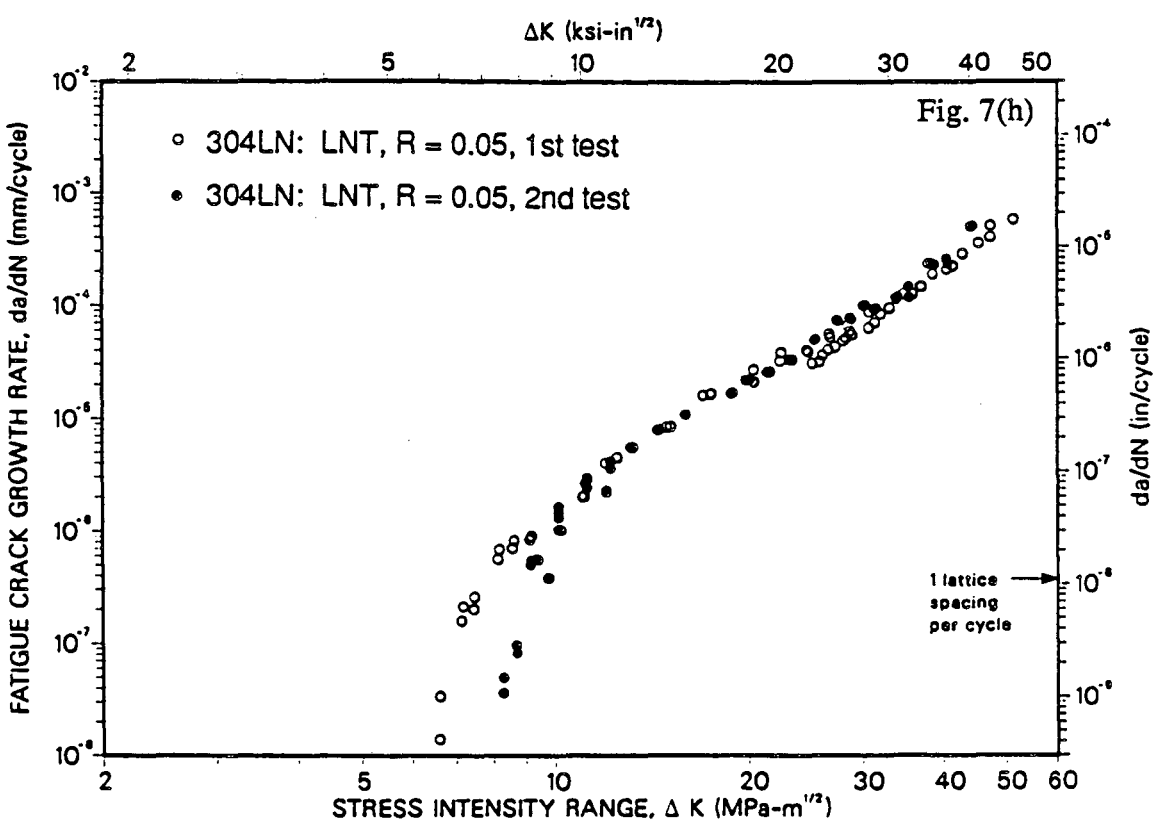

XBL 8811-4050 & XBL 899-3490

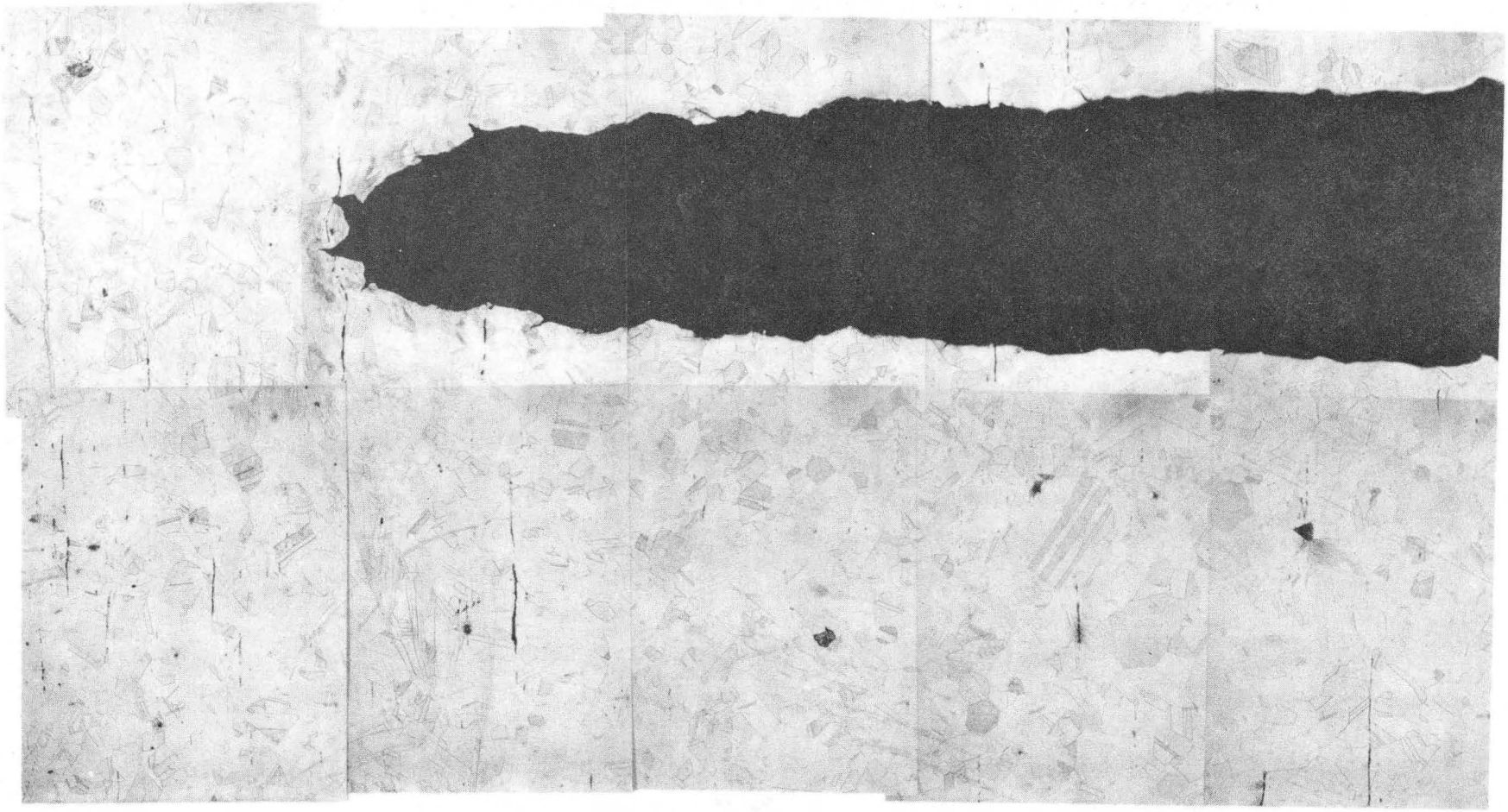

Fig. 8 (a): Optical micrograph of the fatigue crack profile of 304LN tested at 298 K with load-ratio of 0.05.

XBB 879-7964

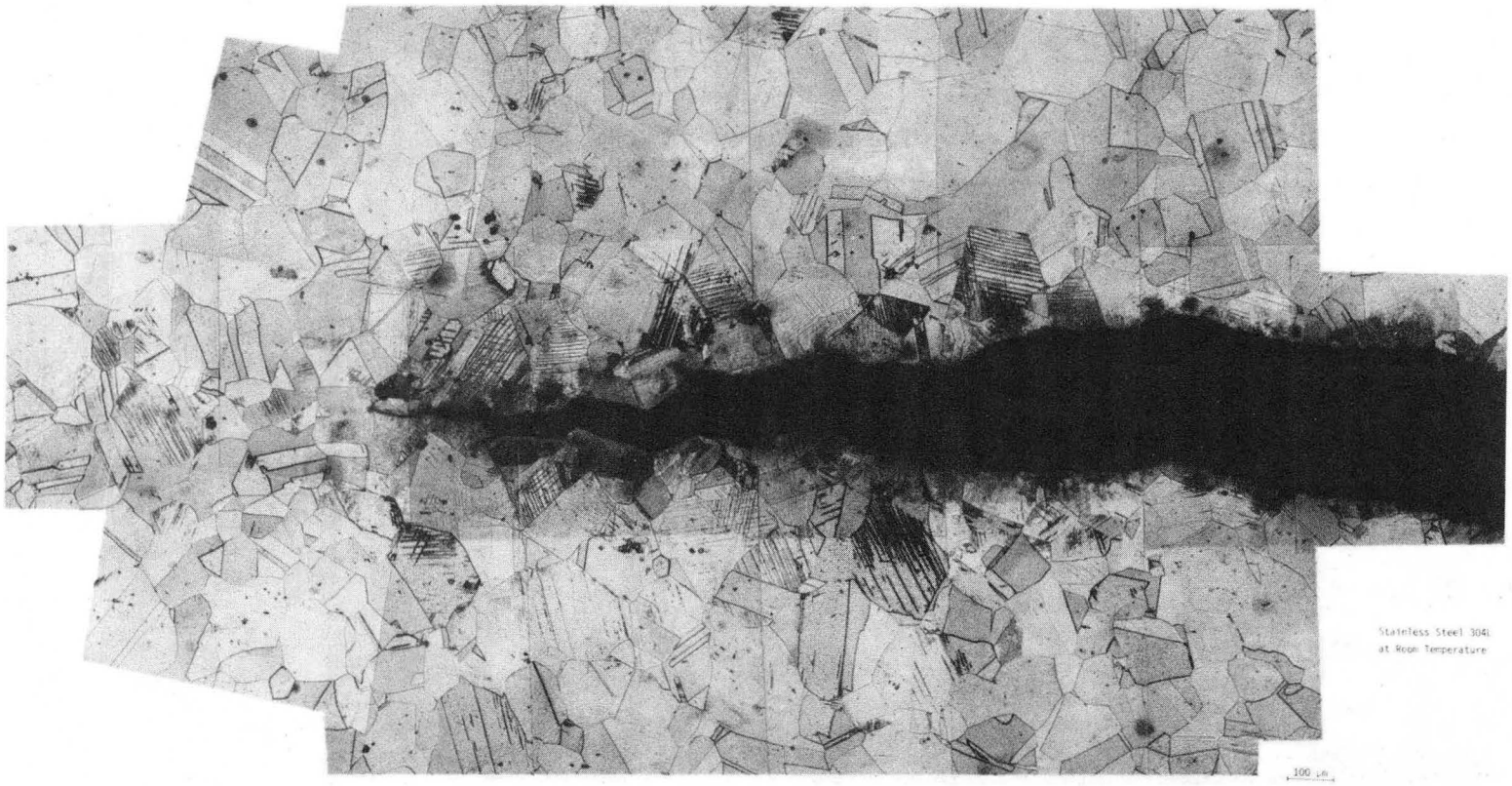

Fig. 8 (b): Optical micrograph of the fatigue crack profile of 304L tested at 298 K with load-ratio of 0.05.

XBB 868-6196

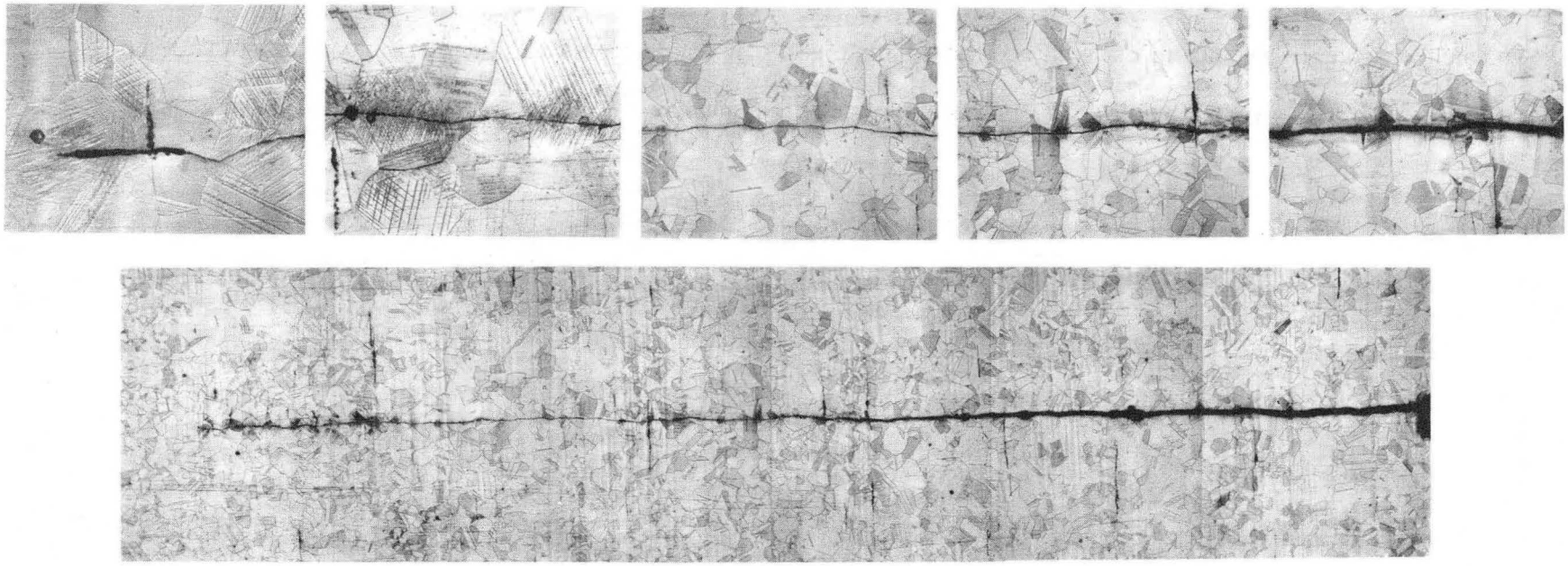

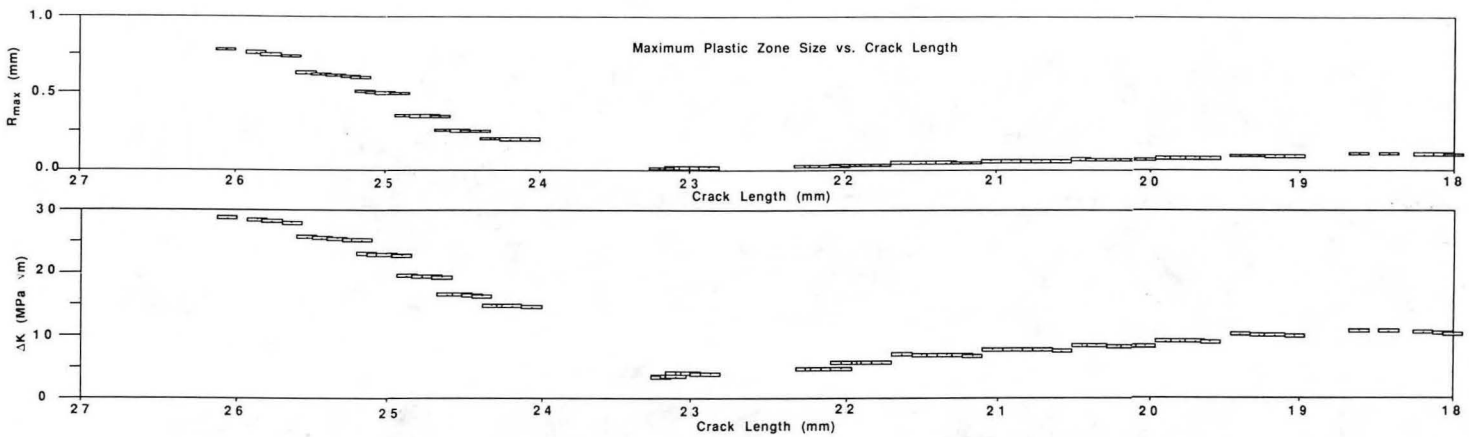

XBB 870-10652

Fig. 8 (c): Optical micrographs of the fatigue crack profile of 304LN tested at 77 K with load-ratio of 0.05, showing the deformation-induced martensite particles. The calculated maximum plastic zone sizes as a function of ΔK are also indicated.

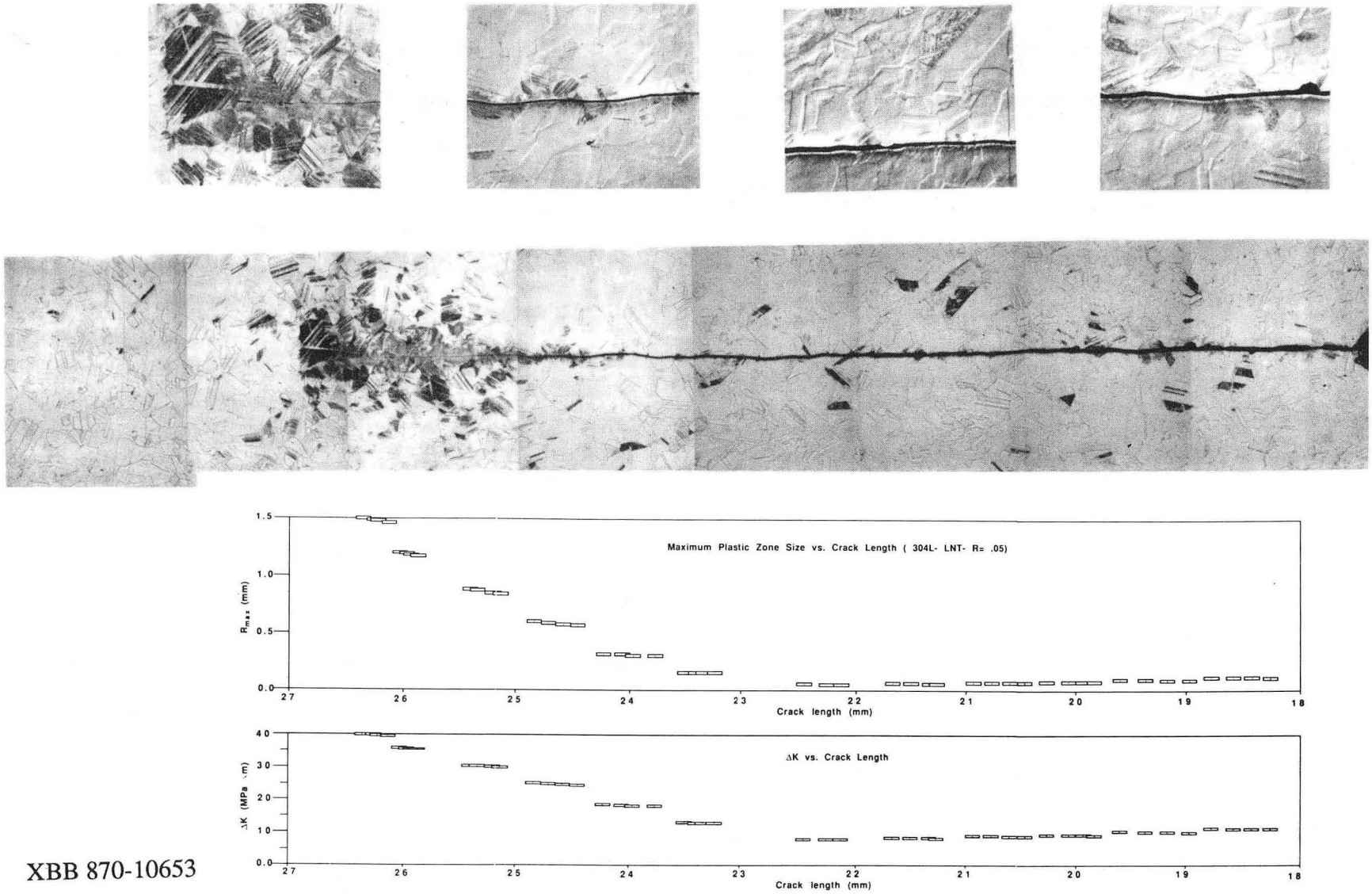

XBB 870-10653

Fig. 8 (d): Optical micrographs of the fatigue crack profile of 304L tested at 77 K with load-ratio of 0.05, showing the deformation-induced martensite particles. The calculated maximum plastic zone sizes as a function of ΔK are also indicated.

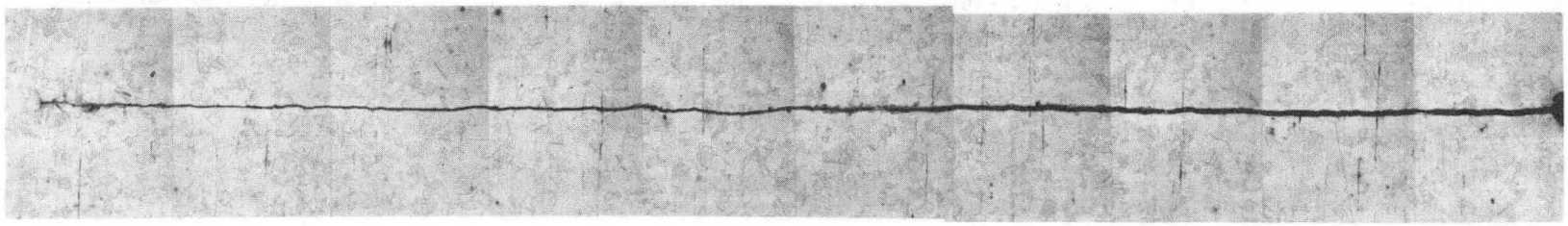

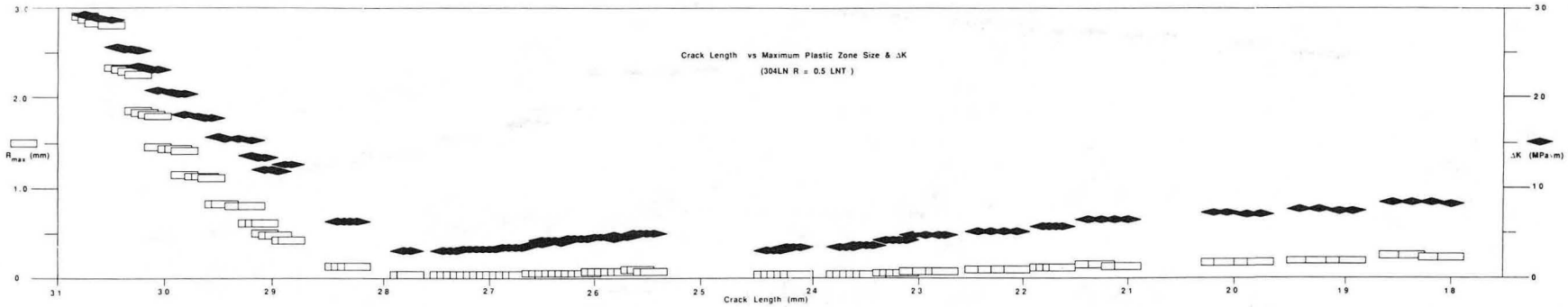

Fig. 8 (e): Optical micrographs of the fatigue crack profile of 304LN tested at 77 K with load-ratio of 0.5, showing the deformation-induced martensite particles.

XBB 870-10649

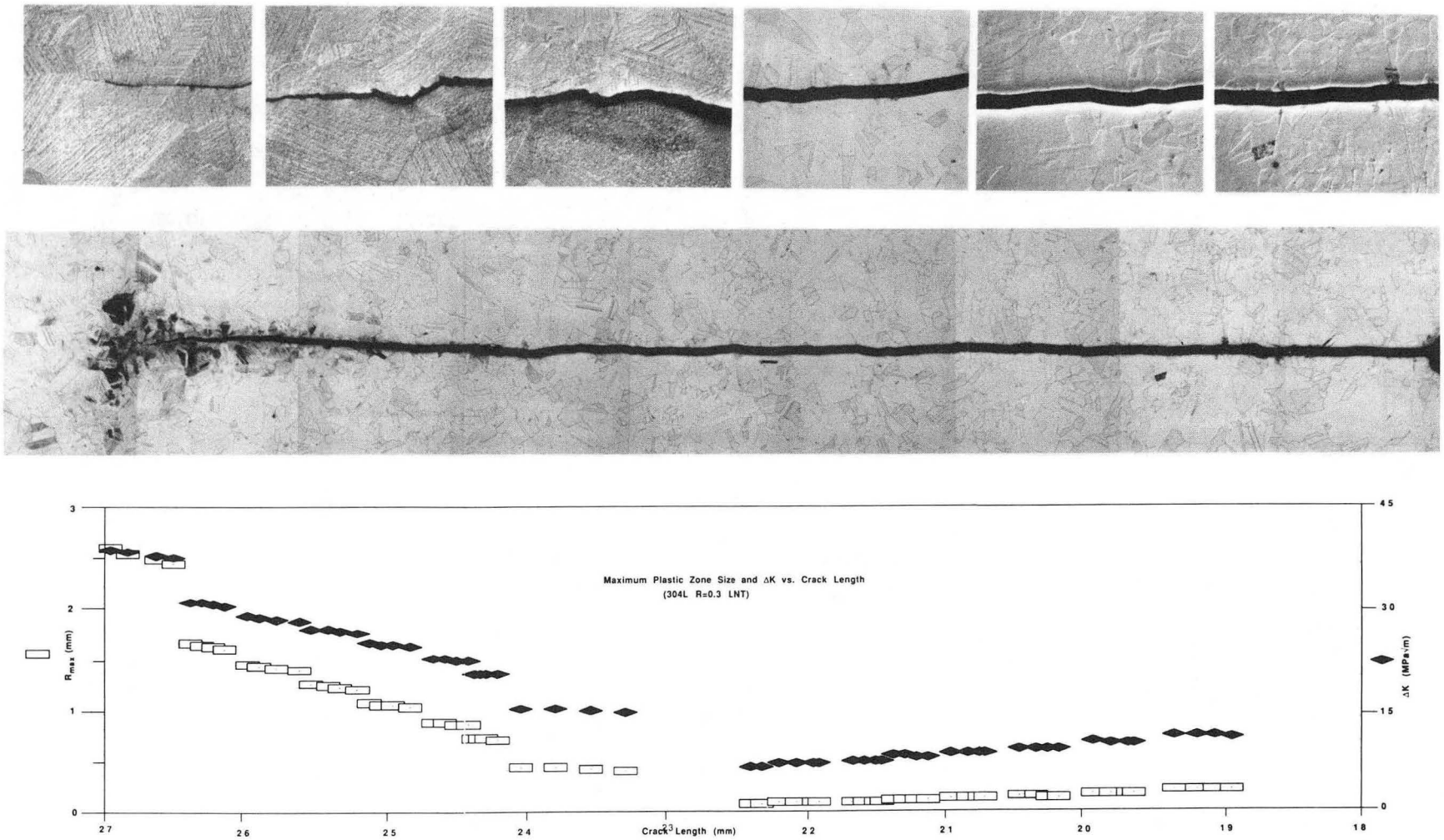

Fig. 8 (f): Optical micrographs of the fatigue crack profile of 304L tested at 77 K with load-ratio of 0.3, showing the deformation-induced martensite particles. The calculated maximum plastic zone sizes as a function of ΔK are also indicated.

XBB 870-10651

Load ratio

The influence of the load ratio on the fatigue crack growth rate at 77 K is illustrated in Figs. 7(f) and 7(g). The plot shows that as the load ratio, R, increases from 0.05 to 0.5 (representing a 1.9 times increase in K_{max} for given ΔK), the fatigue crack growth rate curve shifts sharply to the left for the unstable alloy, 304L, but is essentially unchanged for 304LN except at very high ΔK where some transformation occurs. This result is in agreement with prior work[9] which measured an increase in the fatigue crack growth rate of 304L by a factor of 18 as R increased from 0.1 to 0.75 at 77 K.

An increase in the fatigue crack growth rate with the load ratio is a common phenomenon, but the effect is usually small in the Paris region. Fig. 9 contains a plot of data drawn from the literature on the fatigue crack growth rates of austenitic steels. The fatigue crack growth rate at given R is normalized by dividing it by the growth rate at R = 0.1; the value is approximately the same for all ΔK in the linear, Paris-law region of the da/dN vs. ΔK curve. In all cases the fatigue crack growth rate increases with R, but by an amount that is significantly greater under conditions where the austenite is relatively unstable. These results suggest that the martensitic transformation exaggerates the load ratio effect.

The abnormally large R-ratio effect in metastable austenitic steels is surprising since the extent of the martensitic transformation increases with R at given ΔK. The composition and temperature results suggest that the crack growth rate should <u>decrease</u> with the extent of the martensite transformation. Taken together the results suggest that the reduction in the crack growth rate due to the transformation depends on the load ratio, that is, high tensile mean stress lessens and even eliminates the effect of the transformation. Fig. 10 includes all the crack growth rate data taken in research to date. It shows that as the R-ratio increases the crack growth rate of 304L at 77 K approaches that of 304LN and that of 304L at room temperature where the alloy is stable.

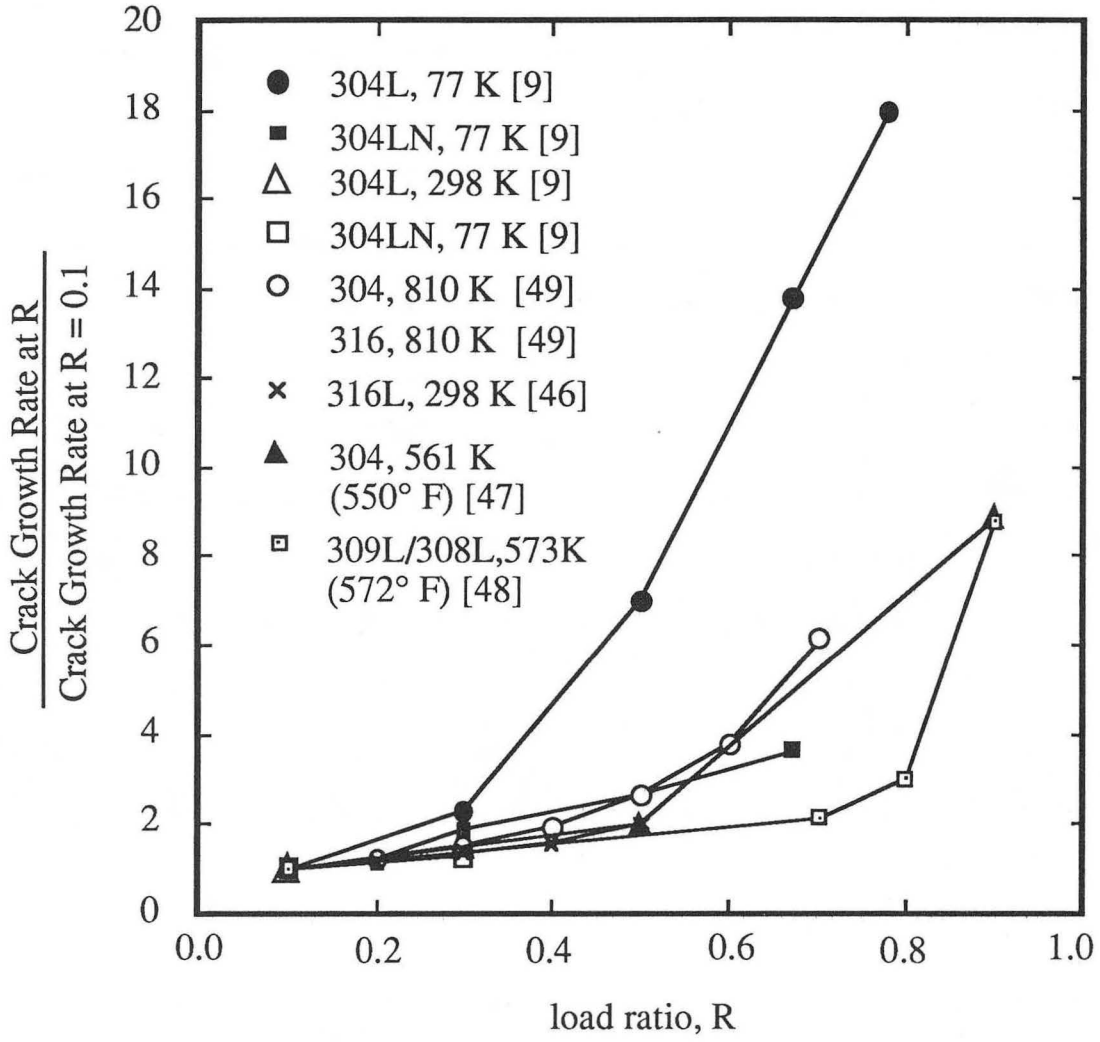

Fig. 9: Plots of the crack growth rates at load ratio R normalized by that at R = 0.1 vs. the load ratio for various austenitic stainless steels at different conditions, showing the abnormally high load ratio effect on crack growth rate for metastable 304L at 77 K.

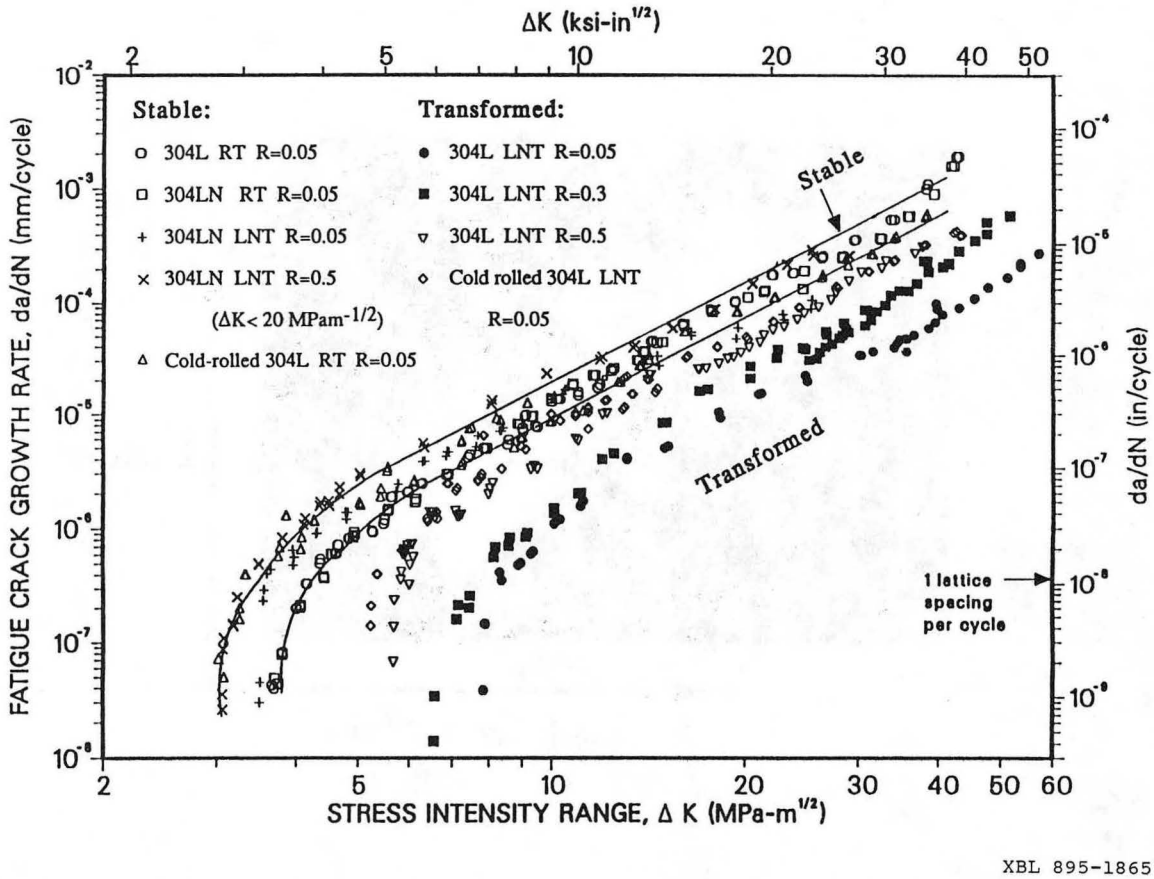

Fig. 10: All fatigue crack growth rate data measured in this research. (XBL 895-1865).

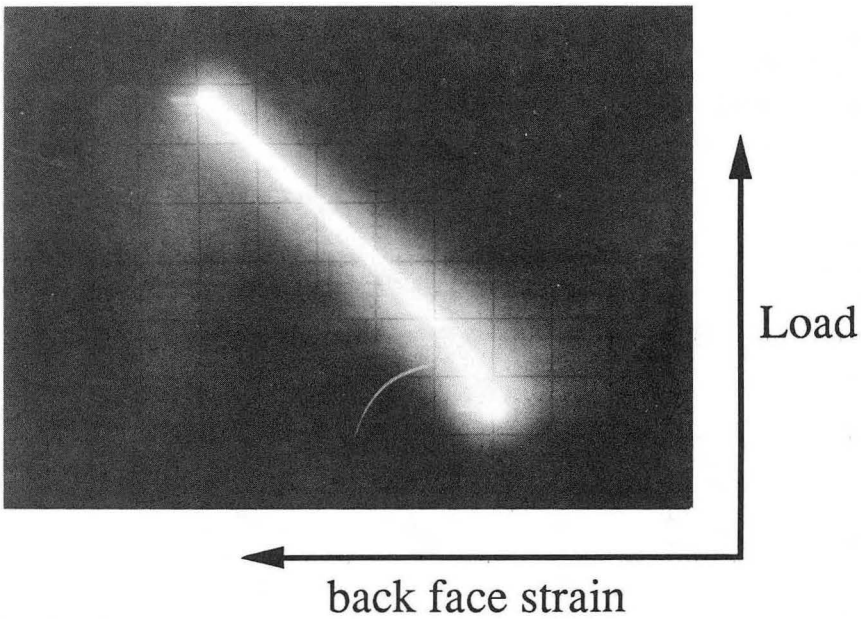

Fig. 11: Picture taken on an oscilloscope, showing the bending of the elastic compliance curve, measured from a back face strain gauge, indicating the crack closure. (XBB 880-9794)

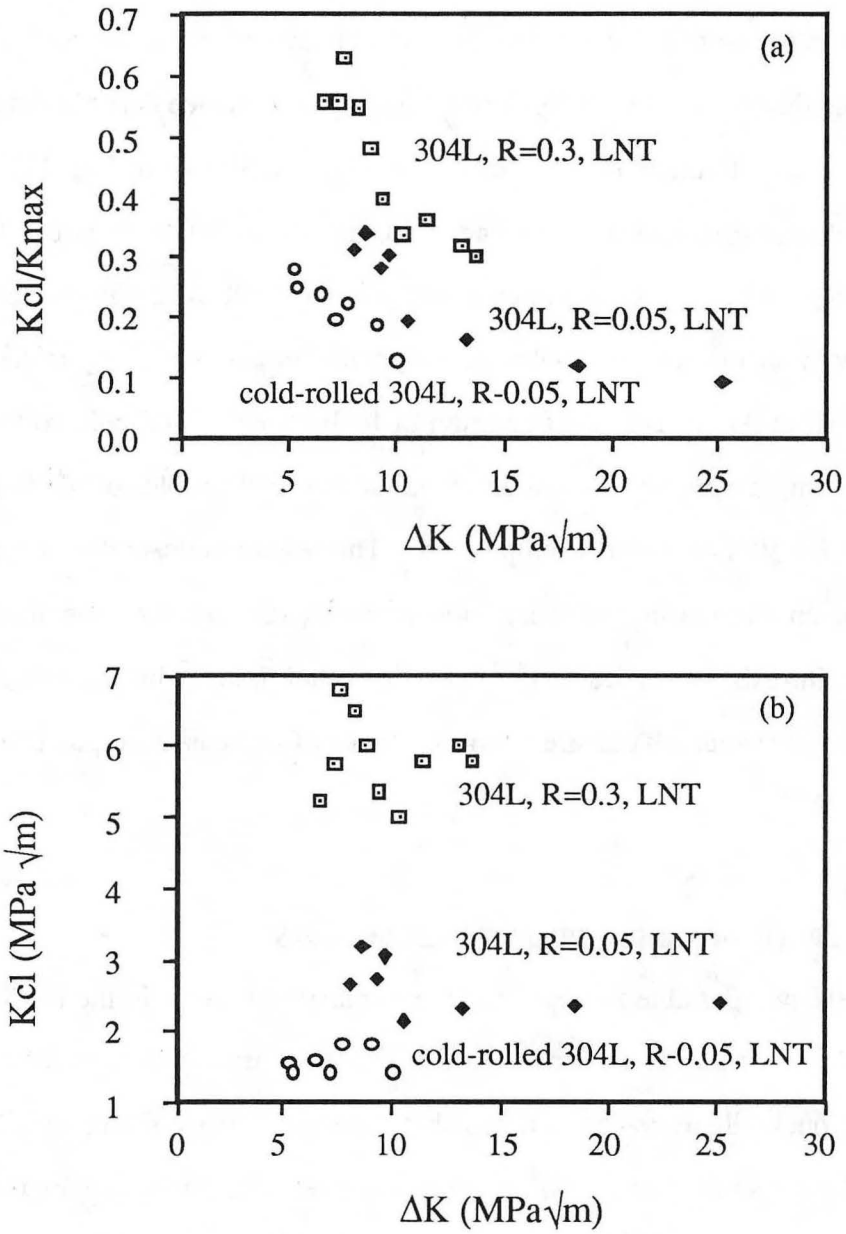

Fig. 12: (a) Stress intensity factor at the crack closure, K_{cl}, normalize by the maximum stress intensity factor, K_{max}, and (b) K_{cl}, as a function of stress intensity factor range.

B. Crack Closure

Crack closure during the fatigue cycle was measured using the back-face strain gauge technique described previously. The unloading compliance curve starts to deviate from linearity when the crack mating surfaces contact, as shown in Fig. 11. The load when the compliance first deviates from linearity is used to calculate the stress intensity at crack closure, K_{cl}. The results are plotted in Fig. 12. Crack closure was only observed in the near-threshold region, and only when the alloy transformed extensively at the crack tip. Closure occurred in the near-threshold region of both annealed and cold-rolled 304L at liquid nitrogen temperature, but was not observed for annealed or cold-rolled 304L at room temperature or for 304LN at either temperature. The results indicate that the martensite transformation on the mating surfaces induces crack closure near the threshold, as discussed by Suresh and Ritchie.[50] On the other hand, the data suggest that transformation-induced crack closure is not the cause of decreased fatigue crack growth rates at higher ΔK.

C. Martensite Transformation around the Fatigue Crack

There are two possible martensitic transformation products in the Fe-Ni-Cr alloy system: the α' (bcc or bct) and ε (hcp) phases. The $\gamma \rightarrow \alpha'$ transformation involves a 2% volume expansion, while the $\gamma \rightarrow \varepsilon$ transformation occurs at nearly constant volume in 304-type alloys. Since both the γ and ε phases are paramagnetic, magnetic etching reveals only the ferromagnetic α' phase. Fig. 13 shows the distribution of α' around a fatigue crack. No evidence of ε-martensite was found in the x-ray diffraction patterns.

To compare the extent of transformation a transformation zone size was arbitrarily defined as the distance from the crack surface at which a 10% martensite transformation occurred. The measurements were made on etched cross-sections, and are hence somewhat imprecise, but do show consistent trends. The data for annealed 304L tested at liquid nitrogen temperature are plotted in Figs. 14 (a) and 14 (b) as functions of ΔK and K_{max},

respectively. Since the transformation is driven by the strain, which varies roughly as $K/\sqrt{r}$ near the crack tip, we had expected that the transformation zone size, δ, would be proportional to K_{max}. Fig. 14(b) shows that this is not the case. Nor is δ a unique function of ΔK. However, the curves in Fig. 14(a) are well fit by an expression of the form

$$\delta = A(\Delta K - C)^2 \tag{4}$$

where A and C are constants whose values change with R (or, equivalently, with K_{max}). Equation (4) implies that there is a threshold value of the cyclic stress intensity for the transformation.

D. Fractography

The fatigue crack is transgranular for all conditions studied, as illustrated by the fatigue crack profiles in Figs. 8(a-f). The fatigue fracture surfaces of 304L (Fig. 15(a)) and 304LN (Fig. 15(b)) tested at 298 K suggest that significant plastic deformation occurs during fracture. On the other hand, the fatigue surfaces of 304LN (Fig. 15(c)) and 304L (Fig. 15(d)) tested at LNT contain flat features that resemble quasi-cleavage. Fig. 15 (g) shows a low magnification optical micrograph of a fatigue fracture surface that was tested half at 298 K and half at 77 K. The part of the surface at 298 K is rough while the part at 77 K is flat, and the grains are visible. The ridges that represent plastic deformation start from the grain boundaries in Fig. 15(d), while the anneal twin boundaries in Fig. 15(e) do not interrupt the ridges. Recalling the shape of the mechanically induced α' shown in Figs. 8(b)-(f), α' features can be identified on the fatigue surfaces in Figs. 15(c and d). Fig. 15(f) shows the form of α' on the fatigue surface of 304L tested at high ΔK and high load ratio where extensive transformation occurs. It is interesting to notice that the α' on the surface appears as if it were deformed in compression, which suggests the possibility of a microscopic crack closure that is not detected by the back-face strain gage technique.

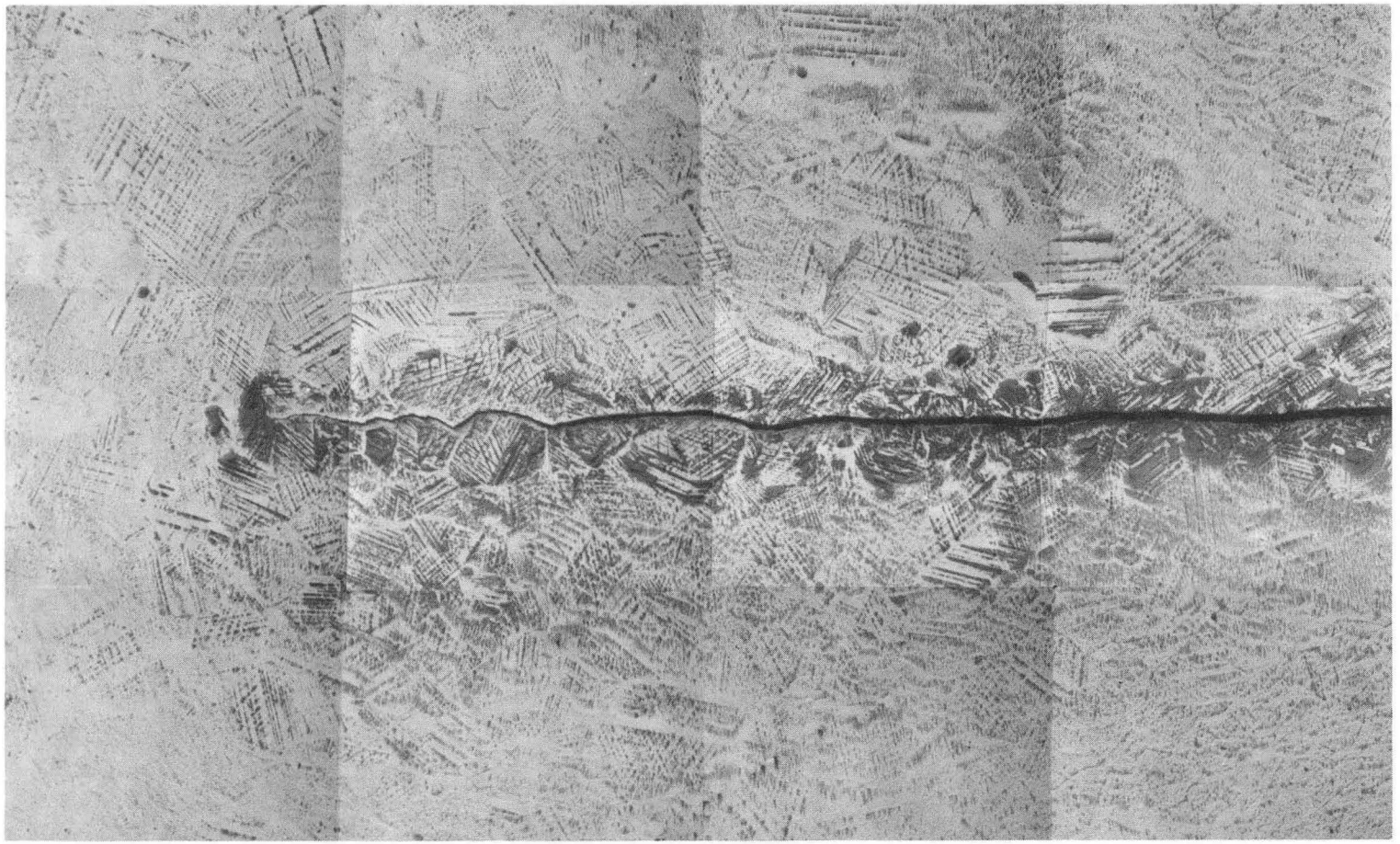

Fig. 13: Optical micrograph of the fatigue crack profile of 304L austenitic stainless steel tested at liquid nitrogen temperature with $\Delta K = 25$ MPa $m^{1/2}$. The sample was covered with a thin layer of ferro-fluid in which 100 Å magnetic particles highlight the magnetic α' martensite. (XBB 884-3426).

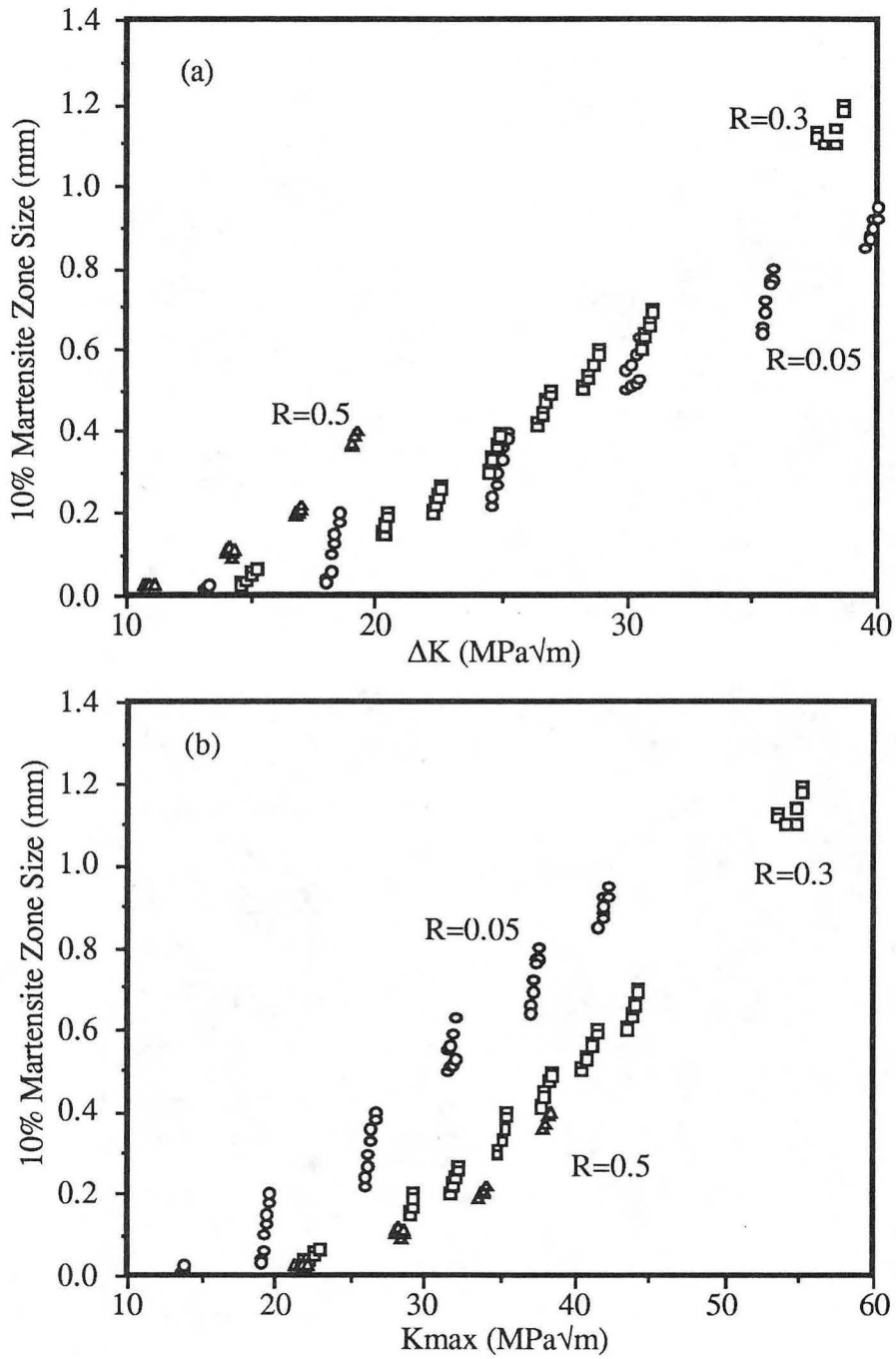

Fig. 14: Martensite zone sizes, determined by metallography, around the fatigue cracks of 304L tested at liquid nitrogen temperature with three load ratios (R) as functions of (a) cyclic intensity factor (ΔK) and (b) maximum stress intensity factor (K_{max}).

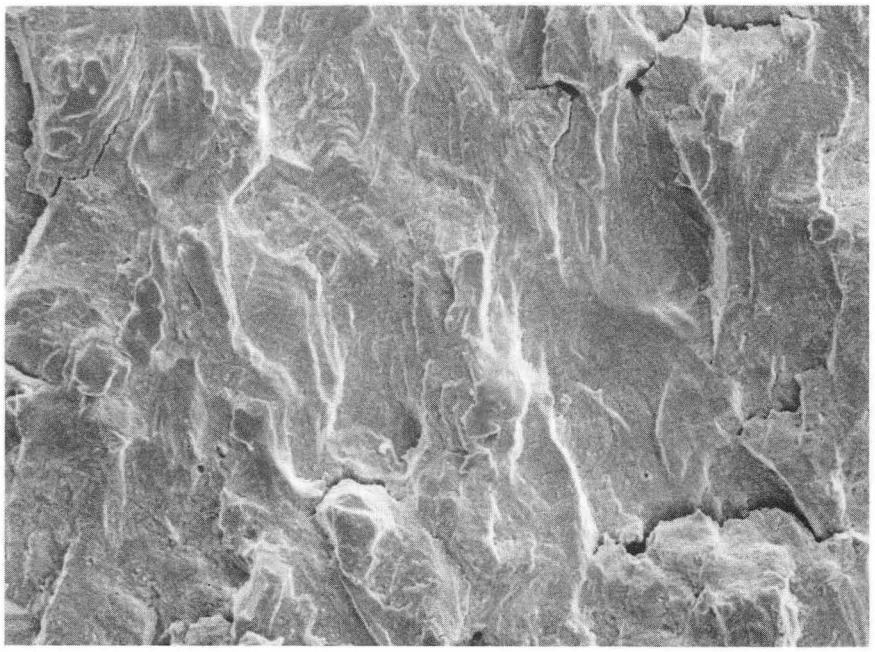

50 μm

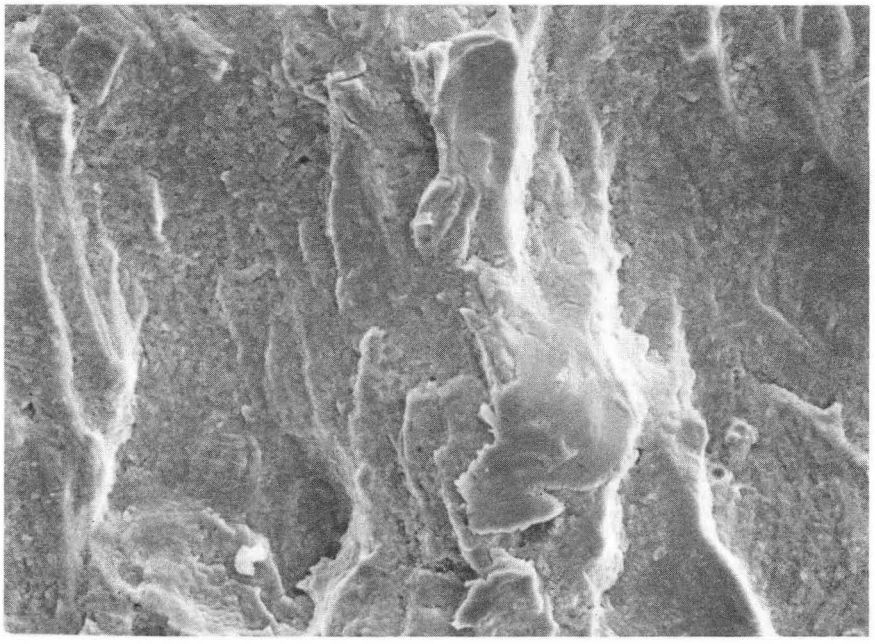

crack propagates

20 um

304LN RT R = 0.05 $\Delta K = 33$ MPa$\sqrt{m}$

Fig. 15 (a): SEM fractographs of 304LN fatigue specimen tested at 298 K with R = 0.05 and $\Delta K \approx 33$ MPa-m$^{1/2}$. XBB 8811-1113

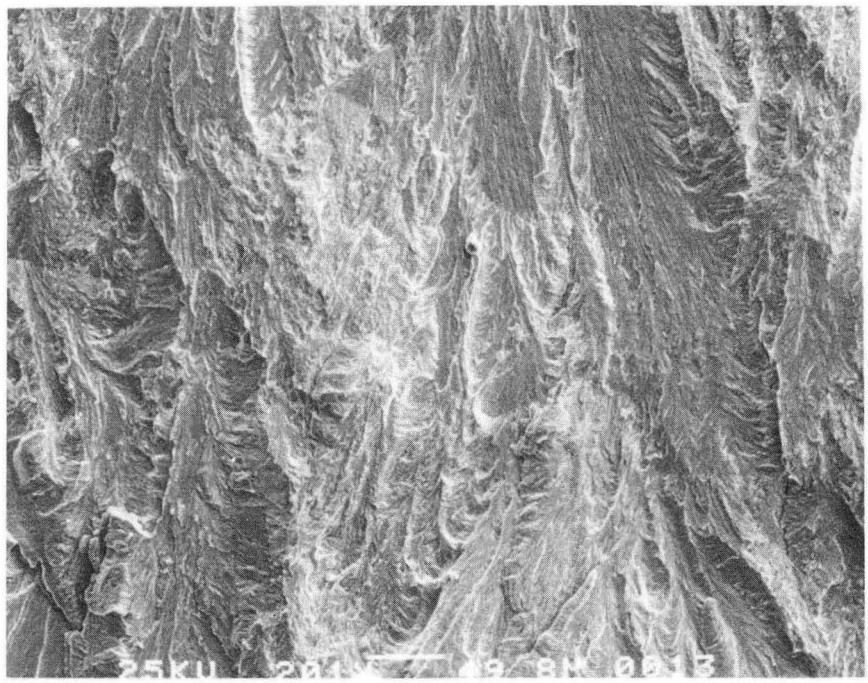

crack propagates

50 um

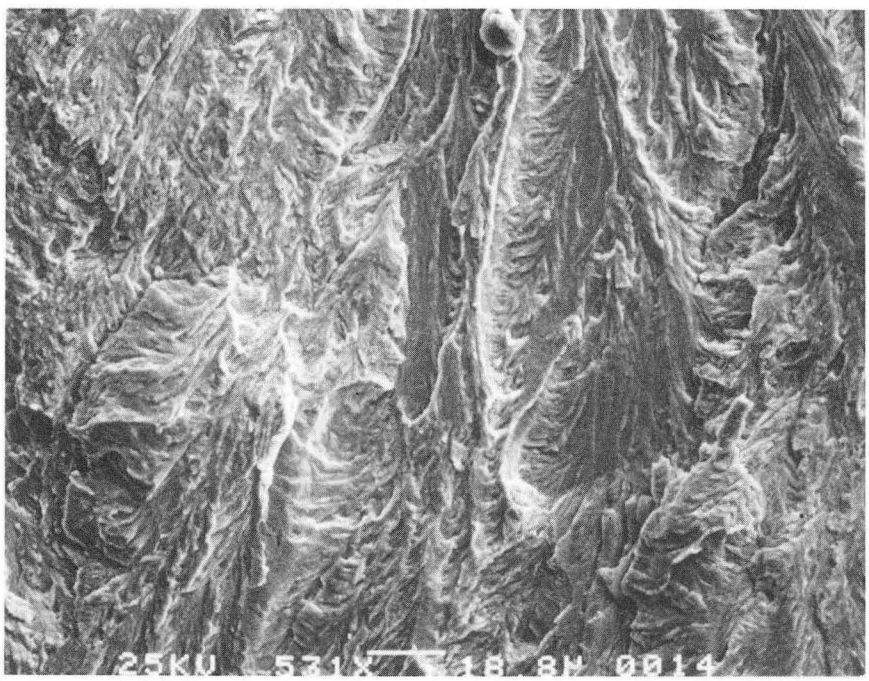

crack propagates

20 um

304L RT R = 0.05 $\Delta K = 20$ MPa$\sqrt{m}$

Fig. 15 (b): SEM fractographs of 304L fatigue specimen tested at 298 K with R = 0.05 and $\Delta K \approx 20$ MPa-m$^{1/2}$. XBB 8811-11108

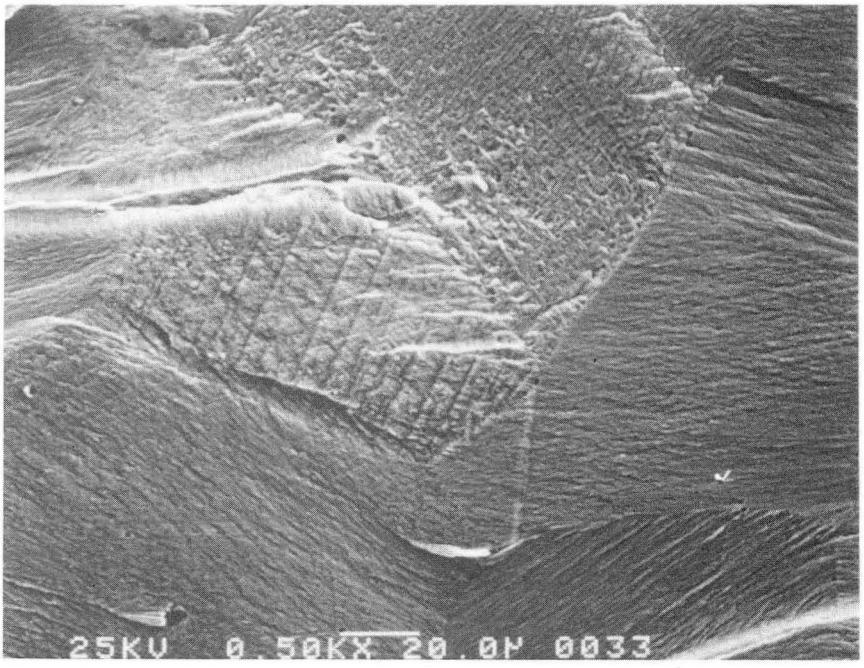

50 µm

crack propagates

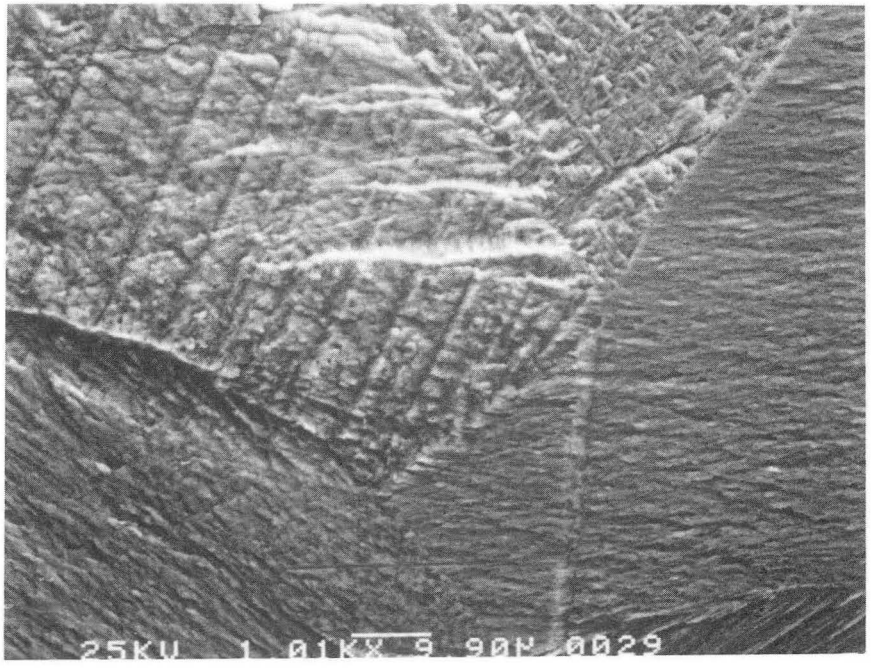

10 µm

Fig. 15 (c): SEM fractographs of 304LN fatigue specimen tested at 77 K with R = 0.05 and $\Delta K \approx 7$ MPa-m$^{1/2}$. XBB 8811-11115

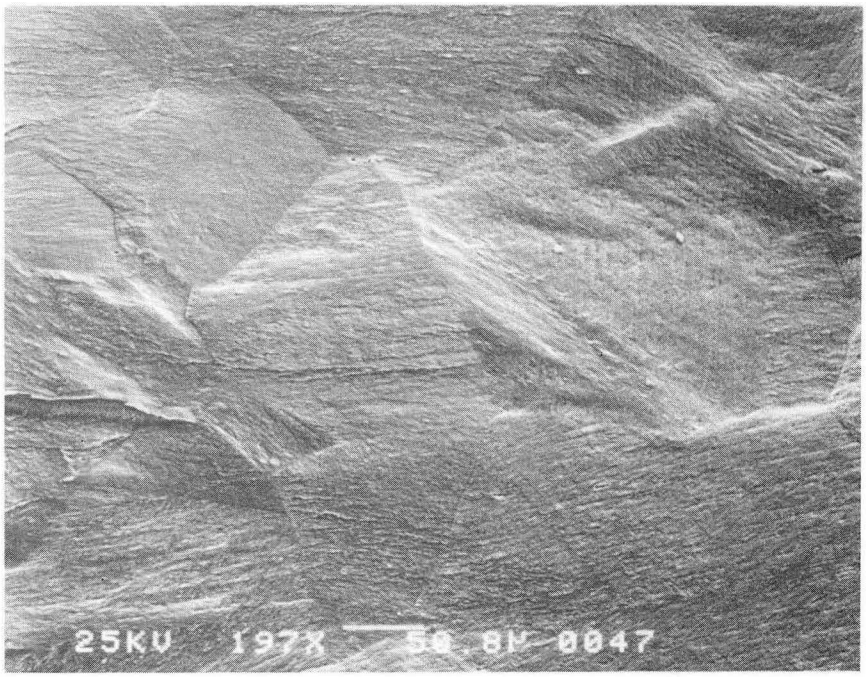

crack propagates

50 µm

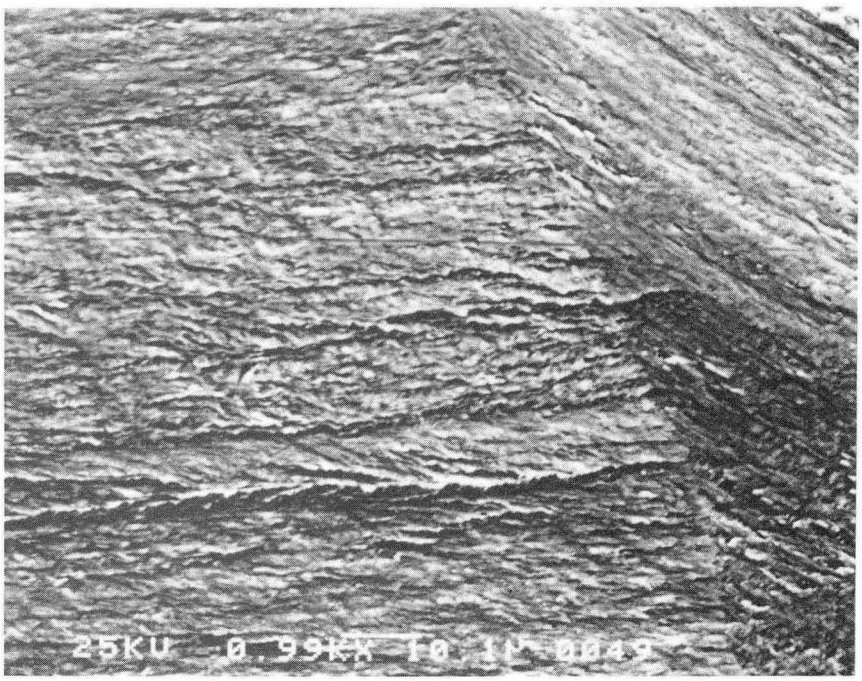

10 µm

Fig. 15 (d): SEM fractographs of 304L fatigue specimen tested at 77 K with R = 0.05 and $\Delta K \approx 8$ MPa-m$^{1/2}$. XBB 8811-11107

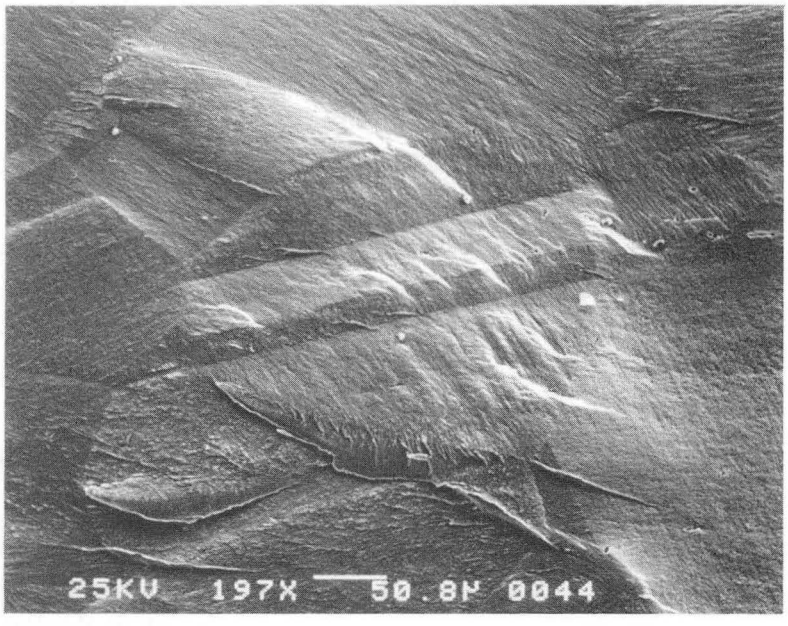

50 µm

crack propagates

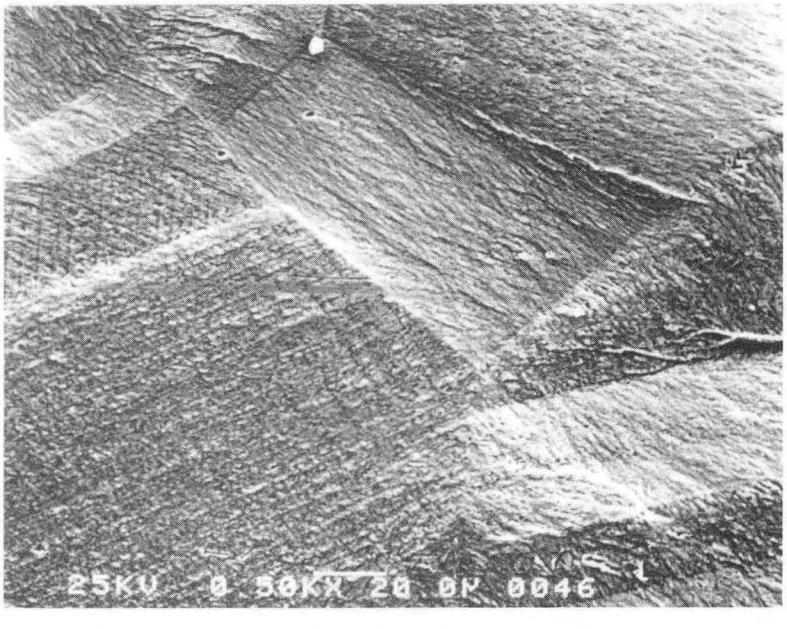

20 µm

Fig. 15 (e): SEM fractographs of 304L fatigue specimen tested at 77 K with R = 0.5 and $\Delta K \approx 6.5$ MPa-m$^{1/2}$. XBB 8811-11109

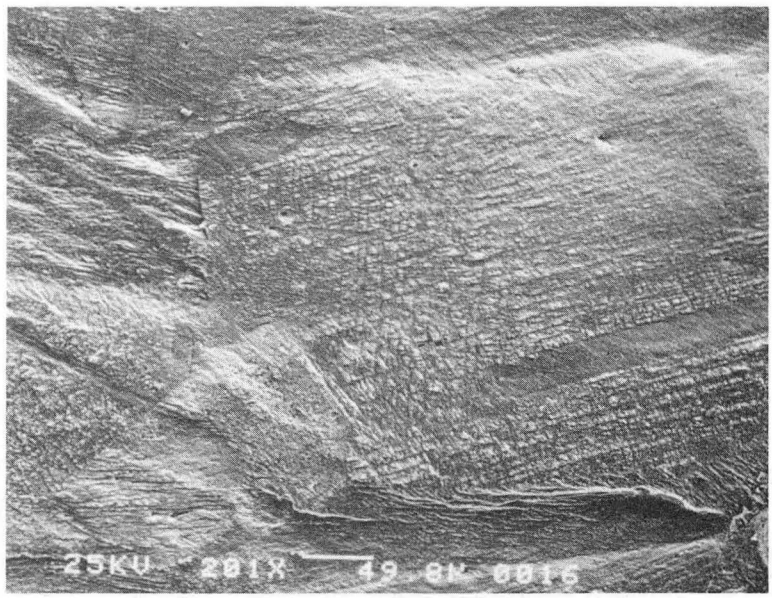

crack propagates

50 μm

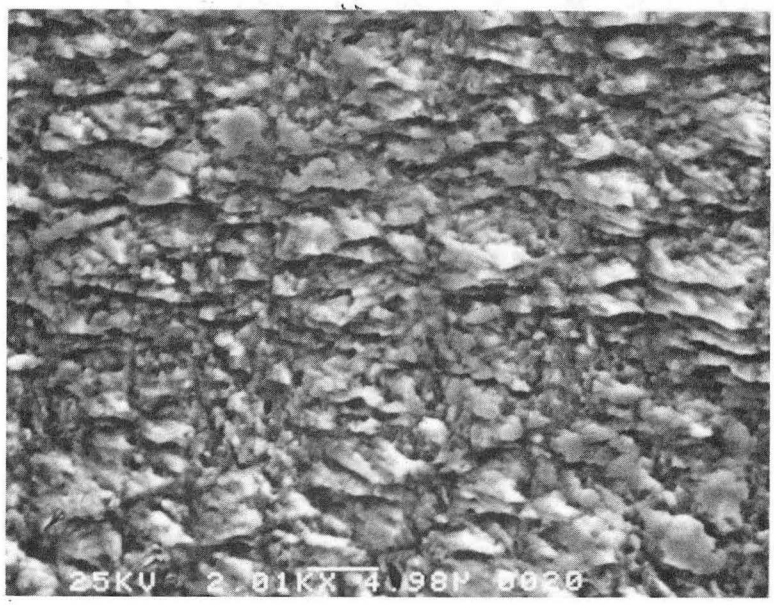

5 μm

Fig. 15 (f): SEM fractographs of 304L fatigue specimen tested at 77 K with R = 0.5 and $\Delta K \approx 18$ MPa-m$^{1/2}$. XBB 8811-11117

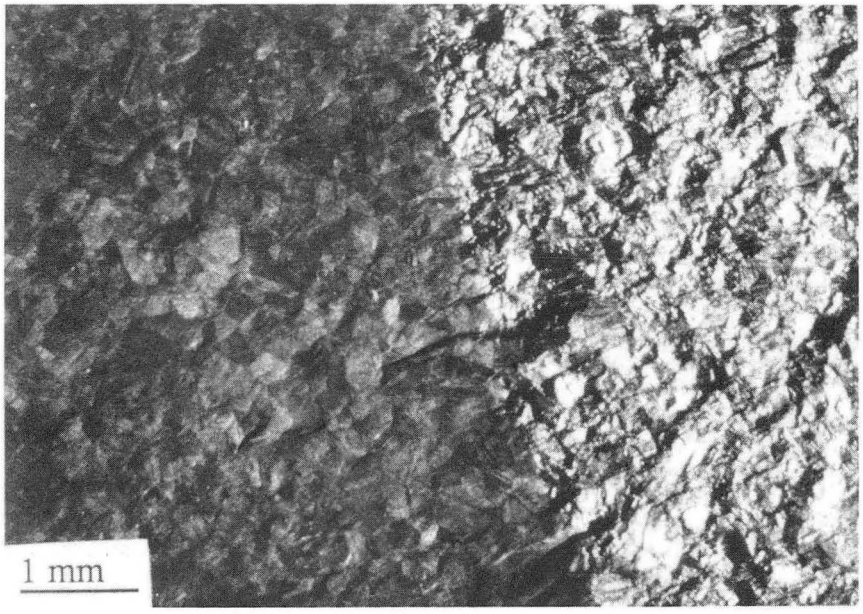

77 K 298 K

XBB 896-5047

Fig. 15 (g): Low magnification optical micrograph of a 304L specimen that was tested half at 298 K and half at 77 K.

IV. DISCUSSION

Fig. 10 includes all the fatigue crack propagation test data. Two conclusions can be drawn. First, the deformation induced martensitic transformation increases fatigue crack growth resistance. The threshold stress intensity increases and the fatigue crack growth rate decreases for all ΔK. Second, the beneficial effect of the transformation decreases as the load ratio increases.

A number of mechanisms have been proposed that may contribute to the influence of the martensite transformation on the crack growth. These include the effect of the volume or shear strain associated with the transformation at the crack tip, the influence of the transformation and the resulting dual-phase microstructure on the crack path, the influence of the transformation on the aggregate mechanical properties of the material at the crack tip, and the influence of the transformation on the fracture mode. We discuss the available models that represent these effects in turn. Among these mechanisms, the effect of the transformation strain appears to be the most important.

A. Influence of the Martensite Transformation on the Crack Tip Stress Field

The most obvious mechanism that influences crack growth in metastable austenitic steels is the perturbation of the crack tip stress field by the strain associated with the transformation. The $\gamma \rightarrow \alpha'$ transformation in 304-type steels involves both a ~2% volume expansion[31-33] and a ~10% shear strain.[33] The influence of the volume expansion is the simpler to treat, and is analyzed in recent works by McMeeking and Evans,[51] and Budiansky, et al..[52,53] The influence of the shear component is much more difficult to analyze. The beginnings of a quantitative analysis appears in recent work by Lambropoulos.[54] These analytic results were used to quantitatively explain the

phenomenon of "transformation toughening" in ceramic materials. Reference [55] provides a good review on this subject.

Volume Expansion

The constraint of the surrounding elastic material on a dilatant transformed region places that region under compression. If a volume of material that is subjected to a remote cyclic tensile load of amplitude (P_{max} - P_{min}) undergoes transformation, both P_{max} and P_{min} are reduced by the associated compressive stress. If P_{min} is large and tensile, the compressive stress does not change the amplitude of the tensile cycle because both P_{max} and P_{min} are reduced by the same amount, but the load ratio changes from (P_{min} / P_{max}) to ([P_{min} - Δ] / [P_{max} - Δ]), where Δ is the reduction of the tension load by the compressive stress. If P_{min} is a small positive number, it may be reduced to a negative value, the amplitude of the tensile cycle is then (P_{max} - Δ), and the load ratio is zero. Since the crack growth rate depends primarily on the amplitude of the tensile cycle and secondarily on the load ratio, the reduction of the amplitude and load ratio by the compressive stress slows the rate of crack propagation. This effect is qualitatively capable of explaining the influence of the transformation on the crack growth rate: the compressive stress reduces the crack growth rate, but the effect is less pronounced as the load ratio increases since a higher load ratio means a higher value of P_{min} and a smaller effect on the amplitude of the tensile cycle.

The influence of the volume expansion on the stress field and stress intensity factor are analyzed below in an attempt to quantify its influence on the fatigue crack growth rate. To do this we must modify previous analyses of the effect.[51,52]

<u>The Stress Field</u>. Let a dilatant cylindrical martensite particle be inserted into an infinitely large elastic body. The stress field outside the cylinder can be calculated by modifying the Lamé solution for a thick-walled tube subjected to an internal pressure,[56]

$$\sigma_{rr} = -P\frac{(R_o/r)^2-1}{(R_o/R_i)^2-1}, \quad \sigma_{\theta\theta} = P\frac{(R_o/r)^2+1}{(R_o/R_i)^2-1}, \quad \sigma_{r\theta} = 0\,. \tag{5}$$

If we let R_o / R_i (the ratio of the outside radius to the inside radius) tend to infinity and use L' Hospital's rule, then the two-dimensional stress field outside the particle is

$$\sigma_{rr} = -P\left[\frac{R_i}{r}\right]^2 \qquad \sigma_{\theta\theta} = P\left[\frac{R_i}{r}\right]^2. \tag{6}$$

The stress field inside the cylinder is constant and hydrostatic

$$\sigma_{rr} = \sigma_{\theta\theta} = -P = -\alpha B\varepsilon^T, \tag{7}$$

where ε^T is the volumetric strain of the martensitic transformation, B is the bulk elastic modulus of the martensitic particle, and α is a parameter, $0 \le \alpha \le 1$, whose value depends on the relative stiffness of the particle and the matrix. If the matrix is much more stiffer than the martensite particle, $\alpha \approx 1$, in the other extreme, $\alpha \approx 0$.

If such a cylindrical martensite particle forms directly in front of a growing crack the driving force for the crack extension is the opening stress, $\sigma_{\theta\theta}$. It follows from equations (6,7) that as the crack approaches the particle it is subject to a tensile stress that varies as r^{-2} and adds to the cyclic stress at the crack tip due to the macroscopic load. The crack does not experience the compressive field of the martensite transformation until it actually penetrates the particle.

<u>The Stress Intensity Factor</u>. The stress field at the tip of a crack in a body under an external tensile load is characterized by the mode I stress intensity factor, K_I. The transformation stress, $\sigma_{\theta\theta}$, changes K_I. The amount of the change, ΔK_I, can be found by calculating the stress intensity factor due to $\sigma_{\theta\theta}$ alone and applying the superposition principle. Given the stress field, $\sigma_{\theta\theta}[r,\theta]$, ΔK_I can be found, as proposed in reference

[57], by evaluating an integral of the K_I solution for a pair of concentrated splitting forces on the crack surface. However, the shape of the transformed zone in front of the crack is not simple, and the stress field is difficult to find.

An alternative method for finding ΔK_I was recently proposed by McMeeking and Evans,[52] who used the Eshelby cycle[58] to find the transformation stress and employed a weight function method[56,58] to evaluate the change in stress intensity. In the Eshelby method the stress and strain fields introduced by a dilatation of magnitude, ε^T, are calculated by summing the fields introduced in a sequence of steps that lead to the final state of the elastic inclusion. A region of the material is cut out and removed from the matrix, then given a volumetric strain, $\boldsymbol{\varepsilon}^T$. This strain is reversed by imposing a surface traction, $\mathbf{T}_c(r,\theta) = -\,\mathbf{n}(r,\theta)\mathbf{C}\boldsymbol{\varepsilon}^T$, where $\mathbf{C}$ is the elastic matrix of the martensite product and $\mathbf{n}(r,\theta)$ is the outward surface normal. The transformed material is then put back to the matrix and rewelded. Since the material inside the transformed region is under the stress, $-\,\mathbf{C}\mathbf{e}^T$, it relaxes against the unstressed matrix. The relaxation is accomplished by applying a traction $\mathbf{T}(r,\theta) = -\,\mathbf{T}_c(r,\theta)$ to the boundary of the particle, since the interface has no traction in its final state. The stress intensity factor generated by the transformation is, hence, equivalent to that generated by a traction, $\mathbf{T}(r,\theta)$, on the boundary of the transformed region. Using the weight function method, the stress intensity factor can be calculated by evaluating the line integral of the scalar product of $\mathbf{T}(r,\theta)$ and the vectorial weight function $\mathbf{h}(r,\theta)$ along the transformed region boundary, S,

$$\Delta K_I = \int_S \mathbf{T}(r,\theta)\cdot\mathbf{h}(r,\theta)\, dl\,. \tag{8}$$

The weight function, $\mathbf{h}(r,\theta)$, is a measure of the contribution of a unit traction at (r,θ) to the stress intensity factor of an elastic crack. If the $\gamma \rightarrow \alpha'$ transformation is a pure

volume expansion, $\mathbf{T}(r,\theta)$ is equal to $[\mathbf{n}(r,\theta)B\varepsilon^T]$. The solution of $\mathbf{h}(r,\theta)$ for a two dimensional infinite solid with a half plane crack was provided in ref. [59],

$$h_x = \frac{1}{2\sqrt{2\pi r}(1-\nu)} \cos\left[\frac{\theta}{2}(2\nu - 1 + \sin\frac{\theta}{2}\sin\frac{3\theta}{2})\right], \tag{9}$$

$$h_y = \frac{1}{2\sqrt{2\pi r}(1-\nu)} \sin\left[\frac{\theta}{2}(2 - 2\nu - \cos\frac{\theta}{2}\cos\frac{3\theta}{2})\right], \tag{10}$$

where ν is Poisson's ratio. The boundary S varies as the crack extends since fresh material is transformed in the propagating crack tip stress field. Evans and McMeeking assumed that the transformation is driven by the hydrostatic stress, and, hence, that the boundary of the transformed zone is a contour of constant pressure:

$$r = \frac{8w}{3\sqrt{3}} \cos^2(\frac{\theta}{2}), \tag{11}$$

where w is a measure of the width of the contour, taken to be one-half the zone width. Their result for ΔK_I is plotted along with the computed zone shape in Figs. 16 (a,b); the stress intensity factor is reduced by an amount, $-\Delta K_I$, that is zero prior to crack extension, then increases and saturates as the crack enters into the zone. Its asymptotic value is

$$\Delta K_I = -\,0.22\left[\frac{E}{1-\nu}\right]V_f\sqrt{w}\varepsilon^T = -0.33\ P\sqrt{w}, \tag{12}$$

where V_f is the fraction of martensite in the zone, E is Young's modulus, ν is Poisson's ratio (approximated as 1/3), and P is the transformation pressure, equal to $BV_f\varepsilon^T$, where B is the bulk modulus..

While equation (12) has apparently been used with some success to treat transformation toughening in ceramics, specific calculation shows that the magnitude of ΔK_I is too small to account for the effects observed in the present work. We therefore modified the Evans-McMeeking solution in two respects that are indicated by the detailed state of the material at the growing crack tip.

1. *Zone Shape.* The martensite zone shape assumed by Evans and McMeeking is determined by a contour of constant hydrostatic stress. However, the $\gamma \rightarrow \alpha'$ transformation in 304 stainless steels involves a greater shear strain (~10% [33]) than volume expansion (~2% [31-33]) and should hence be more strongly affected by the local shear stress. This is true even when the overall transformation stress is nearly hydrostatic; the formation of a sheared martensite plate promotes the local formation of others in twinned orientation that tend to cancel the overall shear. Nonetheless it seems reasonable to assume that the initial transformation, which triggers the process, is determined more by the local shear than by the local hydrostatic stress. This phenomenon is strikingly evident in computer simulations of the stress-induced martensite transformation,[60] and is consistent with observations of the martensite zone shape in this and other work [26,28] which show transformation zones that follow shear stress contours much more closely that hydrostatic stress contours. Figs. 17 (a,b) show two examples, one is the zone induced by the cyclic loading[26], the other one is the zone induced by the static loading.[60]

Using the Von Mises measure of shear stress for the plane strain condition,

$$\bar{\tau} = \sqrt{\frac{1}{2}[(\sigma_{xx}-\sigma_{yy})^2+(\sigma_{yy}-\sigma_{zz})^2+(\sigma_{xx}-\sigma_{zz})^2+6\tau_{xy}]}\,. \tag{13}$$

A contour of constant equivalent shear is specified by the relation,

$$r = wc(v)\cos^2\left(\frac{\theta}{2}\right)\left[3\sin^2\left(\frac{\theta}{2}\right)+(1-2v)^2\right] \tag{14}$$

where c(v) is a factor that fixes the width, w, of the contour. The shapes of the constant hydrostatic stress and constant equivalent stress contours are sketched in Fig. 16(a).

The integral (8) can be solved numerically for ΔK_I as a function of the crack extension for a transformation zone that has the shape given by equation (11). The result is given in Fig. 16(b), and shows that a transformation governed by the equivalent shear stress is more effective in reducing the stress intensity factor than a transformation driven by the hydrostatic stress. Moreover, ΔK is not zero at the beginning of crack growth. The asymptotic value for the plane strain condition with $v = 1/3$ is

$$\Delta K_I = -\,0.5\ P\sqrt{w} \tag{15}$$

which is more than a 50% greater reduction than in the hydrostatic case.

The reason that the shear-controlled transformation is more effective in reducing the stress intensity becomes apparent when the integral (8) is re-expressed as an integral over the area, A, enclosed by the contour, S,[51]

$$\Delta K_I = \int_S B\varepsilon^T \mathbf{n}(r,\theta)\bullet \mathbf{h}(r,\theta)\ \ dl = \int_A B\varepsilon^T \nabla \bullet \mathbf{h}(r,\theta)\ ds$$

$$= \int_A \frac{E\varepsilon^T}{6\sqrt{2\pi}(1-v)} r^{3/2}\cos\left[\frac{3\theta}{2}\right] ds. \tag{16}$$

The integrand in eq. (16) gives the contribution to ΔK_I from a transformed particle located at (r,θ). Because of the factor, $\cos(3\theta/2)$, in the integrand, transformed particles that are located in a wedge-shaped region in front of the crack ($-60° < \theta < 60°$) increase ΔK_I, while particles located outside this region decrease it. When the transformation

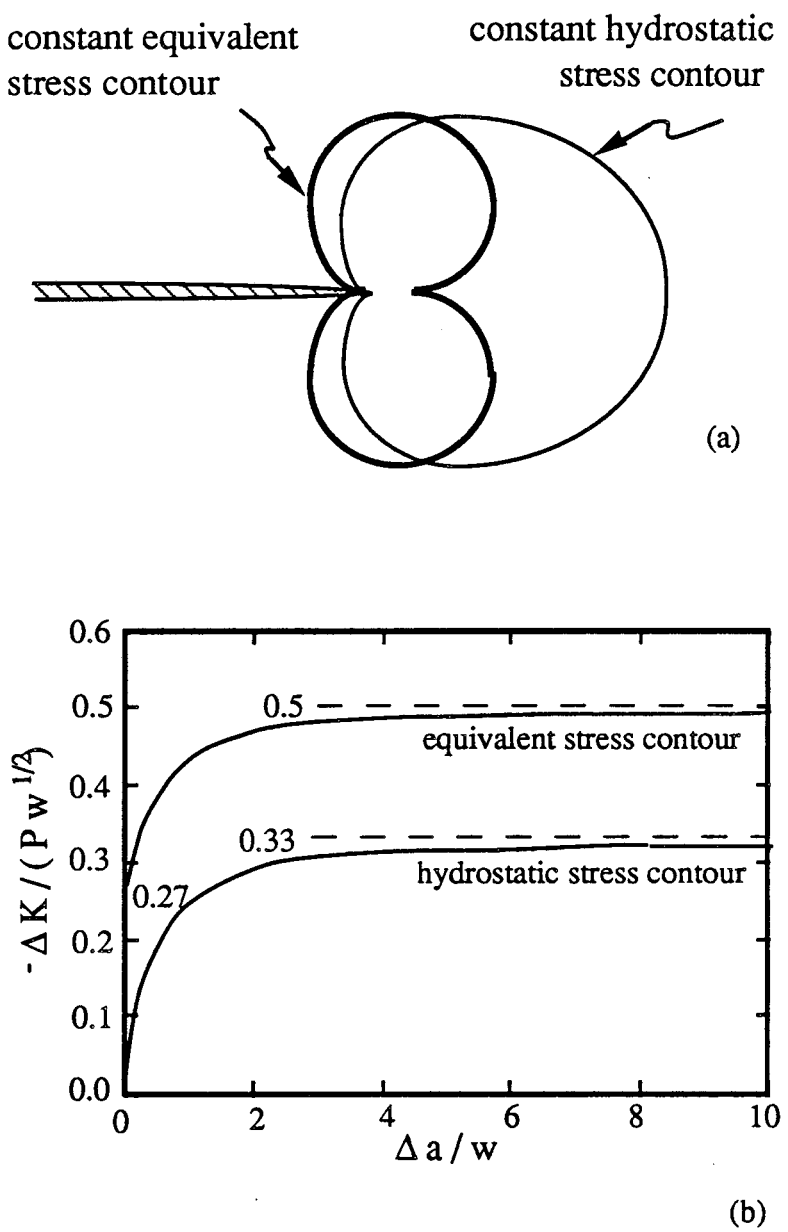

Fig. 16: (a) Assumed transformation zone shapes before the crack propagates into it -- constant hydrostatic stress contour and equivalent stress contour. (b) Predicted R curves for plane strain with Poisson's ratio of 1/3 for the two initial zone shapes.

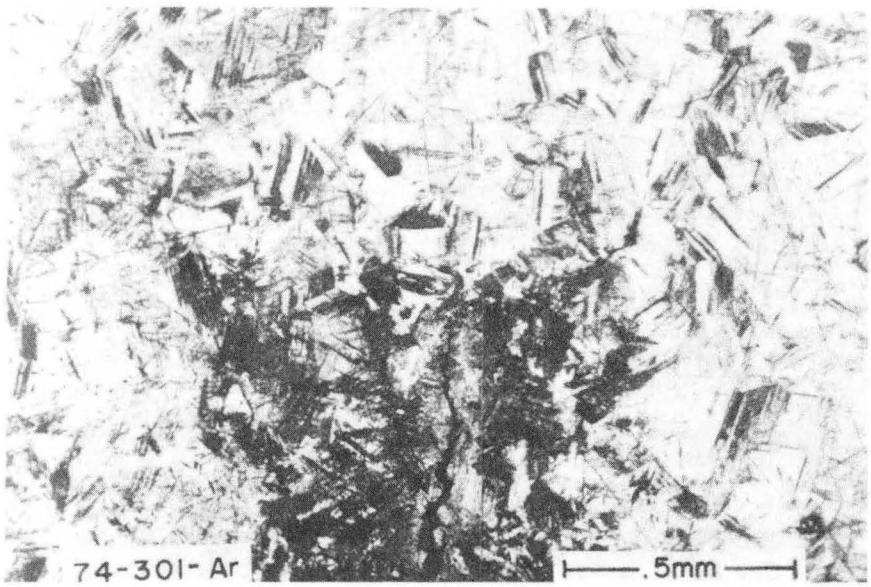

Fig. 17 (a): Deformation-induced martensitic transformation zones in a fatigue specimen of AISI 301 steel,[26] showing the zone shape follow more closely along the constant shear contour than the constant pressure contour.

Transformation Zone

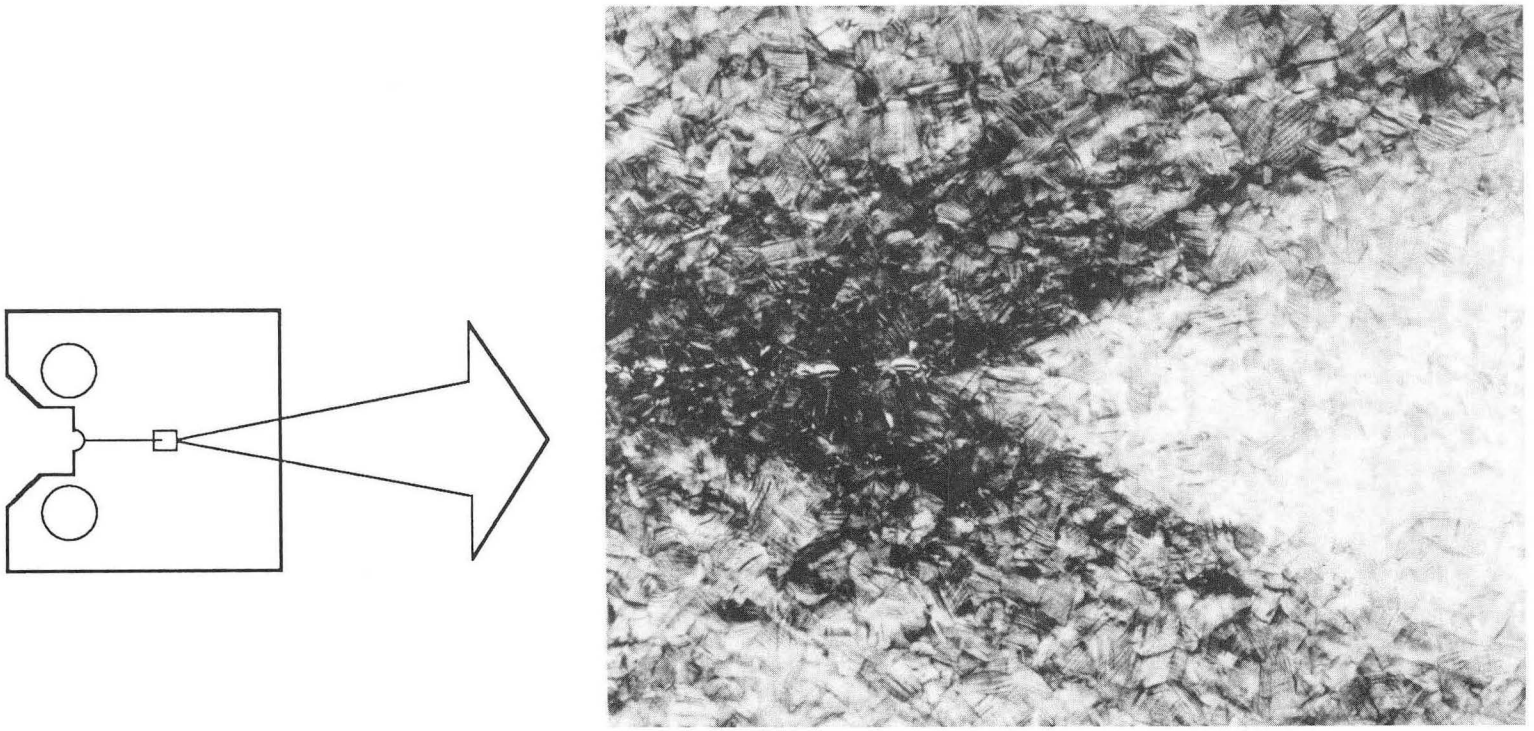

Fig. 17: Deformation-induced martensitic transformation zone about a crack in a J_{IC} test specimen.

XBB 880-9765

occurs within a contour of constant shear a much higher fraction of the transformed region lies in the zone that decreases the stress intensity than when the transformation follows a contour of constant pressure.

2. *Martensite Distribution.* The calculations leading to eqs. (12) and (15) assume that the transformation is homogeneous over the region in which it occurs: the transformed fraction is equal to V_f everywhere inside the transformed zone, and is zero outside. In reality the fraction transformed varies continuously with distance from the crack surface; as shown in Fig. 8(d), for example, the fraction of martensite is high at the crack surface and decreases significantly with distance. It is evident from equation (16) that the inhomogeneity of the martensite distribution is important. Because of the factor $r^{-3/2}$ in the integrand a transformed particle that is close to the crack tip has a much larger effect on the stress intensity than one that is further away.

Eqs. (12,15) can be modified to account for the inhomogeneous martensite distribution. Assume that a zone of width w has a martensite volume fraction, V_i, at the crack surface and let it decrease with distance, x, according to the function, V(x), to the value, $V_0 < V_i$, at the zone boundary. To compute the change in stress intensity we imagine that the zone is created by a sequence of elementary transformations and use the superposition principle. In this picture, the austenite inside the zone of width w transforms to the fraction V_0, then a smaller zone of width x_1 transforms further to $(V(x_1) - V_0)$, a still smaller zone of width x_2 transforms further to create the volume fraction $(V(x_2) - V(x_1))$, and so on until the whole inhomogeneous transformation is taken into account. The value of ΔK_I in each step can be calculated by (12) or (15), and the total change is given by the integral,

$$\Delta K_I = - C\sqrt{w}V_0 + \int_0^w C\sqrt{x}\frac{dV(x)}{dx}dx \qquad (17)$$

where $C = KB\varepsilon^T$, and $K = 0.33$ if eq. (12) is used and $K = 0.5$ if eq. (15) is used. If a linear distribution is assumed,

$$V(x) = V_0 + (V_i - V_0)\left[\frac{w-x}{w}\right] \tag{18}$$

and (17) becomes,

$$\Delta K_I = -C\sqrt{w}V_0 - \int_0^w C\sqrt{x}\frac{V_i - V_0}{w}\,dx$$

$$= -C\sqrt{w}V_0 - \frac{2}{3}C\sqrt{w}(V_i - V_0)\,. \tag{19}$$

The value of V_0 is the martensite fraction at the transformation zone boundary and is about 10% by optical microscopy measurements, while the value of V_i is the martensite fraction at the crack surface and is about 50% by X-ray diffraction measurements. This effect can be significant. For the conditions stated ΔK_I is about 25% larger than the value calculated on the assumption that the volume fraction is homogeneous and equal to its average value.

Given the assumption of a shear-controlled transformation and a linear transformation profile, ΔK_I can be calculated if the transformation zone width, w, is known. In the present work we found the zone width experimentally for 304L at 77 K for three values of the load ratio. After the fatigue tests, transformation zone sizes were measured by optical microscope as a function of ΔK (Fig. 14 (a)). It was found that the three sets of data in Fig. 14(a) could be fit by an relation of the form

$$w = A(\Delta K - C)^2 \tag{20}$$

where the values of A and C depend on the load ratio, R. Substituting this result into eq. (19) yields ΔK_I as a function of ΔK. The resulting values of ΔK_I are plotted in Figs. 18 (a-c) along with the values of K_{max} and K_{min}.

As shown in Fig. 18 the magnitude of ΔK_I increases with ΔK, essentially because a higher ΔK causes a more extensive transformation. On the other hand, the stress intensity at crack closure, K_{cl}, that is measured by the back-face strain gage is nearly independent of ΔK. These results are superficially inconsistent since the crack should close at its tip when $K = |\Delta K_I|$, but closure is not observed until the stress intensity reaches the value $K = K_{cl}$, which is greater than $|\Delta K_I|$ when ΔK is near the threshold, but is much smaller at larger values of ΔK. It does not seem reasonable that the discrepancy is simply due to the approximations in the calculation of $|\Delta K_I|$; however the transformation effect is calculated the increased martensite fraction should lead to a higher value of $|\Delta K_I|$ and hence to earlier crack tip stress relaxation at higher ΔK. We suspect that the discrepancy (and the relatively constant value of K_{cl}) is due to the fact that back-face strain gage measures a qualitatively different phenomenon: the macroscopic closure of the crack over a length sufficient to produce a measurable increase in the modulus. The effect of ΔK_I, on the other hand, is local and specific to the crack tip itself; when $K = |\Delta K_I|$ only the very tip of the crack is relaxed. The macroscopic closure, K_{cl}, reflects a number of phenomena, such as the crack roughness; the transformation may not determine its value. On the other hand, the relaxation at the crack tip itself is determined by ΔK_I, and can induce closure at the crack tip, essentially removing the driving force for crack growth, even when the crack remains open in a more macroscopic sense.

From this perspective the effective cyclic stress intensity, ΔK_{eff}, is limited by the larger of three terms: the minimum stress intensity, K_{min}, the stress intensity for macroscopic closure, K_{cl}, and the transformation stress intensity, $|\Delta K_I|$. If K_{min} is the largest of

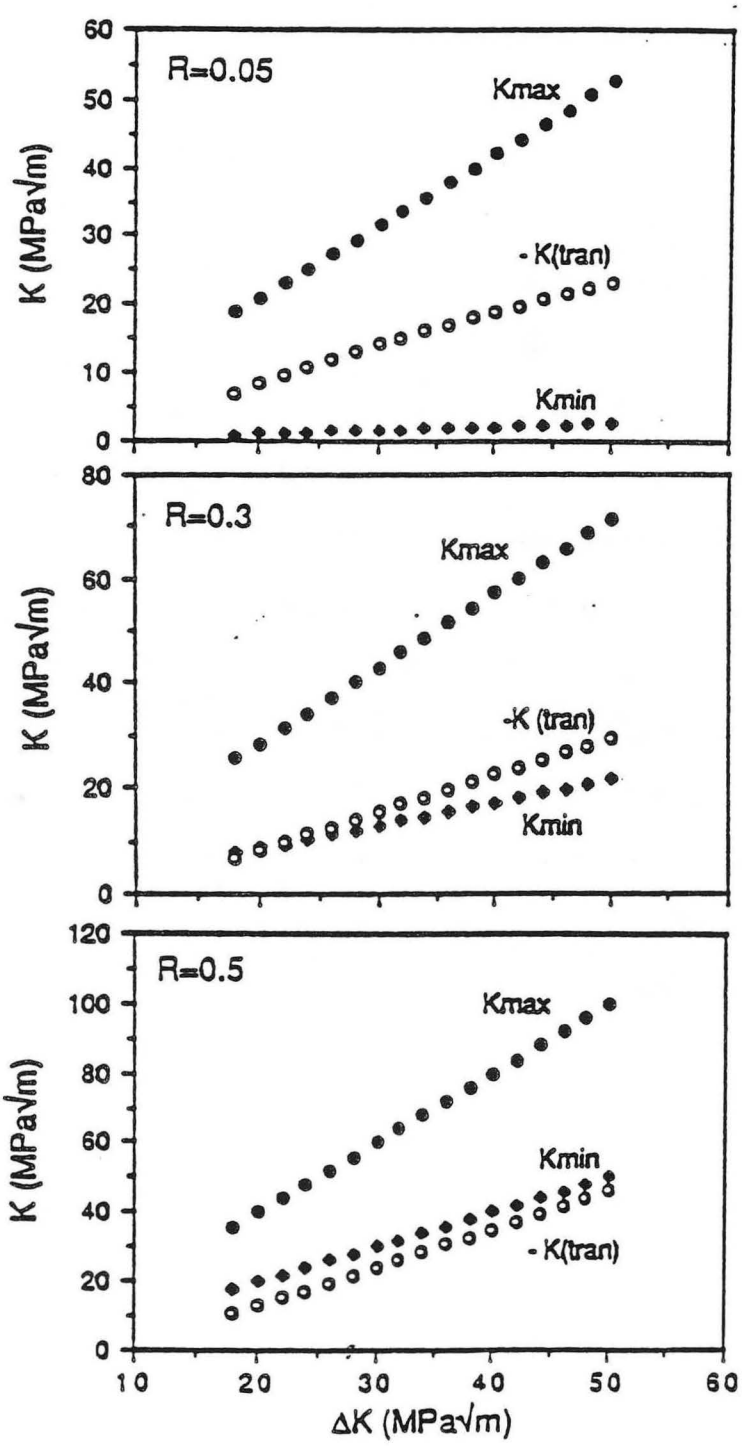

Fig. 18: The reduction of stress intensity factor $-K_{tran}$, calculated from equation (19) and the transformation zone size plotted in Fig. 14 (a), vs. the cyclic stress intensity factor (ΔK) of fatigue tests of 304L at 77 K with load-ratios (R) of (a) 0.05, (b) 0.3, and (c) 0.5. The maximum and minimum stress intensity factors are also plotted for comparison.

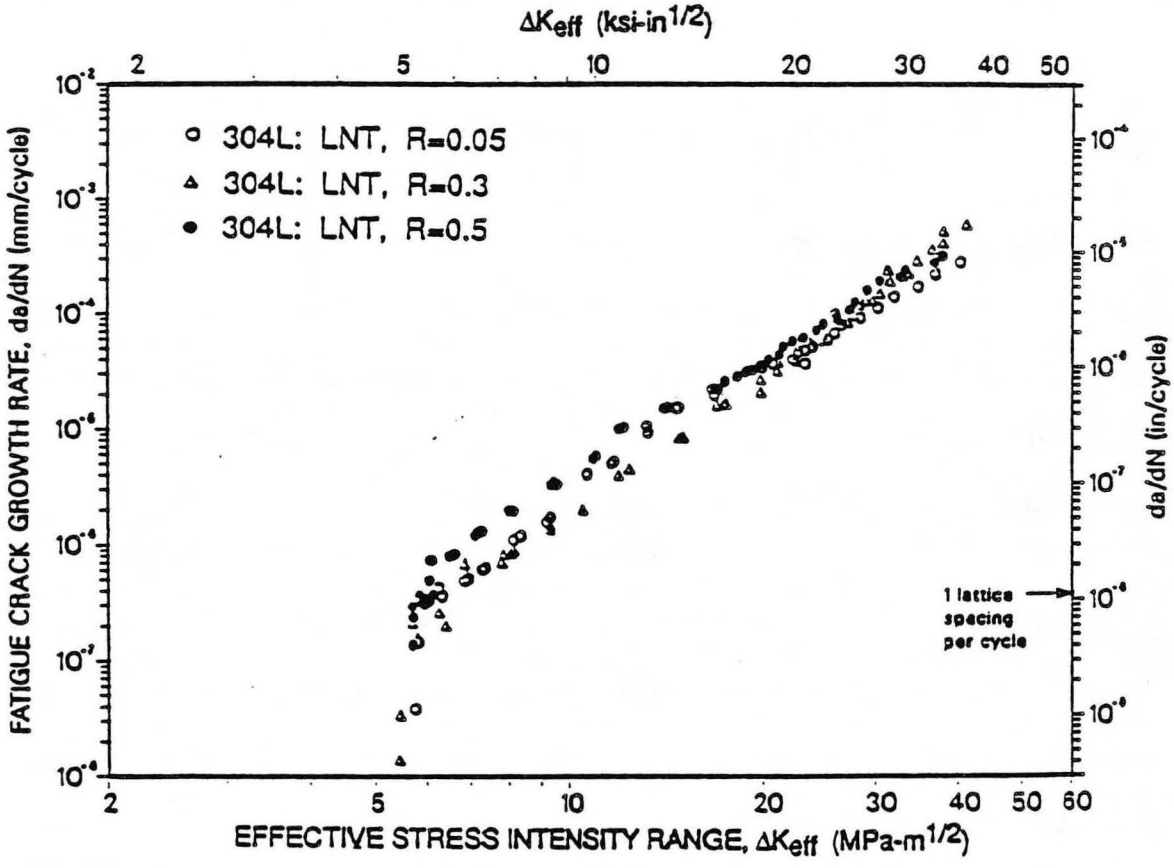

Fig. 19: Crack growth rates vs. effective stress intensity factor range for 304L autenitic stainless steel tested at 77 K with three load-ratios.

the three the crack never closes. If K_{cl} is the largest the lips of the crack touch, possibly at a position slightly away from the crack tip, and relax the crack-tip stress concentration. If $|\Delta K_I|$ is the largest, the stress intensity is relaxed locally at the crack tip. The cyclic stress intensity that should be used in the crack growth law is, then,

$$\Delta K_{eff} = K_{max} - \max\{K_{min}, K_{cl}, |\Delta K_I|\} \tag{21}$$

To test this hypothesis, the fatigue crack growth curves given in Fig. 7(f) are replotted to show the fatigue crack growth rate as a function of the effective stress intensity (ΔK_{eff}) in Fig. 19. While the curves do not completely coalesce, they agree much more closely with one another. Since ΔK_{eff} is determined by ΔK_I, whose value is known only approximately over most of the range plotted, the agreement seems reasonably good.

Shear Strain

The above calculation considers only the volume expansion term in the martensite transformation strain. The shear strain in the transformation should also reduce the stress intensity at the crack tip. Unfortunately, this effect is very difficult to estimate quantitatively. The formation of a martensite particle in a particular variant tends to trigger the formation of adjacent particles in variants with compensating shears. Only the net shear affects the overall strain field. The beginnings of an analysis of this effect were made by Lambropoulos[53], who assumed that the locations and fractions of the different variants of martensite adjust to eliminate the deviatoric component of the macroscopic stress. He was then able to estimate a net value for the transformation strain from this assumption with the additional approximation that the martensite particles are ellipsoidal, so that Eshelby's solution for the elastic field[58] could be employed. The validity of the assumptions is not at all clear, and the results of the calculation for ΔK_I is very sensitive to the assumed orientation

of the martensite particles. However, he concluded that the effect of the shear can be large; ΔK_I due to the shear strain can be double that due to volume expansion alone.

Since the particle orientation in our fatigue experiments was not regular, it was not clear how to apply his results to our case, and we did not attempt to do so. Nonetheless the author of this thesis is continuing to investigate the influence of the shear strain.

B. Other Mechanisms

Metallurgical effects besides the perturbation of the crack-tip stress may also influence fatigue crack growth in a material that undergoes transformation. The following mechanisms are also investigated.

Dual-phase Microstructure

The stress/strain field of a fatigue crack creates an $\gamma + \alpha'$ dual-phase medium in front of the crack, and that medium may be more fatigue-resistant inherently than the single γ phase medium. However, comparison of the crack growth rate in the γ single phase with that in the $\gamma + \alpha'$ dual phase rules out this possibility. The $\gamma + \alpha'$ structure (Fig. 2(b)) produced by cold-rolling as explained previously was fatigue-tested at room temperature, and the results are compared with those of the annealed 304L and 304LN in Fig. 20 (a). The crack growth rates of three steels do not differ very much except in the threshold region. No crack closure was observed. No further transformation was induced during the fatigue testing. In Fig. 20(b) the crack growth rates at liquid nitrogen temperature are compared. The crack growth rate in the cold-rolled 304L in the Paris region is very close to that of 304LN that is stable during fatigue, and not close to that of annealed 304L that transforms to martensite during fatigue. Additional but little martensite transformation occurred during the fatigue test of the cold-rolled 304L at LNT. The crack closure was observed and the measurements are included in Fig. 12. The threshold stress intensity range of the cold rolled 304L is higher in comparison to of 304LN.

These data indicate that crack growth rates in the Paris region do not differ very much in either γ single phase or $\gamma + \alpha'$ dual-phase. Actually the insensitivity of crack growth rate in the Paris region with microstructure is a common phenomenon.[62] The previous research on Al alloys and Ni-based superalloys [63] showed that varying chemical composition does not change the fatigue crack growth rate in Paris region very much, if the environmental effects are not considered. Fatigue crack growth rate in the threshold region on the other hand depends significantly on microstructure, and is related with crack closure phenomenon.

In the cold-rolled 304L specimen, martensite particles are present everywhere within the specimen; while in the annealed 304L, martensite particles exist only about fatigue crack surface. Fatigue crack growth rate is reduced in the annealed 304L but not in the cold-rolled 304L. This indicates that the reduction of crack growth rate must relate with the elastic constraint of the matrix materials on the local transformation, i.e. an effect of residual stress.

Figs. 20 (c, d) show the fractographs of the specimen of cold-rolled 304L tested at room temperature. At the threshold region (Fig. 20 (c)), the fracture surfaces show little or no trace of plastic deformation in comparison with that of annealed 304L tested at room temperature, (Fig. 15 (b)), apparently due to the presence of the martensite particle. The paucity of plastic deformation at the threshold region is possibly the reason for the lower threshold stress intensity range of the cold-rolled 304L than that of annealed 304L (Fig. 20 (a)), for the arguments of the plasticity-induced crack closure. On the other hand, in the Paris region (Fig. 20 (d)), the trace of plastic deformation are apparent, but so are those of secondary cracking.

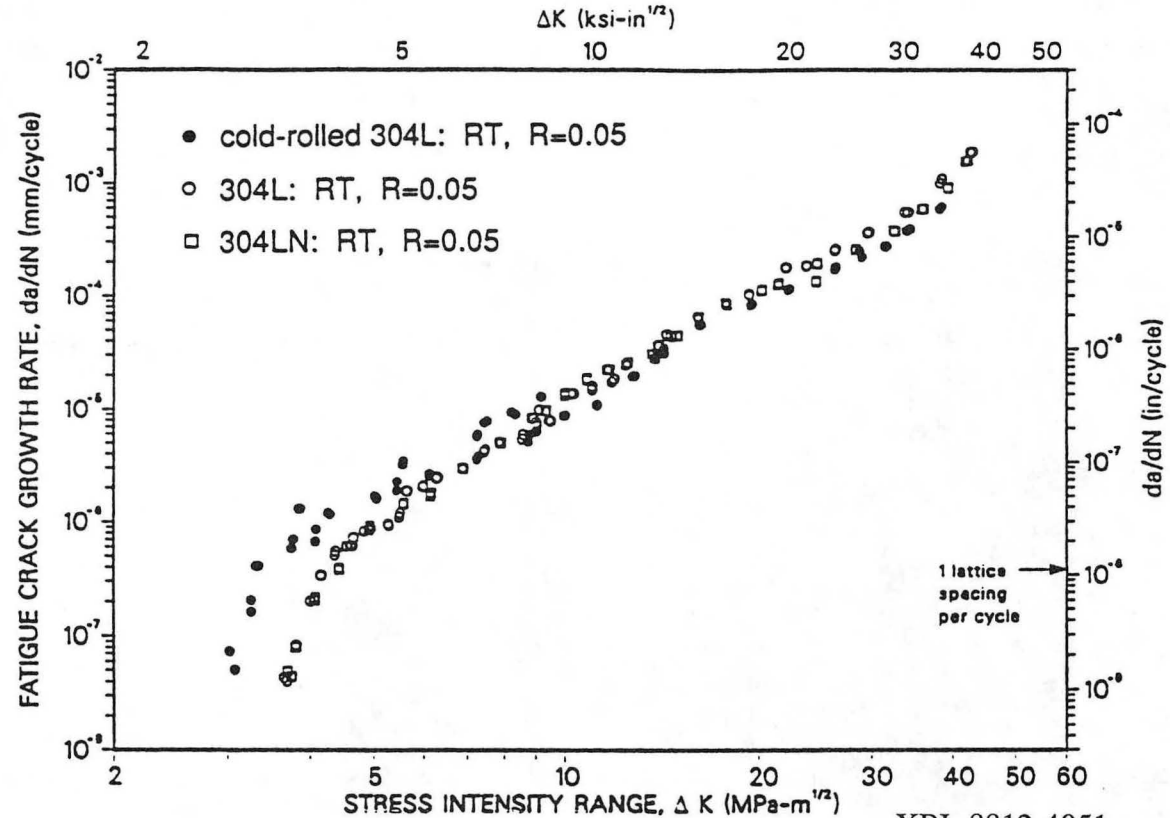

XBL 8812-4051

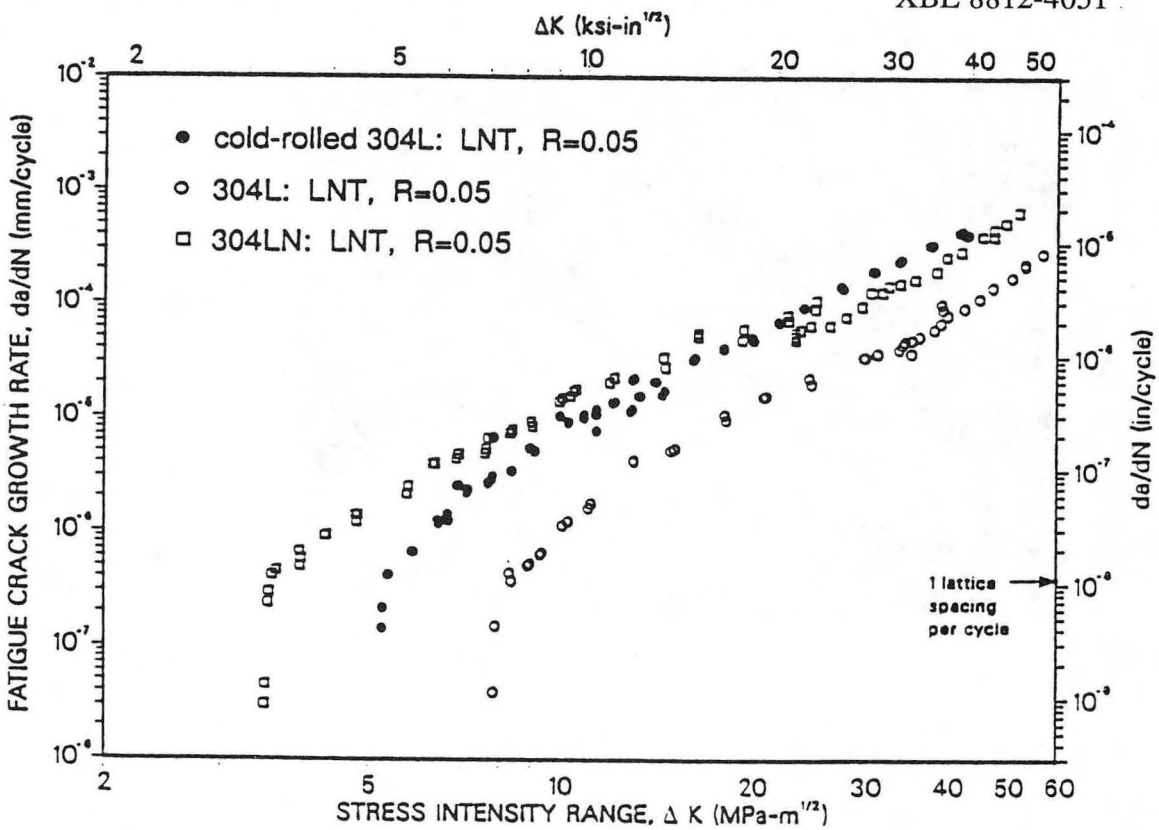

Fig. 20: Crack growth rates vs. stress intensity range of (a) cold-rolled 304L, annealed 304L, and 304LN steels tested with load-ratio 0.05 at (a) 298 K and (b) 77 K.

XBL 8812-4052

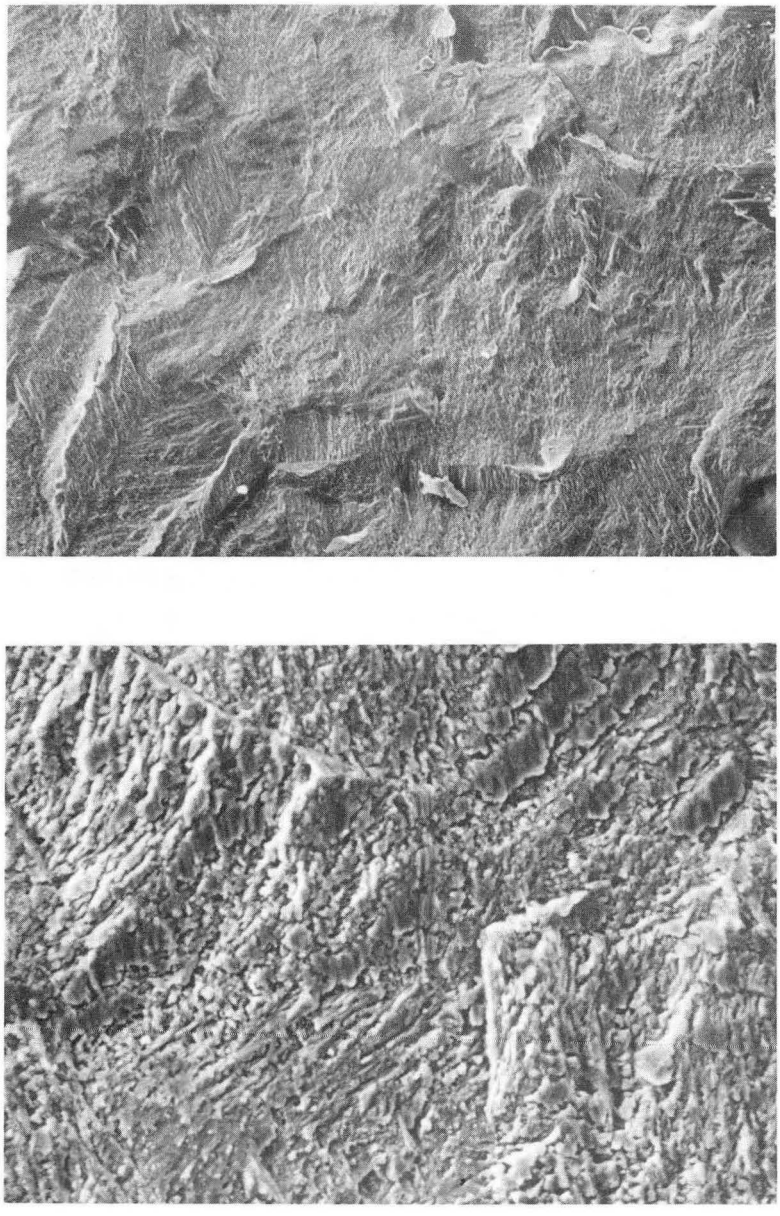

crack propagates

50 um

10 um

Cold-rolled 304L
tested at RT
R = 0.05
$\Delta K = 7$ MPa$\sqrt{m}$

Fig. 20 (c): SEM fractographs of cold-rolled 304L fatigue-tested at 298 K with $\Delta K \approx 4$ MPa-m$^{1/2}$ (threshold region). XBB 8811-11110

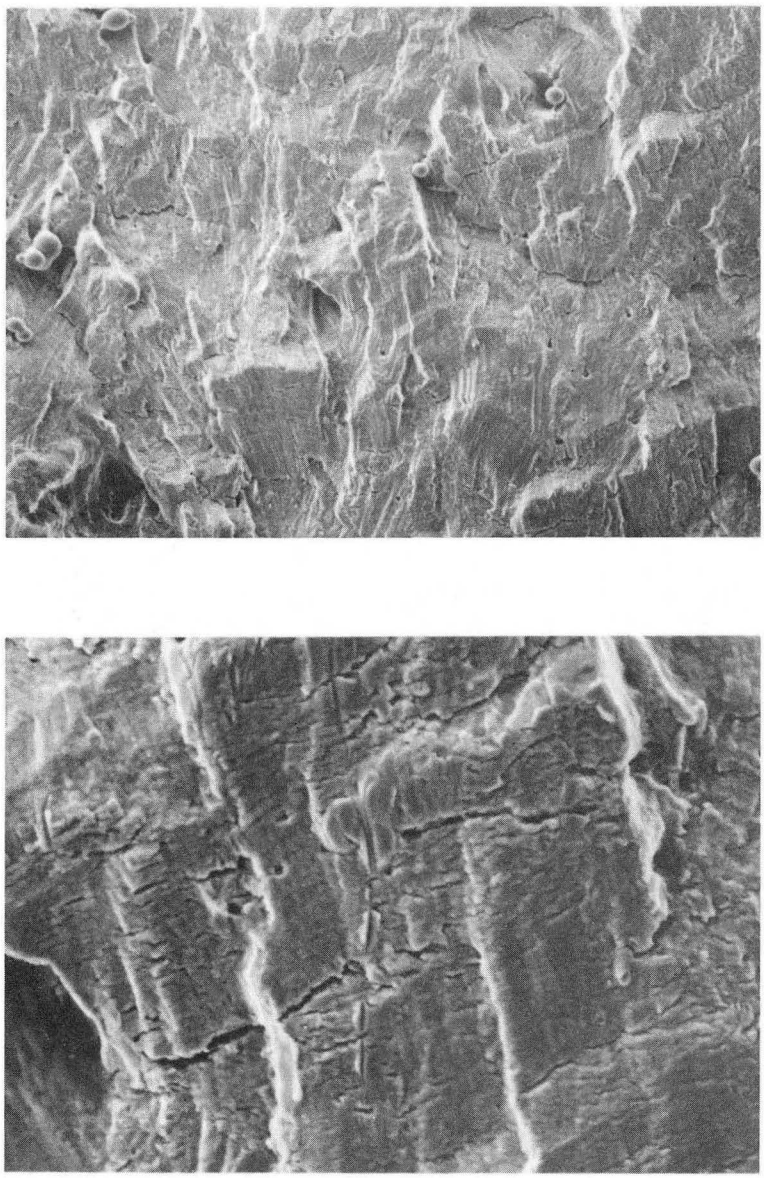

crack propagates

50 um

10 um

Cold-rolled 304L
tested at RT
R = 0.05
$\Delta K = 38$ MPa$\sqrt{m}$

Fig. 20 (d): SEM fractographs of cold-rolled 304L fatigue-tested at 298 K with $\Delta K \approx 35$ MPa-m$^{1/2}$ (Paris region). XBB 8811-11114

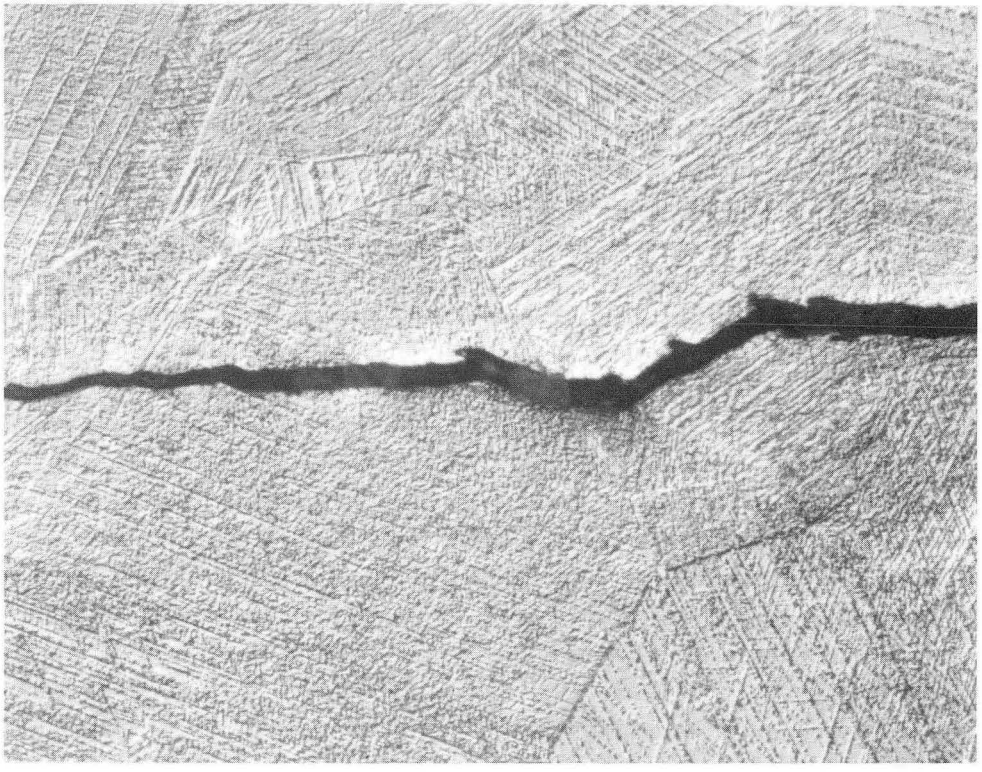

Fig. 21: Optical micrograph of a crack propagated in an extensively transformed area, showing that the tendance for the crack extension between martensite laths produces a zigzag crack path. (XBB 8712-10651 B)

Crack Deflection

As shown in Fig. 21, the crack tends to extend between the martensite laths when material in front of it has transformed extensively. This tendance produces a wavy, zigzag crack path. It has been established in the literature that a crack under a K_I loading advances with a slower speed along a zigzag path than along a flat path. This is because (a) the crack moves through a longer distance along a zigzag path than along a flat path for the same projected length; (b) the externally applied tensile opening loading (K_I) changes to the tensile opening plus sliding loading ($k_1 + k_2$) near the crack tip if the crack deviates from the direction normal to the loading axis. The two effects can be evaluated quantitatively on the basis of the model given in ref. [64].

Let da/dN and $(da/dN)_I$ represent the respective crack growth rates with and without deflection, and let ϕ denote the angle of deflection from the normal direction to the loading axis. The reduction of crack growth rate due to effect (a) is given in ref. [64] as

$$\frac{da}{dn} = \cos\phi \left[\frac{da}{dn}\right]_I. \tag{22}$$

The local stress intensities, k_1 and k_2, of a deflected crack can be expressed as functions of the mode I and II stress intensities due to the external load, K_I and K_{II},[65,66]

$$k_1 = a_{11}(\phi)\, K_I + a_{12}(\phi)\, K_{II}$$

$$k_2 = a_{21}(\phi)\, K_I + a_{22}(\phi)\, K_{II} \tag{23}$$

The first order solutions for the $a_{ij}(\phi)$[67] are very close to the exact solutions,[66] and are,

$$a_{11}(\phi) = \cos^3(\phi/2) \qquad a_{12}(\phi) = -\,3 \sin(\phi/2) \cos^2(\phi/2)$$

$$a_{21}(\phi) = \sin(\phi/2)\cos^2(\phi/2) \qquad a_{22}(\phi) = \cos(\phi/2)\,[1 - 3\sin^2(\phi/2)]. \tag{24}$$

When K_{II} is zero, as it is in the case of interest to us, eq. (23) become

$$k_1 = \cos^3(\phi/2)\,K_I, \qquad k_2 = \sin(\phi/2)\cos^2(\phi/2)\,K_I \tag{25}$$

According to the coplanar strain energy release rate theory,[68] the effective driving force for the crack propagation is,

$$\begin{aligned} k_{eff} &\approx (k_1^2 + k_2^2)^{1/2} \\ &= [\cos^6(\phi/2) + \sin^2(\phi/2)\cos^4(\phi/2)]^{1/2}\,K_I \end{aligned} \tag{26}$$

The maximum value of ϕ measured in these tests was about 30°. Actually, the deformation induced martensite in Fe-Ni-Cr alloys were identified to be plates on $\{111\}_\gamma$ family planes. The half of the angle between (111) and $(\bar{1}11)$ is about 35.3°. If the maximum ϕ is assumed to be 35.3°, the minimum k_{eff} calculated from (26) is 0.908 K_I. It is easy to see that in the case of cyclic loading, $\Delta k_{eff} = 0.908\,\Delta K_I$. Plugging Δk_{eff} into the Paris-law equation, we have

$$\frac{da}{dn} = A\,(\Delta k_{eff})^n = A(0.908)^n(\Delta K)^n \tag{27}$$

For 304L steel, n is roughly equal to 3.7. Therefore, the growth rate of a deflected crack is 0.7 ($\approx 0.908^{3.7}$) times of that of a linear crack. If eq. (22) is also taken into consideration, the crack grows in its irregular path at a rate about 0.57 times that of its growth along a linear path.

While crack deflection certainly affects the crack growth rate in this case, the effect cannot be the major source of the reduced crack growth. Crack deflection reduces the growth rate, at most, 1.75 (= 1/0.57) times, while the experimental data (Fig. 7) indicates that the growth rate is reduced by at least a factor of 4 as a result of the transformation. Moreover, the crack propagates through the martensite particles when the transformation in front of it is not extensive. Therefore, the crack deflection effect only applies when ΔK is large.

Work Hardening

The $\gamma \rightarrow \alpha'$ transformation increases the effective rate of work hardening. This effect is apparent in Table II, which includes the ratios of the ultimate and yield strengths. Pineau and Pelloux[23] proposed that an increase in work hardening rate due to transformation would cause a reduction in the crack growth rate. However, there is no well-developed model that permits us to quantify the effect.

As reviewed by McEvily,[69] the proposed mechanisms of fatigue crack propagation in the Paris region can be divided into two categories. The first category focuses on the plastic sliding-off process at the crack tip, the other emphasizes damage accumulation. In the first type of model, the crack growth rate can be related to the crack tip opening displacement (CTOD)[70],

$$\frac{da}{dN} \approx 0.5(\mathrm{CTOD}) = 0.5\left[\frac{\Delta K^2}{E\sigma_y}\right] \tag{28}$$

where σ_y and E are the yield stress and Young's modulus, respectively. In the damage-accumulation model, a fatigue crack grows an incremental length, Δa, if a critical value of the accumulated plastic displacement is reached, and[71]

$$\frac{da}{dN} = C\left[\frac{\Delta K^4}{E\sigma_y{}^3 D_c}\right] \tag{29}$$

where D_c is the critical plastic displacement. Neither of these relations is experimentally verified. However, both imply that an increase in flow stress causes a reduction in the crack growth rate.

The stress and strain fields at a crack tip in a material that exhibits power law hardening ($\sigma = A\,\varepsilon^n$) under K_I loading have been found, [73,74] and are

$$\sigma_{ij} = \left(\frac{1}{r}\right)^{n/(1+n)}\ \Sigma_{ij}$$

$$\varepsilon_{ij} = \left(\frac{1}{r}\right)^{1/(1+n)}\ E_{ij}, \tag{30}$$

where the matrices Σ_{ij} and E_{ij} are found numerically from the external loading, the work hardening coefficient, n, the crack orientation orientation, and the elastic constants.[68] Work hardening elevates the stress at the crack tip and raises the ratio of the maximum normal stress to equivalent stress.[73] At the same time, work hardening makes the strain at the crack tip more uniform. For example, in a perfectly plastic material the strains vary as r^{-1}, while in a hardenable material the strains vary as $r^{-1/(1+n)}$, where $0 < n < 1$. The plastic zone size decreases as (n) increases.[73]

These analyses suggest that the crack growth rate may vary in either direction with increasing work hardening. Work hardening reduces the CTOD and the plastic zone size, which should decrease the crack growth rate; on the other hand, it enhances the stresses and the normal-to-shear stress ratio, which increases the probability of fracture by cleavage. The net effect is not clear.

Fracture Mode Transition

Finally, there is an evident transition in the local mode of fracture when transformation intrudes in the samples studied here. The fatigue fracture surfaces in the samples that did not transform (Figs. 15 (a)-(b)) are rough and exhibit traces of significant plastic deformation; the surfaces of the samples that did transform (Fig. 15 (c)-(f)) are flat, and show a predominant cleavage or quasi-cleavage fracture mode. It appears that the material becomes brittle after the transformation, which is consistent with the behavior of fresh martensite, and should accelerate crack propagation. The brittleness of the fresh martensite phase may also contribute to the load ratio effect: at low load ratios, the crack growth rate is held down by the compressive residual stress; at high load ratios, the extensive transformation in front of crack and the high static stress promote a low-energy, brittle fracture. However, the experimental data suggests that this effect is not quantitatively large in these steels; the crack growth rate in the cold-rolled material that contains a high fraction of martensite is similar to that in annealed 304L, as shown in Fig. 20 (a).

V. CONCLUSIONS

1. The martensitic transformation that occurs at the tip of a growing fatigue crack in metastable 304-type steels significantly reduces the fatigue crack propagation rate in both the threshold and Paris regions. However, the effect decreases as the load ratio, or mean stress increases.

2. Several mechanisms apparently contribute to the decreased crack growth rate in steels that transform. The most important is the perturbation of the stress field at the crack tip. By modifying previous theories of the influence of the transformation on the crack tip stress intensity, it is possible to obtain a theory that provides a reasonable quantitative fit to the experimental data. To improve this theory it is necessary to develop a good quantitative model that includes the net shear due to the martensite transformation.

3. Other factors contributing to the change in the crack growth rate are the dual-phase microstructure, the crack deflection, the increased work hardening rate, and the relative brittleness of the fresh martensite phase.

PART B: EFFECTS OF LOW TEMPERATURE ON CRACK PROPAGATION IN THE STABLE AUSTENITIC STAINLESS STEEL

I. REVIEW OF PAST WORKS

A limited amount of near-threshold fatigue crack propagation rate data at low temperatures is available for Al alloys,[75-79] Cu alloys,[80] 300 series of AISI austenitic stainless steels,[27-29,80-83] AISI 4340 steel and Zn-22Al superplastic alloy,[84] mild steels,[80] Fe-Si alloys and high strength low alloy steel,[85-90] JBK-75 stainless steel and inconel 706,[91,92] CrMoV steel,[93] and Fe-Cr-Mn alloy.[95] All the data, including fcc, bcc, and hcp metals, indicate that the threshold cyclic stress intensity increases and the near-threshold crack growth rate decreases as the temperature decreases in the range between 298 K to 4 K. This phenomenon were attributed to surface-roughness-induced crack closure,[86,92-94] transformation toughening,[27-29] and thermally activated dislocation movement.[76,85,87,94]

In contrast to the trend found in the threshold region, the crack growth rate in the Paris region may either increase or decrease with the temperature. The relevant data was recently reviewed by Tobler and Cheng,[96] who summarize results for more than 200 material and temperature combinations, including ferritic nickel steels, austenitic stainless steels, Ni-base superalloys, Ti-base alloys, and Al-base alloys. Another extensive review was done by Verkin and et al.[97]

For most bcc alloys that exhibit the DBTT (Ductile to Brittle Transition Temperature) behavior, the plots of da/dN vs. ΔK at low and high temperatures cross each other, as shown in Fig. 22 (a). At small ΔK, da/dN at the low temperature is slower than that at high temperature; while at large ΔK, the reverse is true. The examples of that

phenomenon are seen in the studies of Fe-Si and Fe-Ni bcc alloys,[98] AISI 4340 steel,[84] and Fe-9Ni alloy.[99]

For most fcc alloys, the plots of da/dN vs. ΔK at low and high temperatures usually do not cross each other, so that da/dN at low temperature is slower than that at high temperature for all ΔK values, as shown in Fig. 22(b). Although the slope of the logarithmic fatigue crack growth rate, that is, the parameter (n) in the Paris Law: $da/dN = A(\Delta K)^n$, increases as the temperature decreases. The value of (n) for most metals at 298 K is in the range 2 - 4, and may increase to 5 - 8 at cryogenic temperature. The examples of this behavior are seen in the studies of Cu alloys,[100] Fe-Ni-Cr superalloy,[94] and Al alloys.[78,79] The increase in (n) reflects the fact that materials become more brittle at lower temperature, the value of (n) is more than 100 for ceramics.[101]

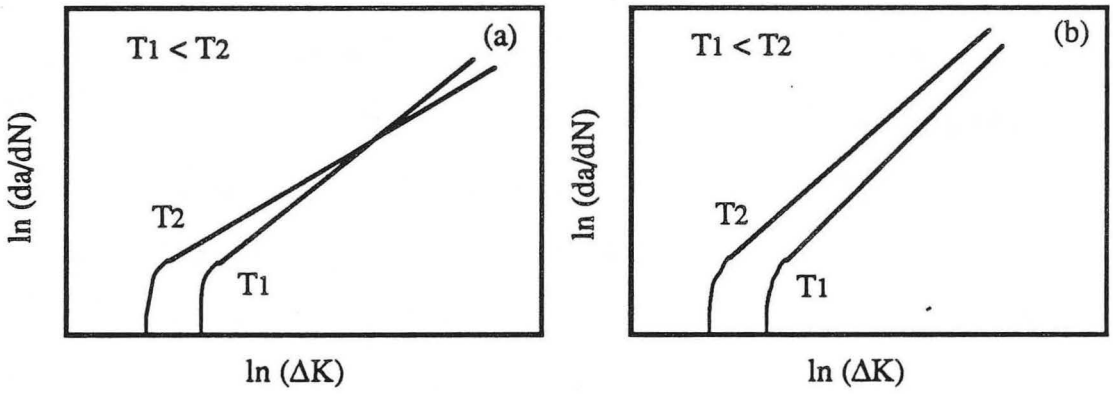

Fig. 22: Sketch showing the variation of the da/dn vs. ΔK plots with the temperature for (a) most of bcc alloys, and (b) most of fcc alloys.

II. EXPERIMENTAL PROCEDURE

The chemical composition of the commercial grade AISI 310 stainless steel used in this study was, in weight percent, 24.73Cr-19.23Ni-1.73Mn-0.51Si-0.26Mo-0.16Cu-0.15Co-0.066N-0.021C-0.023P-0.008S. The steel was annealed at 1050 C for 1 hour and then quenched in water. The grain size was ≈100 mm (Fig. 24).

The fatigue crack growth rate was determined according to the similar procedure described in section Part I. The tests at 4 K were done by immersing the specimen and the compression tube into a cryostat filled with liquid helium, the temperature was monitored by a superconducting detector.

The fatigue crack profiles were observed by optical microscopy. The fatigue fracture surfaces were studied by scanning electron microscopy (SEM) to determine fracture mode, by X-ray diffractometry to check for evidence of phase transformation, and by surface profilometry to characterize surface roughness.

III. RESULTS

A. Fatigue Crack Growth Rate

Fig. 23 includes measured fatigue crack growth rates for 310 austenitic stainless steel at room temperature, liquid nitrogen temperature, and liquid helium temperature. The parameters n and A in the Paris Law formula ($da/dN = A\ \Delta K^n$), and the threshold stress intensity range are listed in Table IV.

Table IV - Power-Law Fatigue Equation Parameters and Threshold Stress Intensities of AISI 310 Austenitic Stainless Steel Tested at Various Temperatures

Temperature	Slope, n	A	Threshold (MPa$\sqrt{m}$)
298 K	3.79	1.50×10^{-9}	3.5
77 K	3.67	8.45×10^{-10}	4.8
4 K	4.51	7.97×10^{-12}	-

The results differ somewhat from those reported by Tobler, et al. for the same material.[102] They found essentially equal crack growth rates, da/dN, at LNT and LHT which were about one-half those measured at RT for the same ΔK. Moreover, their crack growth rates were uniformly lower than those measured here; if their RT data were plotted in Fig. 23, it would appear just on the right side of our 310 LHT data line. However, their data include only a small section (between 3×10^{-6} to 2×10^{-4} mm/cycle) of the whole fatigue propagation curve. It may also be relevant that their fatigue specimen thickness was between 25.4 mm and 50.8 mm (1 in - 2 in) while ours was 12.7 mm (0.5 in). In earlier

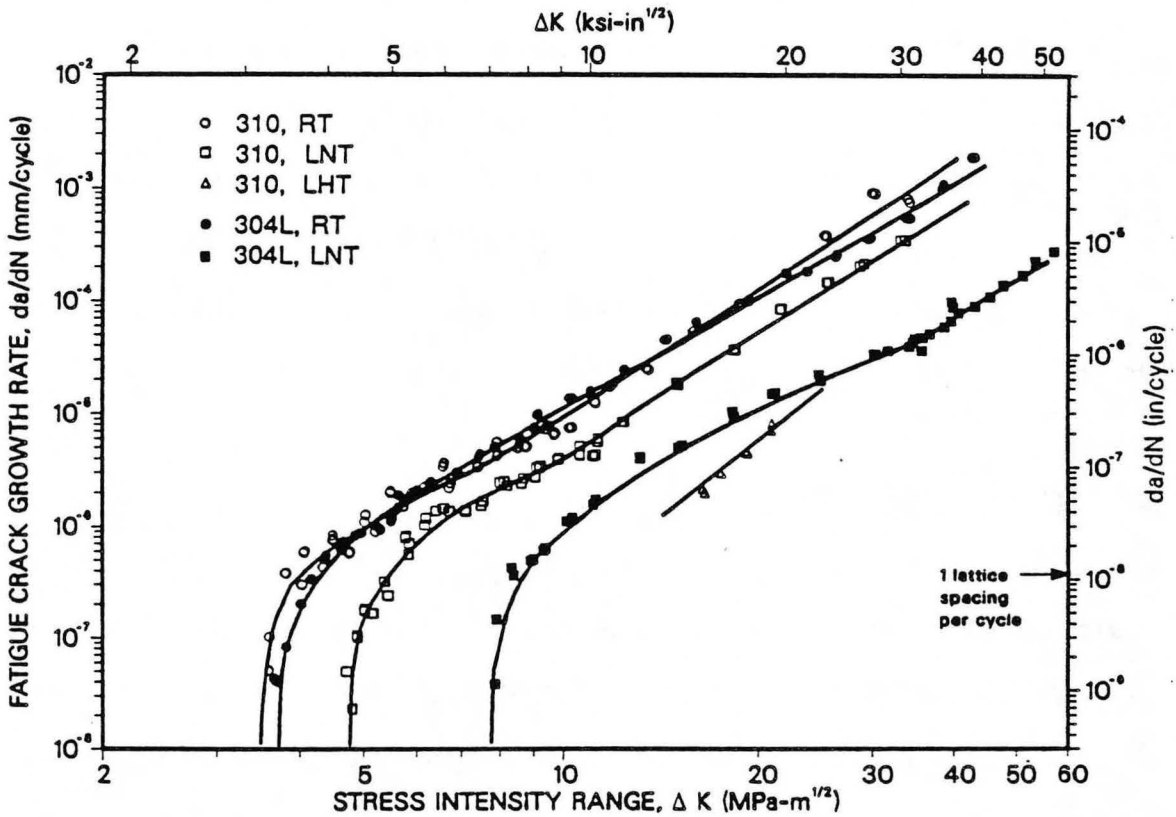

Fig. 23: Crack growth rate vs. stress intensity range of 310 and 304 austenitic stainless steels at room, liquid nitrogen, and liquid helium temperatures. (XBL 897-2552).

work, we did observe a specimen thickness effect on the fatigue crack propagation in 304L austenitic stainless steel, the origin is still under investigation; however the magnitude of this effect seems too small to explain the large difference between their data and the current data.

The crack growth rates of 304L austenitic stainless steel at RT and LNT, are also plotted in Fig. 23. For this alloy, the increase in the threshold stress intensity range and the reduction in the crack growth rate with decreasing temperature is a result of the deformation-induced martensitic transformation that occurs at LNT in addition to inherent temperature effects. Alloy 310 remains austenitic when tested at RT, LNT, and LHT, yet also shows an increase in the threshold stress intensity range and a reduction in the crack growth rate with decreasing temperature.

B. Crack Profile and Fractography

Optical microscopy revealed that fatigue cracks propagate in 310 stainless steel in a zigzag path. The cracks are kinked and branch at all temperatures. Crack branching is most prominent at LHT as shown in Figs. 24 (a)-(c). The direction of crack propagation almost invariably changes at grain boundaries, and may also change within a single grain to produce a sawtooth pattern. The crack path appears to be a consequence of two competing tendencies: preferential crack growth along particular crystallographic planes, and maximal driving force for crack propagation perpendicular to the axis of loading. The result is a zigzag path. Kinks and branches reduce the crack growth rate for two reasons: the crack passes through a longer distance along a zigzag path than along a straight path, and the effective stress intensity factor is smaller if the crack deviates from the plane normal to the external load.[64]

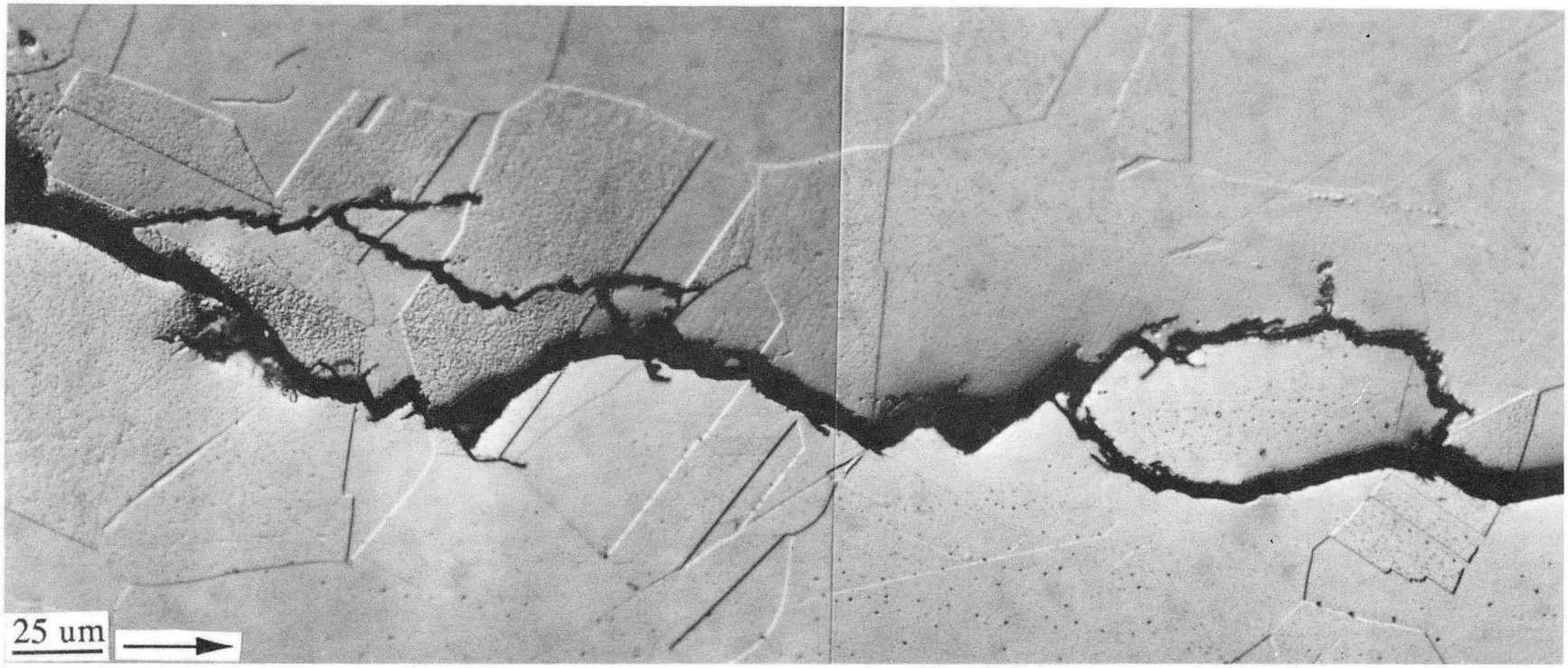

Fig. 24: Optical micrograph of fatigue crack profile of the 310 stainless steel specimen tested at liquid helium temperature.

XBB 897-5501

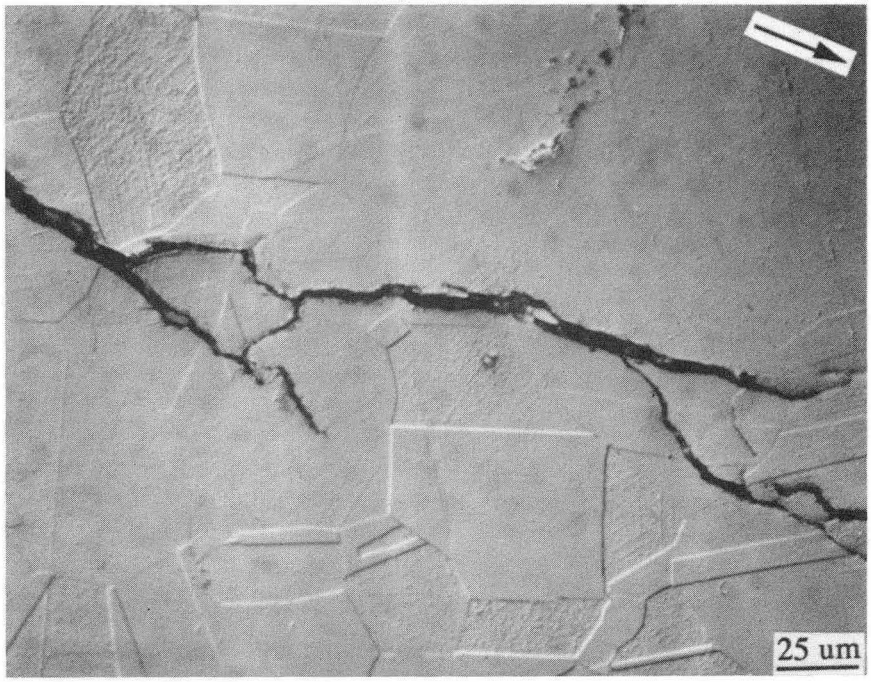

XBB 897-5840

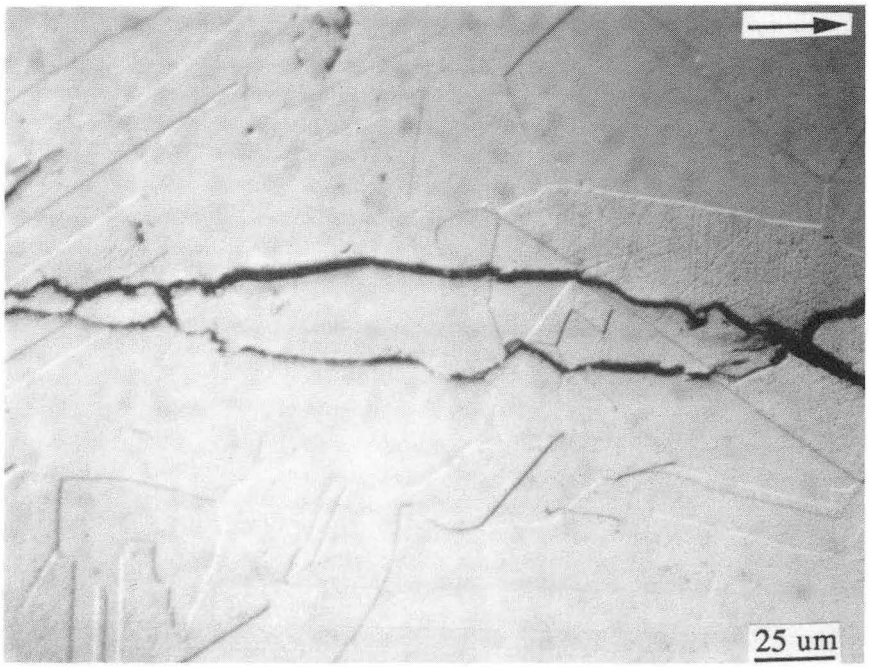

Fig. 24 -1: Optical micrographs of fatigue crack profile of 310 stainless steel specimen tested at 4 K.

Fig. 25 (a)-(d) are scanning electron micrographs of the fatigue fracture surfaces. The crack propagation directions are marked by arrows. For the specimen tested at RT, fatigue striations are easily seen when ΔK is larger than $\approx$ 32 MPa-m$^{1/2}$. The striation spacing is close to the crack extension per cycle. It is interesting that the striations have different orientations in different grains, for example grain A and B in Fig. 25 (a). Fatigue striations were not seen in the specimens tested at LNT and LHT. When ΔK is smaller than $\approx$ 32 MPa-m$^{1/2}$, the fracture surface at RT resembles that at LNT and LHT. At all three temperatures, the cracks propagate in a quasi-cleavage mode. As shown in Fig. 25 (b) and 25 (c) the flow of the river pattern is in the direction of crack propagation, and the pattern changes across grain boundaries. These features are characteristic of the cleavage fracture mode.[103] Note that the crack profile, Fig. 24, also shows that the crack changes its propagation direction across grain boundaries.

C. Surface Roughness and Crack Closure

No crack closure was detected during the fatigue tests at RT and LNT by the back-face strain gauge technique, although the measurement of surface roughness and observation of crack profile led us to believe that crack closure should occur. An experimental error with the back-face strain gauge prevented the study of closure at LHT. To clarify the influence of surface roughness on fatigue crack propagation the fracture surfaces of the fatigue specimens were characterized by profilometry. Fig. 26 shows two line scans for each of three specimens tested at RT, LNT, and LHT. The profilometer scanning direction was along the fatigue crack propagation direction. The roughness of the surfaces was quantified by the parameter R defined as

$$R = \frac{\int_0^L |y(x) - \bar{y}|\,dx}{L} \tag{31}$$

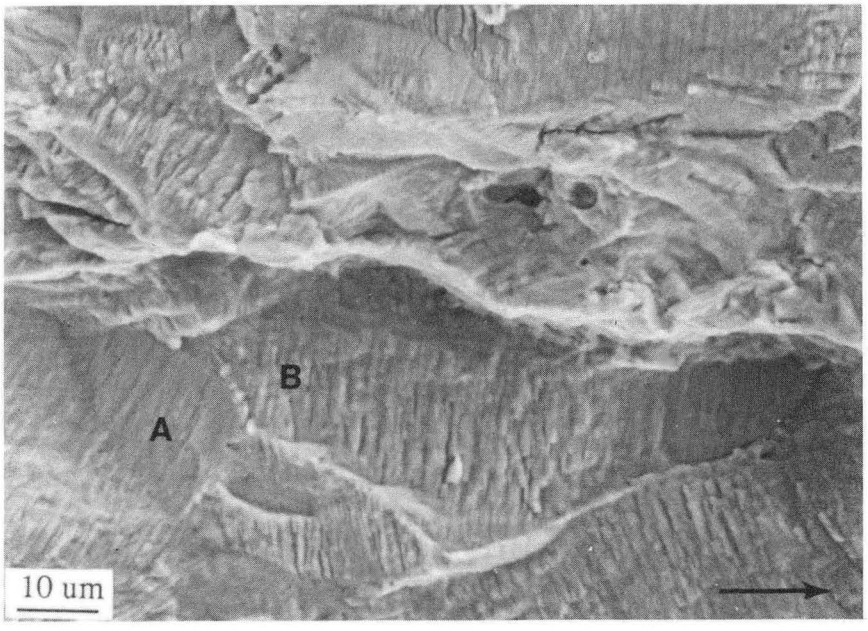

(a) XBB 896-5051A

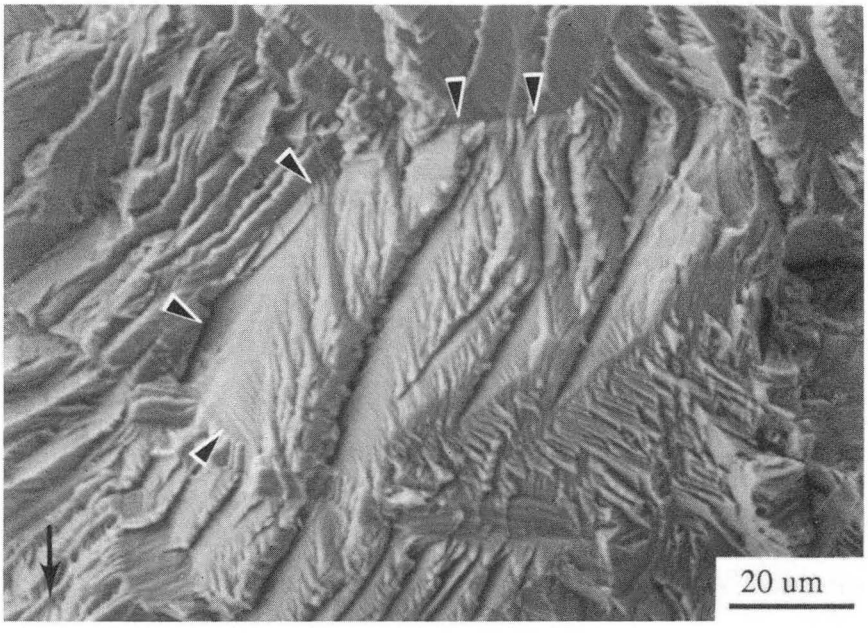

(b) XBB 896-5059A

Fig. 25: SEM fractographs of 310 stainless steel specimens fatigue-tested at (a) 298 K with $\Delta K \approx 32$ MPa-m$^{1/2}$ and da/dN ≈ 1 μm/cycle, and at (b) 77 K with $\Delta K \approx 10.5$ MPa-m$^{1/2}$ and da/dN $\approx 1.1 \times 10^{-2}$ μm/cycle.

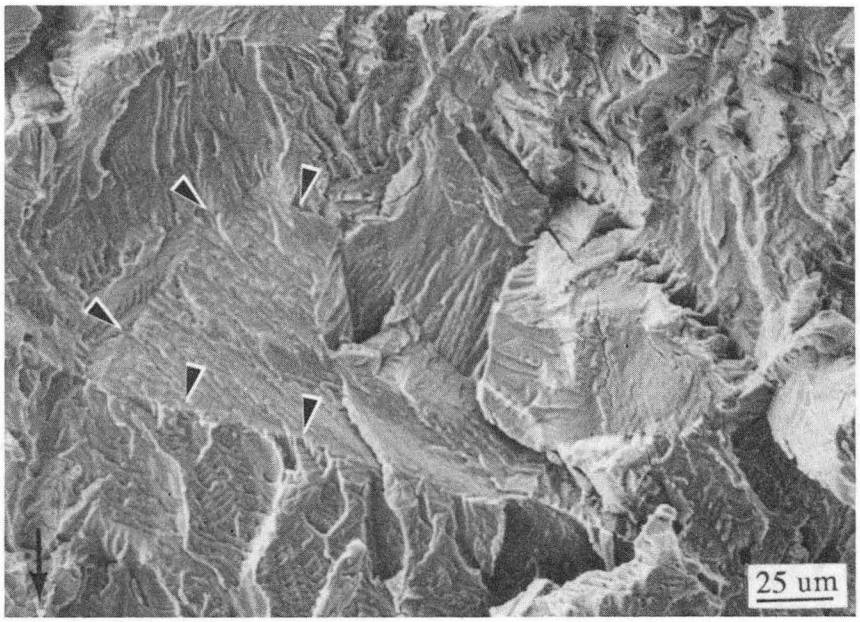

(c) XBB 896-5061A

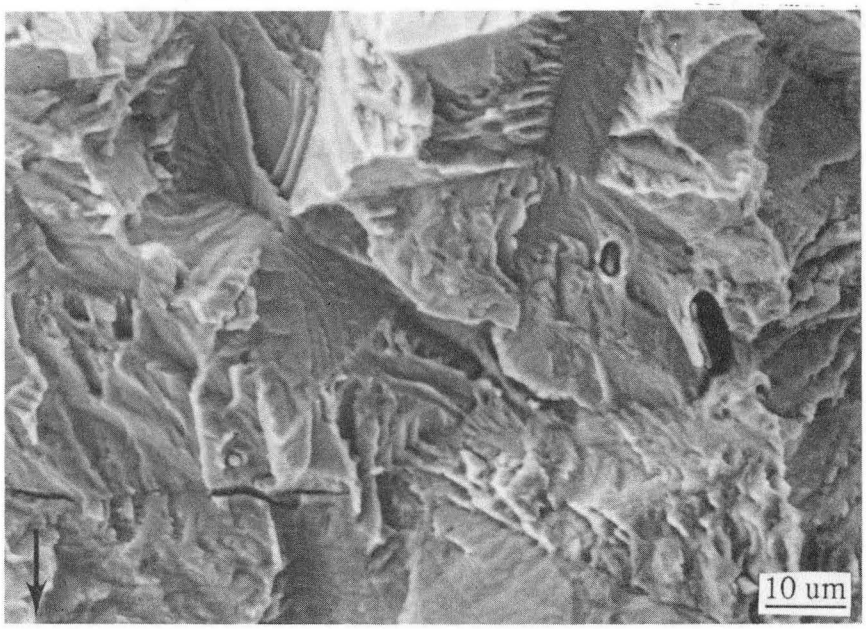

XBB 896-5060

(d)

Fig. 25: (c, d) SEM fractographs of 310 stainless steel specimens fatigue-tested at 4 K with $\Delta K \approx 20$ MPa-m$^{1/2}$ and da/dN $\approx$ da/dN $\approx 7 \times 10^{-3}$ μm/cycle.

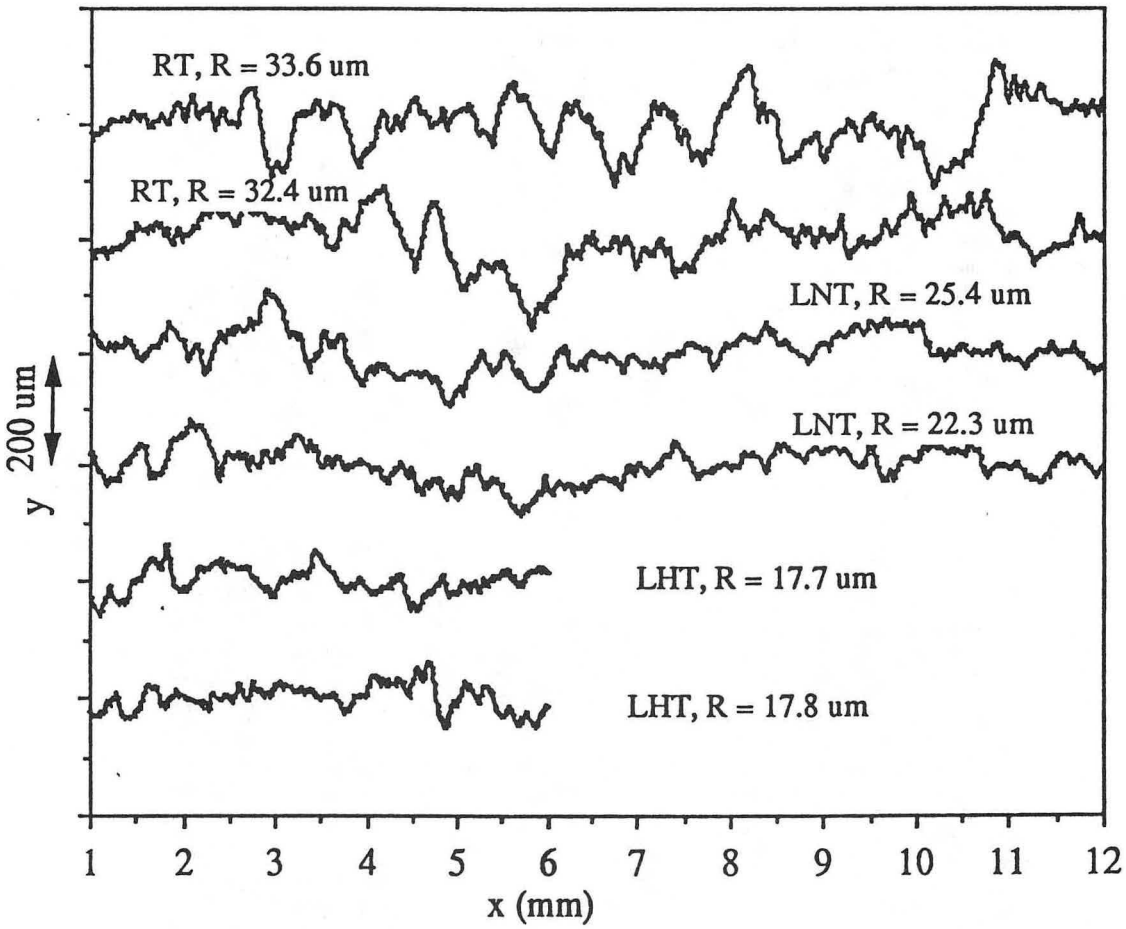

Fig. 26: Profilometer line scannings of the fatigue fracture surfaces of the specimens that were tested at room, liquid nitrogen, and liquid helium temperatures. (XBL 899-3488).

where y (x) is the surface line-scanning data denoting the surface height y as function of horizontal position x, $\bar{y}$ is the average surface height, L is the line-scanning distance. The results document the decrease in roughness as the temperature decreases. The roughness of the fatigue fracture surface should depend on the grain size, fracture mode, and the amount of plastic deformation during fracture. Observations of the fracture surface (Fig. 25) and the crack profile (Fig. 24) indicate that at all three temperatures (RT, LNT, and LHT) the fatigue crack extends in a quasi-cleavage mode. The roughness of the fatigue fracture surface is then decided by the plasticity. The larger the plastic zone size (as the temperature increases), the rougher the fracture surface becomes.

B. X-ray Diffraction and Texture

The results of X-ray diffraction measurements of the fatigue fracture surfaces confirm our expectation that 310 austenitic stainless steel is stable with respect to deformation-induced martensite at cryogenic temperatures. Fig. 27 (a) shows the diffraction data for the LHT fatigue specimen. No martensite peaks appear. But the X-ray diffraction data is of interest in another respect. Comparing the spectrum of the fatigue fracture surface (Fig. 27 (a)) with that of the surface 3 mm below the fatigue fracture surface (Fig. 27 (b)), we see an increase in intensity of the 002 peak. Figs. 28 (a,b) present the pole figures under these two conditions. This same phenomenon was observed on the LNT and RT fatigue specimens, and may indicate the development of a preferential texture as a result of the plastic deformation near the crack tip. While it is well known that a preferential texture develops during monotonic straining, the development of texture during cyclic plastic strain has not been studied. Another possibility is that the crack propagates preferentially along 002 crystallographic planes to create a fracture surface that exposes many 002 planes. These two possible explanations are currently under further investigation.

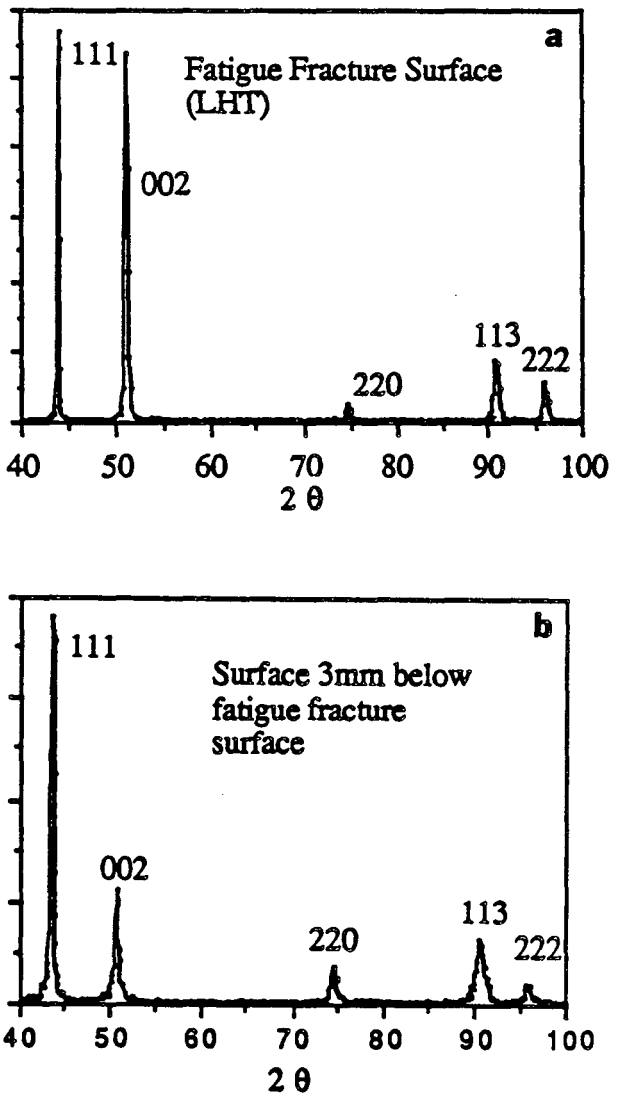

Fig. 27: X-ray diffraction data of (a) fracture surface of the fatigue specimen tested at liquid helium temperature and (b) the surface 3mm below the fracture surface.

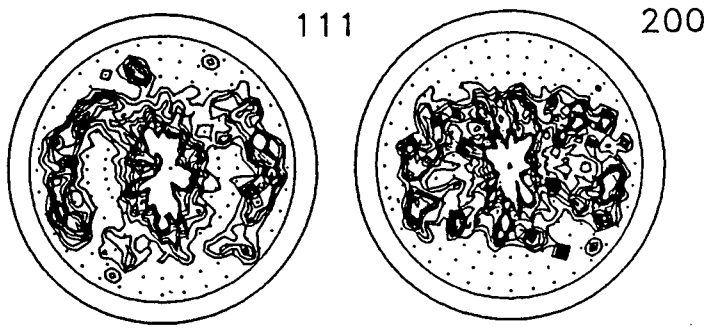

(a) Fatigue Fracture Surface

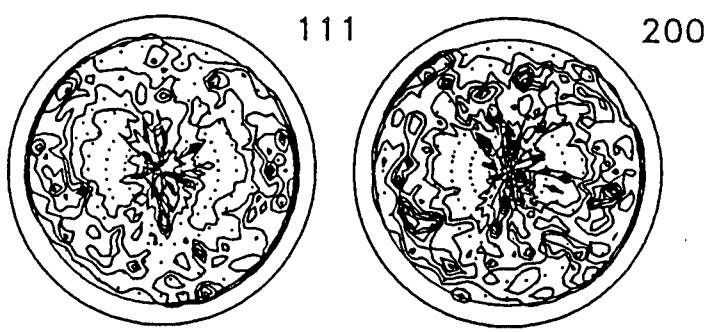

(b) Matrix

MAXIMUM = 34.18

MINIMUM = 0.00

CONTOUR(1) = 0.50

CONTOUR(2) = 1.00

CONTOUR(3) = 1.50

ETC.

Fig. 28. Pole figures of (a) fracture surface of the fatigue specimen tested at liquid helium temperature and (b) the surface 3mm below the fracture surface.

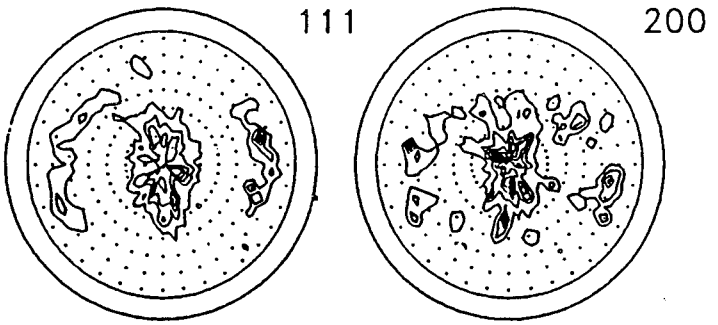

(a) Fatigue Fracture Surface

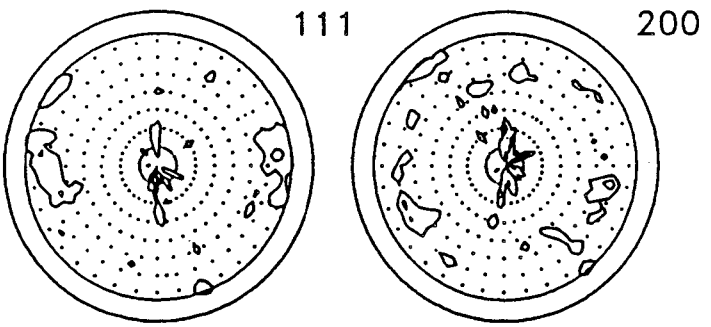

(b) Matrix

MAXIMUM = 34.18

MINIMUM = 0.00

CONTOUR(1) = 2.00

CONTOUR(2) = 4.00

CONTOUR(3) = 6.00

ETC.

Fig. 28 - 1: Same as Fig. 28 but with a different scale.

IV. DISCUSSION

The fatigue crack propagation rate of 310 austenitic stainless steel decreases and threshold cyclic stress intensity increases as the temperature decreases from 298 K to 4 K. Two mechanisms have been proposed to explain this effect. The first is crack closure due to the crack surface roughness,[86,92-94] which, as discussed above, is not true in the present study, because the surface roughness measured by profilometry decreases with decreasing temperature.

A second possible explanation for the temperature dependence relates it to the thermal activation of the dislocation motion that drives plastic crack extension. Models of fatigue crack propagation through the dynamic motion of dislocations have been proposed by Yokobori et al.[104] and by Gerberich et al.[105] and successfully explain some experimental data.[87,106] In these models the dislocation movement is related to the crack extension. Since the dislocation movement is a thermally activated process, the crack propagation is also thermally activated with the same activation energy. If these models apply, a plot of ln(da/dN) vs. 1/T should be a straight line with a slope equal to the activation energy, Q, for thermally activated dislocation motion. As shown in Fig. 29, however, the data are not linear on a plot of this type; the crack growth rate at lower temperature is higher than that allowed by the thermally activated process. The nonlinear relation between ln(da/dN) and 1/T suggests that the rate of fatigue crack propagation is not limited by thermally activated dislocation motion; at lower temperature cracks propagate by not only plastic deformation but also fracture process that is probably not a thermally activated process.

The data obtained here make it appear that the fatigue crack growth behavior of alloy 310 is also limited by the metallurgy of the alloy, and closely associated with the fracture mode. As temperature decreases crack propagation is increasingly anisotropic.

The fracture surfaces are made up of relatively flat facets on well-defined crystallographic planes. The deviation of the preferred plane from the plane of maximum tension and the increasing degree of branching at low temperature reduce the driving force for crack propagation, raising the threshold value and decreasing the crack growth rate.

While anisotropy in the crack growth is the most evident feature that affects the fatigue behavior of alloy 310, it should be kept in mind that its behavior is not anomalous. The threshold value of the cyclic stress intensity increases as the temperature drops in almost all alloys.[75-95] The increase in the exponent (n) is also a common observation.[96] These observations suggest that there are common underlying factors governing the threshold and crack growth exponent that remain to be understood.

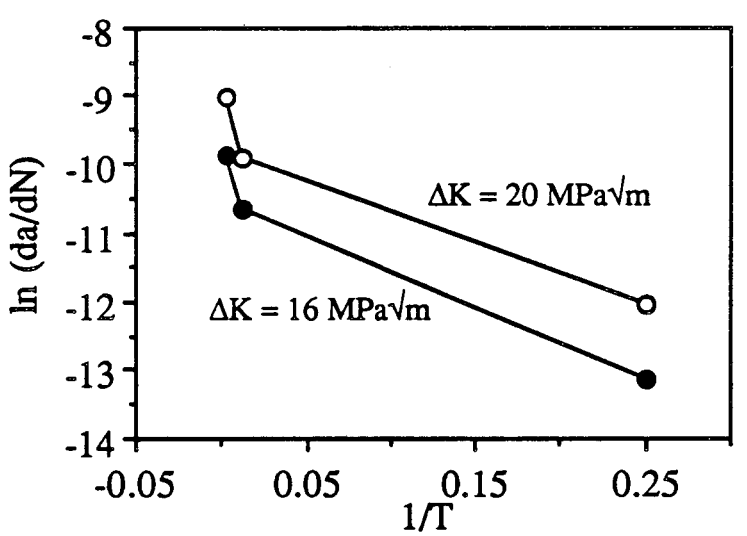

Fig. 29: Plots of ln(da/dN) vs. 1/T at $\Delta K = 20$ and 16 MPa-m$^{1/2}$.

V. CONCLUSIONS

1. In the range between 298 K to 4 K, as temperature decreases, the fatigue crack growth rate in 310 austenitic stainless steel decreases while the threshold stress intensity increases. The fatigue crack propagates in a quasi-cleavage mode along a zigzag path. The propagating crack branches to an extent that increased as the temperature decreased.

2. The reason for the decreased growth rate and increased threshold at low temperature is not the surface-roughness induced crack closure. It is likely that at the threshold region, crack growth rate is controlled by a thermo-activated process while in the Paris region, or as the stress intensity increases, the fracture due to static load operates concurrently with the thermo-activated processes.

3. A grain orientation texture due to the cyclic load was observed, that phenomenon needs to be further studied.

ACKNOWLEDGEMENT

It has been 2 years and 8 month since I entered my Ph. D program, and 5 years and 5 months since I came to Berkeley to start my graduate study. As I am about to file my dissertation, my heart is full with joy. I would like to put my research supervisor, Professor J. W. Morris, Jr. on the top of my acknowledgement list. Without his guidance, encouragements, supports, and patience, this study would not have been possible. I am also deeply indebted to Professor R. O. Ritchie and his students Drs. W. Yu and J. Shang, for their valuable discussions throughout the whole research. It is my great honor to have Professors J. W. Morris, Jr., R. O. Ritchie, F. Hauser as my thesis committee members. I will always remember my qualifying examination committee members, Professors R. O. Ritchie, G. Thomas, T. Devine, and F. Hauser, not only their names but also tough questions they asked during the exam..

I would like to express my gratitude to all my fellow graduate students in Morris group, especially to G. Chang, Dana Tribular, Mark McCormack, Jin Chan, Judy Glazer, Steve Shaffer, Anne Sunwoo, Tammy Summers, and Choongun Kim, for their valuable discussions, assistance in doing experiments, and help with my English.

This work was supported by the Director, Office of Energy Research, Office of Fusion Energy, Development and Technology Division of the U. S. Department of Energy, under Contract No. DE-AC03-76SF00098.

I dedicate my dissertation to my mother Meiying Guan and wife Ping Xu.

REFERENCES

1. L. Summers, Lawrence Livermore National Laboratory, private communication, 1989.
2. H. I. McHenry, Austenitic Steels at Low Temperatures, R. P. Reed and T. Horiuchi, eds., Plenum Press, New York and London, 1982, p. 1.
3. R. P. Reed, Austenitic Steels at Low Temperatures, R. P. Reed and T. Horiuchi, eds., Plenum Press, New York and London, 1982, p. 41.
4. D. Bhandarkar, V. F. Zackay, and E. P. Parker, *Metall. Trans.*, 1972, vol. 3 A, p. 2619.
5. P. Manganon Jr. and G. Thomas, *Metall. Trans.*, 1970, vol. 1, p. 1587.
6. A. Rosen, R. Jago, and T. Kjer, *J. of Mat. Sci.*, 1972, vol. 7, p. 870.
7. P. C. Maxwell, A. Goldberg, and J. C. Shyne, *Metall. Trans.*, 1974, vol. 5 A, p. 1319.
8. R. L. Tobler, R. P. Reed, and D. S. Burkhalter, Materials Studies for Magnetic Fusion Energy Applications at Low Temperatures III, NBSIR 80-1627, R. P. Reed, ed., National Bureau of Standards, Boulder, Colorado, 1980, p. 51.
9. G. M. Chang, M. S. Thesis, University of California at Berkeley, 1983.
10. G. B. Olson and M. Azrin, *Metall. Trans.*, 1978, vol. 9A, p. 713.
11. V. F. Zackay, E. R. Parker, D. Fahr, and R. Busch, *Trans. ASM*, 1967, vol. 60, p. 252.
12. S. D. Antolovich and B. Singh, *Metall. Trans.*, 1971, vol. 2 A, p. 2135.
13. W. W. Gerberich, P. L. Hemmings, and V. F. Zackay, *Metall. Trans.*, 1971, vol. 2A, p. 2243.
14. W. W. Gerberich, P. L. Hemmings, and V. F. Zackay, Fracture 1969, Pl L. Pratt, ed., Chapman and Hall, Ltd., London, 1969, p. 288.

15. G. R. Chanani, D. Eng. Thesis, University of California at Berkeley, 1970, UCRL-19620.

16. G. R. Chanani, and S. D. Antolovich, *Metall. Trans.*, 1974, vol. 5, p. 217.

17. G. Baudry, and A. Pineau, *Mater. Sci. Eng.*, 1977, vol. 28, p. 229.

18. D. Hennessy, G. Steckel and C. Alstetter, *Metall. Trans.*, 1976, vol. 7A, p. 415.

19. F. R. Schwartzberg and J. A. Shepic, Materials Studies for Magnetic Fusion Energy Applications at Low Tempertures, vol. I, National Bureau of Standards, Boulder, Colorado, Apirl 1978.

20. G. Franke and C. Altstetter, *Metall. Trans.*, 1976, vol. 7A, p. 1719.

21. G. R. Chanani, S. D. Antolovich, and W. W. Gerberich, *Metall. Trans.*, 1972, vol. 3A, p. 2661.

22. C. Bathias and R. M. Pelloux, *Metall. Trans.*, 1973, vol. 4A, pp. 1265-73.

23. A. G. Pineau and R. M. Pelloux, *Metall. Trans.*, 1974, vol. 5A, pp. 1103-12.

24. R. L. Tobler and R. P. Reed, *J. of Testing and Evaluation*, 1984, vol. 12, no. 6, pp. 364-70.

25. G. Schuster and C. Altstetter, *Metall. Trans.* , 1983, vol. 14A, pp. 2077-83.

26. G. Schuster and C. Altstertter, Fatigue Mechanisms, ASTM STP 811, pp. 445-63.

27. A. J. McEvily, W. Zagrany and J. Gonzalez, Basic Mechanisms in Fatigue of Metals, P. Lukas and J. Polak, eds., Elsevier, New York, 1988, pp. 271-79.

28. K. Katagiri, M. Tsuji, T. Okada, Kohji, R. Ogawa, G. M. Chang, and J. W. Morris, Jr., *Adv. Cryog. Eng.*, 1989, vol. 36, to be published.

29. Z. Mei, G. M. Chang, and J. W. Morris, Jr., Cryogenic Materials '88, R. P. Reed, Z. S. Xing, and E. W. Collings, eds., ICMC, Boulder, Colorado, 1988, vol. 2, p. 491.

30. E. Hornbogen, *Acta Metall.*, 1978, vol. 26, p. 147.

31. H. Fiedler, B. Averbach and M. Cohen, *Trans. ASM*, 1955, vol. 47, p. 276.

32. R. Reed, *Acta Metall.*, 1962, vol. 10, p. 865.

33. P. L. Mangonon, Jr., Ph. D Thesis, University of California, Berkeley, 1968.

34. G. H. Eichelman and F. C. Hull, *Trans. Am. Soc. Met.*, 1953, vol. 45, pp. 77-104.

35. I. Williams, R. G. Williams and R. C. Capellaro, Proceedings of the Sixth International Cryogenic Engineering Conference, IPC Science and Technology Press, Guildford, Surrey, England, 1976, pp. 337-41.

36. Annual Book of ASTM Standards, E 647 - 83, American Society for Test and Materials, Philadephia, PA., 1983, pp. 739-59.

37. Metals Handbook, 9th edition, vol. 8, America Society for Metals, Metals Park, Ohio, 1985, pp.386-402.

38. J. F. Knott, Fundamentals of Fracture Mechanics, Butterworths, London, 1973.

39. M. D. Halliday and C. J. Beevers, The Measurement of Crack Length and Shape During Fracture and Fatigue, C. J. Beevers, ed., Engineering Materials Advisory Services LTD, West Middlelands, U. K., 1981, pp. 85-112.

40. T. C. Lindley, Subcritical Crack Growth due to Fatigue, Stress Corrosion and Creep, L. H. Larsson ed., Elsevier Applied Science, London and New York, 1981, pp. 167-213.

41. R. O. Ritchie and W. Yu, Small Fatigue Cracks, R. O. Ritchie and J. Lankford, eds., TMS-AIME, Warrendale, PA, 1986, pp. 167-89.

42. W. F. Deans and C. E. Richards, *J. Test. Eval.*, 1979, vol. 7, pp. 147-154.

43. Metals Handbook, ASM, Metals Park, OH, 1985, 9th ed., vol. 9, pp. 63-70.

44. R. J. Gray, Revealing Ferromagnetic Microstructures with Ferrofluids, ORNL-TM-368, Oak Ridge National Laboratory, Oak Ridge, Tenn., March 1972.

45. T. H. Coleman and D. R. F. West, *Metals Technology,* Feb. 1976, pp. 49-53.

46. B. Yahiaoui and P. Petriquin, Note Technique RAM (73) 567, Division de Metallurgie et D 'Etude des Combustibles Nucleaires, Centre d'Etudes Nucleaires de Saclay, December 1973.

47. L. A. James, Fatigue Crack Growth Measurement and Data Analysis, ASTM STP 738, American Society for Testing and Materials, 1981, pp. 45-57.

48. J. L. Bernard and G. S. Slama, *Nuclear Technology*, 1982, vol. 59, No. 1, pp. 136-47.

49. L. A. James, Report HEDL-TME 75-20, Westinghouse Hanford Company, February, 1975.

50. S. Suresh and R. O. Ritchie, Fatigue Crack Growth Threshold: Concepts, D. L. Davidson and S. Suresh, eds., TMS-AIME, Warrendale, PA, 1984, pp. 227-61.

51. R. M. McMeeking and A. G. Evans, *J. Am. Ceram. Soc.*, 1982, vol. 65, No. 5, pp. 242-46.

52. B. Budiansky, J. W. Hutchinson and J. C. Lambropoulos, *Int. J. Solids Structures*, 1983, vol. 19, No. 4, pp. 337-55.

53. J. W. Hutchinson, Harvard University Report DEAP 58,1974.

54. J. C. Lambropoulos, *Int. J. Solids Structures*, 1986, vol. 22, No. 10, pp. 1083-1115.

55. A. G. Evans and R. M. Cannon, *Acta Metall.*, 1986, vol. 34, No. 5, p. 761.

56. N. I. Muskhelishvili, Some Basic Problems of the Mathematical Theory of Elasticity, P. Noordhoff Ltd, Groningen, Holland, 1953, pp. 225-7.

57. H. Tada, P. C. Paris, and G. R. Irwin, The Stress Analysis of Cracks Handbook, Del Research Corporation, Hellertown, Pa. 1973, pp. F.1-F16, and pp. C.1-C20 .

58. J. D. Eshelby, Proc. Roy. Soc. London, 1957, A 241, pp. 376-96.

59. P. C. Paris, R. M. McMeeking, and H. Tada, Cracks and Fractures, ASTM STP 601, American Society for Testing and Materials, Philadelphia, 1976, pp. 471-89.

60. S. Chen, A.G. Khachaturyan and J.W. Morris, Jr., Proceedings, ICOMAT 1979, W.S. Owen, ed., M.I.T, 1980, pp. 94-9.

61. J. W. Chan, J. Glazer, Z. Mei, P. A. Kramer, and J. W. Morris, submitted to *Acta Metall.*

62. R. O. Ritchie, Class Notes of MSE 212, 1987, University of California, Berkeley, Chapter of Fatigue Crack Growth, Mechanics and Fatigue Mechanisms, Fig. 7.

63. K. Chang, General Electric Co., and R. Sawtell, Aluminum Company of America, private communications.

64. S. Suresh, *Metall. Trans. A*, 1983, vol. 14, p. 2375-85.

65. A. A. Khrapkov, *Int. J. of Fract. Mech.*, 1971, vol. 7, pp. 373-82.

66. B. A. Bilby, G. E. Cardew, and I. C. Howard, Fracture 1977, D. M. R. Taplin, ed., University of Waterloo Press, 1977, vol. 3, pp. 197-200.

67. B. Cotterell and J. R. Rice, *Int. J. Fract.*, 1980, vol. 16, pp. 155-169.

68. P. C. Paris and G. C. Sih, Stress Analysis of Cracks, ASTM STP 381, American Society for Testing and Materials, Philadephia, PA, 1965, p. 30-40.

69. A. J. McEvily, Fatigue Mechanisms, ASTM STP 811, American Society for Testing and Materials, 1983, pp. 283-312.

70. F. A. McClintock, Fatigue Crack Propagation, ASTM STP 415, American Society for Testing and Materials, 1967, p. 170.

71. J. Weertman, "Fatigue Crack Propagation Theories", Fatigue and Microstructure, ASM, Metal Park, 1979, p. 279.

72. W. Yu, Prof. R. Ritchie's group, Lawrence Berkeley Laboratory, private communication, and G. H. Aronson and R. O. Ritchie, J. test. Eval., vol. 7, 1979, pp. 208-15.

73. J. R. Rice and G. F. Rosengren, *J. Mech. Phys. Solids*, 1968, vol. 16, pp. 1-12.

74. J. W. Hutchinson, *J. Mech. Phys. Solids*, 1968, vol. 16, pp. 13-31.

75. J. Glazer, S. L. Verzasconi, E. N. C. Dalder, W. Yu, R. A. Emigh, R. O. Ritchie, and J. W. Morris, Jr., *Adv. Cryog. Eng.*, 1986, vol. 32, p. 397.

76. J. Mckittrick, P. K. Liaw, S. I. Kwun, and M. E. Fine, *Metall. Tran.*, 1981, vol. 12A, p. 1535.

77. D. H. Park and M. E. Fine, TMS-AIME Symposium on Fatigue Crack Growth Threshold Concepts, D. L. Davidson and S. Suresh, eds, Philadelphia, 1983, p. 145.

78. S. Ya. Yarema, O. P. Ostash, V. M. Beletskii, V. N. Belyaev, and A. N. Zboromirskii, *Fiziko-Khimicheskaya Mekhanika Materialov*, 1977, vol. 13, no. 2, p.5.

79. O. P. Ostash, S. Ya. Yarema, and V. A. Stepanenko, *Fiziko-Khimicheskaya Mekhanika Materialov*, 1977, vol. 13, no. 3, p.26.

80. E. Tschegg and S. Stanzl, *Acta Metall.*, 1981, vol. 29, p. 33.

81. R. L. Tobler and Y. W. Cheng, *Int. J. Fatigue*, 1985, vol. 7, p. 191.

82. R. L. Tobler, *Adv. Cryog. Eng.*, 1986, vol. 32, p. 321.

83. R. P. Reed, R. L. Tobler and R. P. Mikesell, *Adv. Cryog. Eng.*, 1975, vol. 22, p. 68.

84. Y. Katz, A. Bussiba, and H. Mathias, *Adv. Cryog. Eng.*, 1982, vol. 30, p. 339.

85. J. P. Lucas and W. W. Gerberich, *Mater. Sci. Eng.*, 1981, vol. 51, p. 203.

86. W. W. Gerberich, W. Yu, and K. Esaklul, *Metall. Trans.*, 1984, vol. 15A, p. 875.

87. W. Yu, K. Esaklul, and W. W. Gerberich, *Metall. Trans.*, 1984, vol. 15A, p. 889.

88. K. A. Esaklul, W. K. Yu, and W. W. Gerberich, Fatigue at Low Temperatures, ASTM STP 857, R. I. Stephens, ed., ASTM, Philadelphia, 1985, p. 63.

89. V. K. Jata, W. W. Gerberich, and C. J. Beevers, Fatigue at Low Temperatures, ASTM STP 857, R. I. Stephens, ed., ASTM, Philadelphia, 1985, p. 102.

90. W. Yu and W. W. Gerberich, *Scripta Metallurgical*, Vol. 17, p.105.

91. P. K. Liaw, W. A. Logsdon, and M. H. Attaar, Fatigue at Low Temperatures, ASTM STP 857, R. I. Stephens, ed., ASTM, Philadelphia, 1985, p. 173.

92. P. K. Liaw, and W. A. Logsdon, *Acta. Metall.*, 1988, vol. 36, pp. 1731-44.

93. P. K. Liaw, A. Saxena, V. P. Swaminathan, and T. T. Shih, *Metall. Trans.*, 1983, vol. 14A, p.1631.

94. P. K. Liaw and W. A. Logsdon, *Engi. Fracture Mech.*, 1985, vol. 22, p. 585.

95. O. P. Ostash, S. Ya. Yarema, K. A. Yushchenko, V. I. Belotserkovets, V. T. Zhmur-Klimenko, and A. N. Vashchenko, *Fiziko-Khimicheskaya Mekhanika Materialov*, 1977, vol. 13, no. 6, p.56.

96. R. Tobler and Y. Cheng, Fatigue at Low Temperatures, ASTM STP 857, R. I. Stephens, ed., ASTM, Philadelphia, 1985, p. 5.

97. B. I. Verkin, N. M. Grinberg, V. A. Serdyuk and L. F. Yakovenko, *Mater. Sci. Eng.*, 1983, vol. 58, p.145.

98. N. R. Moody and W. W. Gerberich, *Mater. Sci. Eng.*, 1979, vol. 41, p.271.

99. R. L. Tobler and R. P. Reed, *Adv. Cryog. Eng.*, 1975, vol. 22, p. 35.

100. H. Ishii and J. Weertman, *Metall. Trans.*, 1971, vol. 2, p.3441.

101. R. H. Dauskardt, D. B. Marshall, and R. O. Ritchie, *J. Am. Ceram. Soc.*, to be published.

102. R. L. Tobler, R. P. Mikesell, R. L. Durcholz, and R. P. Reed, Semi-Annual Report, NBS, October, 1974.

103. R. W. Hertzberg, Deformation and Fracture Mechanics of Engineering Materials, second edition, John Wiley & Sons, Inc., 1983, p. 255.

104. T. Yokobori, S. Konosu, and A. T. Yokobori, Jr., Proceedings, International Conference of Fracture, vol. 1, Pergamon Press, New York, 1978, p.665.

105. W. W. Gerberich and K. A. Peterson, Micro and Macro Mechanics of Crack Growth, K. Sadananda, B. B. Rath, and D. J. Michel, eds., TMS-AIME, Warrendale, PA, 1982, p. 1.

106. T. Yokobori, I. Maekawa, Y. Tanabe, Z. Jin, and S. I. Nishida, Fatigue at Low Temperatures, ASTM STP 857, R. I. Stephens, ed., ASTM, Philadelphia, 1985, p. 121.

LAWRENCE BERKELEY LABORATORY
CENTER FOR ADVANCED MATERIALS
1 CYCLOTRON ROAD
BERKELEY, CALIFORNIA 94720